TOPICAL REVIEW — Magnetism, magnetic materials, and interdisciplinary research

The magnetic properties and magnetocaloric effects in binary R–T (R = Pr, Gd, Tb, Dy, Ho, Er, Tm; T = Ga, Ni, Co, Cu) intermetallic compounds*

Xin-Qi Zheng(郑新奇)[1] and Bao-Gen Shen(沈保根)[2,†]

[1] School of Materials Science and Engineering, University of Science and Technology Beijing, Beijing 100083, China
[2] Institute of Physics, Chinese Academy of Sciences and University of Chinese Academy of Sciences, Beijing 100190, China

(Received 5 December 2016; revised manuscript received 15 December 2016; published online 10 January 2017)

In this paper, we review the magnetic properties and magnetocaloric effects (MCE) of binary R–T (R = Pr, Gd, Tb, Dy, Ho, Er, Tm; T = Ga, Ni, Co, Cu) intermetallic compounds (including RGa series, RNi series, $R_{12}Co_7$ series, R_3Co series and RCu_2 series), which have been investigated in detail in the past several years. The R–T compounds are studied by means of magnetic measurements, heat capacity measurements, magnetoresistance measurements and neutron powder diffraction measurements. The R–T compounds show complex magnetic transitions and interesting magnetic properties. The types of magnetic transitions are investigated and confirmed in detail by multiple approaches. Especially, most of the R–T compounds undergo more than one magnetic transition, which has significant impact on the magnetocaloric effect of R–T compounds. The MCE of R–T compounds are calculated by different ways and the special shapes of MCE peaks for different compounds are investigated and discussed in detail. To improve the MCE performance of R–T compounds, atoms with large spin (S) and atoms with large total angular momentum (J) are introduced to substitute the related rare earth atoms. With the atom substitution, the maximum of magnetic entropy change (ΔS_M), refrigerant temperature width (T_{width}) or refrigerant capacity (RC) is enlarged for some R–T compounds. In the low temperature range, binary R–T (R = Pr, Gd, Tb, Dy, Ho, Er, Tm; T = Ga, Ni, Co, Cu) intermetallic compounds (including RGa series, RNi series, $R_{12}Co_7$ series, R_3Co series and RCu_2 series) show excellent performance of MCE, indicating the potential application for gas liquefaction in the future.

Keywords: magnetocaloric effect, magnetic entropy change, magnetic property, neutron diffraction, magnetic structure

PACS: 75.30.Sg, 75.50.Cc, 75.50.Ee **DOI:** 10.1088/1674-1056/26/2/027501

1. Introduction

Magnetocaloric effect (MCE) is the intrinsic property of magnetic materials and magnetic refrigeration based on MCE is demonstrated as a promising alternative to the conventional gas compression/expansion refrigeration for its high energy efficiency and environmental friendliness.[1–4] Lots of efforts have been made to explore advanced room temperature MCE materials for the potential application on household refrigerators or air conditioners and the reported typical MCE materials are $Gd_5Si_2Ge_2$, $La(Fe,Si)_{13}$, $MnAs_{1-x}Sb_x$, $MnFeP_{1-x}As_x$, NiMnGa, NiMnSn, etc.[5–13] In recent years, people also pay much attention on the MCE materials with low transition temperatures, and these materials are promising to be used for gas liquefaction in the future. Lots of low-temperature MCE materials have been studied and rare earth (R)-based material is one important category among them, such as (Gd,Er)NiAl, $ErCo_2$, DyCuAl, HoCuSi,[14–17] and so on. People usually use the following parameters to evaluate the potentiality in application of an MCE material: isothermal magnetic entropy change (ΔS_M), adiabatic temperature change (ΔT_{ad}), refrigerant temperature width (T_{width}), and refrigerant capacity (RC). According to the works in the past years, MCE materials with several magnetic transitions usually show advantages in the MCE performance.[18,19]

In the recent years, our group and other groups have devoted great efforts to study the R-based MCE materials with low temperature transitions. In this paper, we review the magnetic properties and magnetocaloric effects of binary R–T (R = Pr, Gd, Tb, Dy, Ho, Er, Tm; T = Ga, Ni, Co, Cu) intermetallic compounds. Most of the R–T compounds undergo several magnetic transitions with temperature increasing and the magnetic properties are complex and interesting. The magnetic properties and magnetic transitions are studied in detail by several approaches including neutron powder diffraction (NPD). The magnetocaloric effects and MCE enhancements with atom substitutions are also studied in detail. In addition, the special shape of MCE curves is discussed deeply and the related physical mechanism is clarified. The overview of

*Project supported by the National Natural Science Foundation of China (Grant Nos. 11274357, 51501005, 51590880, and 11674008), the Fundamental Research Funds for the Central Universities, China (Grant No. FRF-TP-15-010A1), the China Postdoctoral Science Foundation (Grant No. 2016M591071), and the Key Research Program of the Chinese Academy of Sciences (Grant No. KJZD-EW-M05).

†Corresponding author. E-mail: shenbg@aphy.iphy.ac.cn

magnetic properties and magnetocaloric effects in binary *R*–*T* compounds (including *R*Ga series, *R*Ni series, $R_{12}Co_7$ series, R_3Co series, and RCu_2 series) would be highly beneficial for the comprehension over the complex magnetic properties and exploration of excellent magnetic functional materials including MCE materials.

2. *R*Ga compounds

The crystal structure of *R*Ga compounds have been investigated before. The *R*Ga binary compounds crystallize in the orthorhombic CrB-type structure (space group *cmcm* #64). The structure was described as the stacking of the slabs of trigonal prisms with *R* atoms at the corners of the prism and the Ga atoms nearly at the corner.[20,21] Both *R* and Ga atoms are in the same crystallographic 4(c) sites with the C_{2v} point symmetry described as (0 0 0; 0.5 0.5 0.5) + (0 y 0.25; 0 $-y$ 0.75).[22,23] The axes of the prisms are parallel to the crystallographic *b* axis, displaced by (0.5, 0.5, 0), so that each Ga atom has seven neareat *R* neighbors.[20] The basic magnetic properties of *R*Ga compounds have also been studied. Magnetization and susceptibility measurements have been done on the *R*Ga (R = Pr, Nd, Sm, Gd, Tb, Dy, Ho, Er) compounds. The Curie temperatures are determined to be 32 K, 44 K, 108 K, 183 K, 158 K, 116 K, 63 K, and 32 K, respectively. And the calculation of effective paramagnetic moments indicates that only *R* atoms contribute to the magnetic moment in *R*Ga compounds.[24] According to the magnetization measurements on polycrystalline and single crystal *R*Ga compounds, these compounds are ferromagnetic with large magneto-crystalline anisotropy at low temperatures.[22,24–26] A non-collinear ferrimagnetic structure is observed for ErGa compound by neutron diffraction experiments.[27] According to the researches on the single crystal *R*Ga compounds, the easy direction of magnetization for PrGa compound is found to be *c* axis.[22] The spin reorientation (SR) of *R*Ga compounds have been studied by Mössbauer spectrum experiments.[20,28] SR in NdGa, SmGa, HoGa, and ErGa compounds is observed obviously. The magnetic moments of GdGa show a direction with $\theta = 30^\circ$ or a direction with $\theta = 60^\circ$ below T_{SR}, but they point to an identify direction with $\theta = 57.3^\circ$ above T_{SR}. In other words, the moments rotate towards the *b* axis in the *ab* plane with temperature increasing. The direction of the moments for ErGa below T_{SR} is complex. But it is proved that the moments also rotate toward *b* axis with temperature increasing.[20] The Curie temperature of PrGa compound is determined to be 36 K with a large derivation with previous results.[20,22,24] The SR transition of HoGa and GdGa was studied in detail by Susilo *et al*.[29,30] The MCE of GdGa compound is also studied, but the temperature range is between 100 K and 265 K, which is not large enough to study the influence of SR on MCE.[31]

In the following sections, the magnetic properties, magnetic transitions and MCEs of *R*Ga compounds will be studied and discussed in detail.

2.1. The crystal structure and magnetic structure of *R*Ga compounds

The polycrystalline *R*Ga (R = Pr, Gd, Tb, Dy, Ho, Er, Tm) compounds were prepared by arc melting R and Ga in argon atmosphere. And the purity of the starting elements is more than 99.9%. In order to make the ingots homogenous, they were turned over and melted several times. Then the samples were wrapped in molybdenum foils, sealed in a high-vacuum quartz tube and annealed at 800 °C for 7 days. After annealing they were quenched into liquid Nitrogen. To confirm purity and crystal structure of the samples, we carried out powder x-ray diffraction (XRD) experiments with Cu $K\alpha$ radiation. The XRD patterns of *R*Ga (R = Gd, Tb, Dy, Er, (Gd, Er)) compounds are shown in Fig. 1.[32,34] And the inset of Fig. 1 is the rietveld refined powder XRD patterns of TbGa compound. Results show that all of the peaks can correspond to the Bragg positions of the orthorhombic CrB-type structure (space group *Cmcm*), which indicates that the prepared compounds are of single phase. The crystal structure of *R*Ga compounds has been described before,[20,22] but we can also describe it from another view. The detailed crystal structure of PrGa compound is shown in Fig. 2. All of the atoms distribute in a form of layers perpendicular to a-axis, and Pr and Ga atoms are connected in a form of hexagon rings within each layer. Other *R*Ga compound has the same crystal structure.

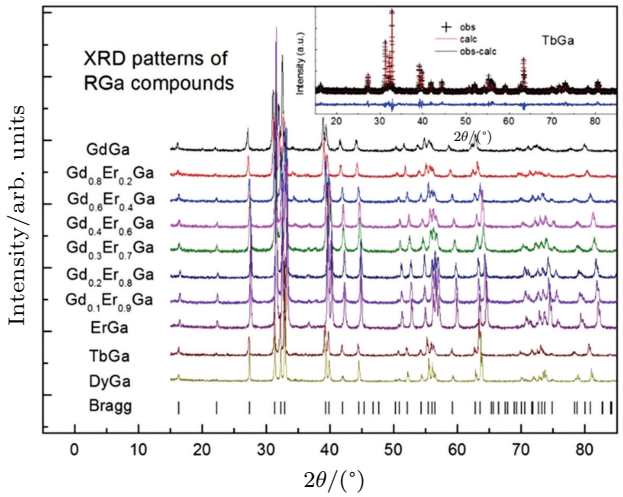

Fig. 1. (color online) The x-ray powder diffraction patterns of binary *R*Ga (R = Gd, Tb, Dy, Er) compounds and pseudo-binary $Gd_xEr_{1-x}Ga$ ($0 \le x \le 1$) compounds. The inset is the observed (cross symbols) and Rietveld fitted (lines) powder diffraction patterns of TbGa compound. The calculated positions of the Bragg peaks are shown as vertical bars just below the plots of the observed and calculated intensities. The differences between the observed and calculated intensities are shown at the bottom of the plot.[32]

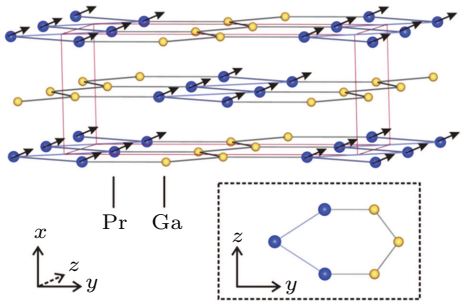

Fig. 2. (color online) The Crystal and magnetic structure of PrGa compound. Distribution of magnetic moments in each unit cell and the distribution of atoms connected in form of the hexagon ring in yz crystal plane.[33]

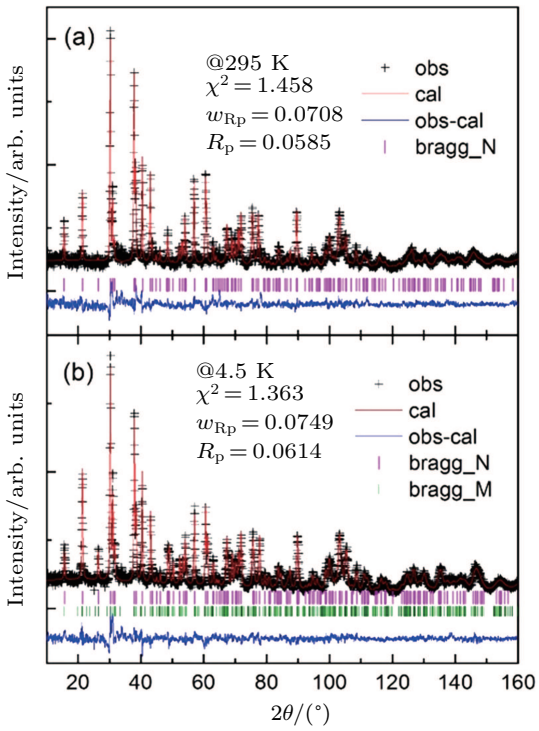

Fig. 3. (color online) The neutron powder diffraction pattern of PrGa at 295 K (a) and 4.5 K (b), respectively. The observed data and the calculated patterns are plotted in cross and solid line, respectively. The solid line at the bottom is the difference between the observed and calculated data. The Bragg positions for the nuclear and magnetic structure are marked as short vertical lines. Only nuclear model is considered in the refinement at 295 K and both nuclear model and magnetic model are considered in the refinement at 4.5 K.[33]

High resolution neutron powder diffraction (NDP) experiment was then employed to study the magnetic structure of PrGa compound. The NPD experiments were performed at 295 K and 4.5 K, respectively. Fitting and calculations were carried out by Rietveld refinement method afterwards. The observed and the calculated neutron powder diffraction patterns at 295 K and 4.5 K are shown in Figs. 3(a) and 3(b). NPD results at 295 K show that PrGa compound has a pure phase and it crystalizes in a CrB-type orthorhombic structure (space group #63 *cmcm*). Both the nuclear and the magnetic structure models are involved in the calculation at 4.5 K. The magnetic moments are FM-ordered along crystallographic *c* axis and the ordered magnetic moment is determined to be 2.6 μ_B at 4.5 K.[33] Figure 4 shows the isothermal magnetization curve at 11K and the inset of Fig. 4 shows the temperature dependence of χ^{-1} up to 300 K, where χ is the magnetic susceptibility. The linear relationship of χ^{-1} and temperature in the high temperature range indicates that the Curie–Weiss law is appropriate here. According to the Curie–Weiss law and the definition of χ, $M_{\rm eff}$ is calculated to be 3.6 μ_B from the slope of the linear fitting curve.[33] The MH curve at 5 K (not shown in Fig. 1) has also been measured and it is almost coincided with the MH curve at 11 K in high field range. For the isothermal magnetization curve at 5 K and 11 K, the magnetization increases with field increasing and reaches its saturation value rapidly, indicating that it is reasonable to calculate saturated magnetization (M_s) from the MH curve at 5 K or 11 K. M_s's at these two temperature are calculated to be the same value of 2.0 μ_B, which is the average value per Pr atom.[33] The value of M_s is similar to the ordered magnetic moment obtained from NPD experiments at 4.5 K but considerably smaller than that of $M_{\rm eff}$.

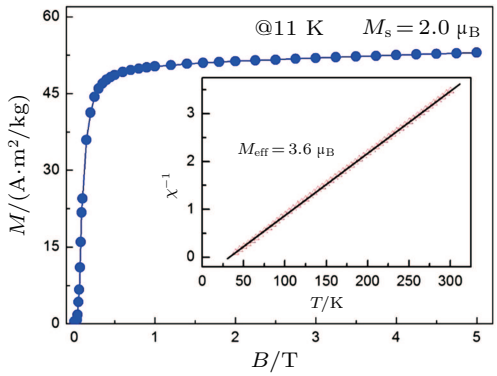

Fig. 4. (color online) Isothermal magnetization curve of PrGa compound up to 5 T at 11 K for PrGa compound and the inset is the temperature dependence of the magnetic susceptibility inverse.[33]

In order to study the magnetic ground state of PrGa compound at low temperature, we investigated the degree of magnetic order, which is known as magnetic entropy (S_M). The total entropy can be calculated from the integration of the heat capacity data:

$$S(T) = S(T_{\rm ref}) + \int_{T_{\rm ref}}^{T} \frac{C_H}{T}\,{\rm d}T, \quad (1)$$

where $T_{\rm ref}$ is the reference temperature, C_H is the heat capacity under a field of H. The heat capacity data at zero field for PrGa and YGa was measured. We first took $T = 10$ K as reference temperature and calculated the total entropy of PrGa and YGa compound, respectively. Then we can obtain S_M of PrGa by subtracting $S_{\rm tot}$ of YGa from $S_{\rm tot}$ of PrGa, and the above method has been used before.[35,36]

$$S_{\rm M}(T) = S_{\rm M}(10\ {\rm K}) + \int_{10\ {\rm K}}^{T} \frac{C_{H=0,{\rm PrGa}} - C_{H=0,{\rm YGa}}}{T}\,{\rm d}T. \quad (2)$$

Now we introduce a new function $f(T)$.

$$f(T) = S_{\rm M}(T) - S_{\rm M}(10\ {\rm K})$$

$$= \int_{10\ \mathrm{K}}^{T} \frac{C_{H=0,\mathrm{PrGa}} - C_{H=0,\mathrm{YGa}}}{T}\,\mathrm{d}T. \quad (3)$$

The right-hand side of Eq. (3) can be calculated and the curve was plotted in Fig. 5. S_{M} increases as temperature goes up. When the temperature exceeds T_{C}, S_{M} changes slowly and reaches its maximum value gradually.

$$f(T)_{\max} = S_{\mathrm{M}}(T)_{\max} - S_{\mathrm{M}}(10\ \mathrm{K}) = 57.03\ \mathrm{J/kg\cdot K}, \quad (4)$$

S_{M} in PM zone can be calculated from the following equation[37]

$$S_{\mathrm{M}}(\mathrm{PM}) = S_{\mathrm{M}}(T)_{\max} = Nk_{\mathrm{B}}\ln(2J+1), \quad (5)$$

where N is the number of magnetic moments, k_{B} is the Boltzmann constant, and J is the total angular quantum number. Therefore we can obtain S_{M} (10 K) = 29.65 J/kg·K.[33] PrGa compound is in stable FM ordered state below 11 K. So the large value of S_{M} at 10 K is unusual. This indicates that the magnetic moments of PrGa are not parallel completely at 10 K, and more complex magnetic structure may exist. This conclusion is in accord with the results of NPD experiments and the analysis of M_{s} and M_{eff}.

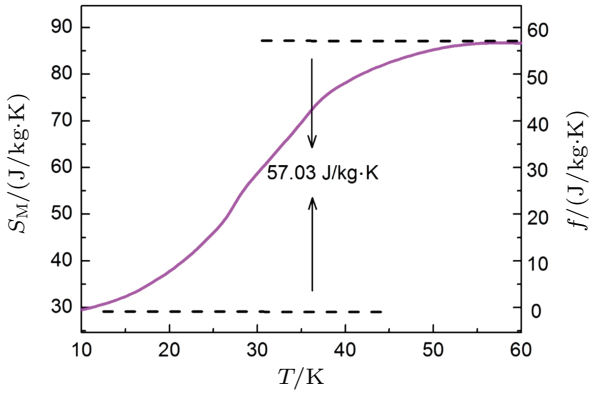

Fig. 5. (color online) The entropy contributed from magnetic moments. The temperature dependence of the magnetic entropy of PrGa compound.[33]

Considering that M_{s} is much smaller than M_{eff} and S_{M} at 10 K is considerably larger than zero, we can assume that the magnetic moments point to different directions but with a fixed deviation angle from c axis and the value of 2.5 μ_{B} is the projection of the magnetic moments on c axis.[33] If we draw all of the magnetic moments at the same atom site, we can see that they are distributed randomly within a conical surface. The sketch of the magnetic structure of PrGa is shown in Fig. 6. The real magnetic moment is M_{eff} and every magnetic moment can be resolved into two components. M_z and M_{xy} are the components along the c axis and within the ab crystal plane, respectively.[33] Furthermore, M_z is long-range FM-ordered but M_{xy} is distributed randomly without any long-range order. M_{eff}, M_z, and M_{xy} have the following relation:

$$M_{\mathrm{eff}}^2 = M_z^2 + M_{xy}^2. \quad (6)$$

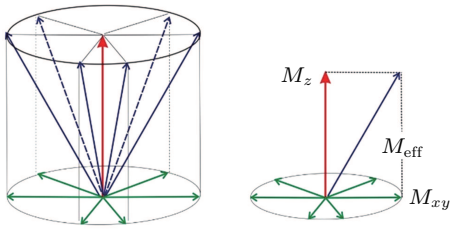

Fig. 6. (color online) The cone-surface distribution of the actual magnetic moments in PrGa compound and the vector decomposition of the magnetic moments.[33]

2.2. The magnetic properties and magnetic transitions of *R*Ga compounds

Spin reorientation has been observed in some of the *R*Ga compounds, such as PrGa, SmGa, HoGa, and ErGa according to the results of Mössbauer spectrum experiments.[20] Here we studied the magnetic properties of *R*Ga compounds in detail including PrGa, GdGa, TbGa, DyGa, HoGa, ErGa, and TmGa compounds. First of all, we analyze the magnetic properties and magnetic transitions of heavy-rare-earth *R*Ga compounds. Figure 7 is the thermal magnetization curves of GdGa, TbGa, DyGa, HoGa, and ErGa compounds under a field of 0.01 T. And the inset of Fig. 7 shows the zero-field-cooled (ZFC) thermal magnetization and field-cooled (FC) thermal magnetization curves of TmGa compound under a field of 0.04 T. All of the M–T curves show hight-variability twice as temperature increases. Besides of the drastic change around Curie temperature (T_{C}), another obvious change of magnetization is observed in low temperature ranges, which is described as SR transition and the transition temperature is marked as T_{t}.[19,32,34,38] The transition temperatures for SR are determined to be 66 K, 31 K, 25 K, 20 K, and 15 K for GdGa, TbGa, DyGa, HoGa, and ErGa compounds, respectively. The Curie temperatures are determined to be 181.9 K, 154 K, 113 K, 69 K, and 30 K for GdGa, TbGa, DyGa, HoGa, and ErGa compounds, respectively. It is clearly that T_{C} decreases steadily as the atomic number of R atoms increases, but the alteration of T_{t} is not as

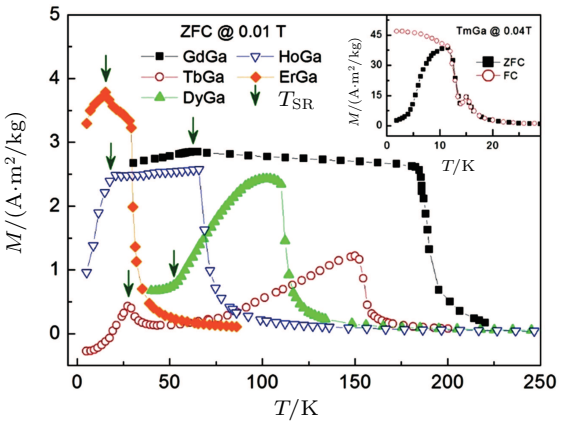

Fig. 7. (color online) The temperature dependences of magnetization curves of *R*Ga (*R* = Gd, Tb, Dy, Ho, Er) compounds at a field of 0.01 T. The inset is the zero-field-cooling and field-cooling curves under a field of 0.01 T for TmGa compound.

obvious as R atom changes. The value of spin quantum number (S) decreases with the atomic number of R atoms increases, and T_C is positively correlated with S. Figure 8(a) shows the isothermal magnetization curves at different temperatures for ErGa compound. All of the M–H curves at the temperature range above T_C show typical FM characteristic. That is, magnetization increases as magnetic field goes up and reaches its saturation value quickly. Therefore, the SR magnetic transition is also ferromagnetic (FM) to FM transition. TmGa compound exhibits two successive magnetic transitions: ferromagnetic (FM) to antiferromagnetic (AFM) transition at $T_t = 12$ K and AFM to paramagnetic (PM) transition at $T_C = 15$ K.[39] The ZFC and FC curves are well overlapped above T_C, indicating that thermal hysteresis is very small as observed in other MCE materials with a second-order magnetic transition.[16] However, there is an obvious bifurcation at temperatures below T_t and it is likely due to a domain wall pinning effect as described in literature.[40] All of the transition temperatures are listed in Table 1.

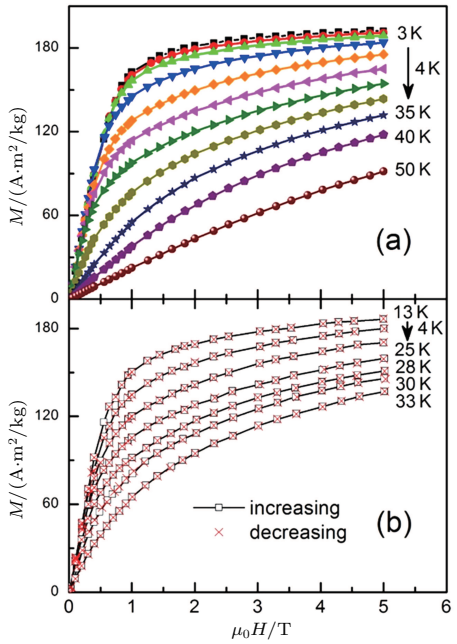

Fig. 8. (color online) (a) The isothermal magnetization curves up to 5 T at a temperature range from 3 K to 50 K for HoGa compound. (b) The isothermal magnetization curves up to 5 T obtained with field increasing and decreasing at a temperature range from 13 K to 33 K.

Table 1. The transition temperatures and magnetocaloric parameters of RGa (R = Pr, Gd, Tb, Dy, Ho, Er, Tm) compounds and $Gd_xEr_{1-x}Ga$ ($0 \le x \le 1$) compounds.[34]

Materials	T_t/K	T_C/K	MCE_0–2 T			MCE_0–5 T			Ref.
			$-\Delta S_M(T)_{max}$/(J/kg·K)	T_{width}/K	RC/(J/kg)	$-\Delta S_M/T_{max}$/(J/kg·K)	T_{width}/K	RC/(J/kg)	
PrGa	27	37	7.0	10.6	59.3	10.7	18.1	158.7	[41]
GdGa	66	181.9	2.7	99.8	182.6	5.3	159.4	616.1	[34]
TbGa	31	154	3.7	135.9	181.8	8.3	155.5	620.6	[32]
DyGa	25	113	2.3	101.2	92.8	5.8	112.7	381.9	[32]
HoGa	20	69	8.8	16.7	113.2	17.1	83	455	[38]
ErGa	15	30	10.9	22.6	166	21.3	30.9	494	[19]
TmGa	12	15	20.6	9.9	149	34.3	14.2	359.7	[39]
$Gd_{0.1}Er_{0.9}Ga$	20.6	49	4.8	48.6	184.7	11.4	56.2	535.2	[34]
$Gd_{0.2}Er_{0.8}Ga$	21.4	76.4	4.9	74.4	244.8	10.9	80.9	659.4	[34]
$Gd_{0.3}Er_{0.7}Ga$	22.9	98.7	3.2	95.9	222.7	7.3	108.3	685.3	[34]
$Gd_{0.4}Er_{0.6}Ga$	21	115.8	2.6	94.1	170.4	5.7	129.3	629.9	[34]
$Gd_{0.6}Er_{0.4}Ga$	26.7	146.8	3.2	153.6	250.4	6.5	162.8	707.2	[34]
$Gd_{0.8}Er_{0.2}Ga$	28.8	167.7	2.7	168.3	254	5.6	185.5	715.3	[34]

Figure 8(b) shows that the M–H curves measured in field increasing and decreasing mode almost coincide, which means good magnetic reversibility. The ZFC and FC of ErGa compound also show no thermal hysteresis around T_C. According to the Banerjee criterion,[42] a magnetic transition is expected to be of the first order when the slope of M^2 versus H/M plot is negative, whereas it will be of the second order when the slope is positive. The relationship between H/M and M^2 has been calculated for ErGa compound and the arrott plot is not shown here. The positive slopes of plot around T_C confirm that the FM–PM transition is of second order,[42] which accords well with the case where both thermal and magnetic hysteresis are absent. Further results show that all of the RGa (R = Pr, Gd, Tb, Dy, Ho, Er, Tm) compounds are of second order transition materials.

The thermal magnetization curves of $Gd_xEr_{1-x}Ga$ ($0 \le x \le 1$) compounds are measured at a field of 0.1 T and the temperature dependence of the magnetization is shown in Fig. 9. Sharp decrease is observed on each M–T curve around T_C, and another anomaly is observed in low temperature range for all the samples. In the compounds with a low content of Gd, the magnetic properties are similar to ErGa compound. And when the content of Gd is large, such as $Gd_{0.6}Er_{0.4}Ga$ and $Gd_{0.8}Er_{0.2}Ga$, the magnetic properties show similar feature to GdGa compound.[34] According to previous analysis, the transition in low temperature range is SR transition for most

$Gd_xEr_{1-x}Ga$ ($0 \leq x \leq 1$) compounds and we marked that transition temperature as T_{SR}. For $Gd_{0.3}Er_{0.7}Ga$ and $Gd_{0.4}Er_{0.6}Ga$ compounds, the transition in low temperature range is an AFM to FM transition, which will be discussed later. And we mark that transition temperature as T_t in this case. In fact, the SR transition of ErGa and GdGa has been studied carefully by Mössbauer spectrum.[20] The magnetic moment points to different directions at different temperatures and it results from the competition between exchange interaction and crystal field interaction. The magnetic moments of GdGa show a direction with $\theta = 30^\circ$ or a direction with $\theta = 60^\circ$ below T_{SR}, but they point to an identify direction with $\theta = 57.3^\circ$ above T_{SR}.[20] In other words, the moments rotate towards the b axis in the ab plane with temperature increasing. The direction of the moments for ErGa below T_{SR} is complex. But it is proved that the moments also rotate toward b axis with temperature increasing.

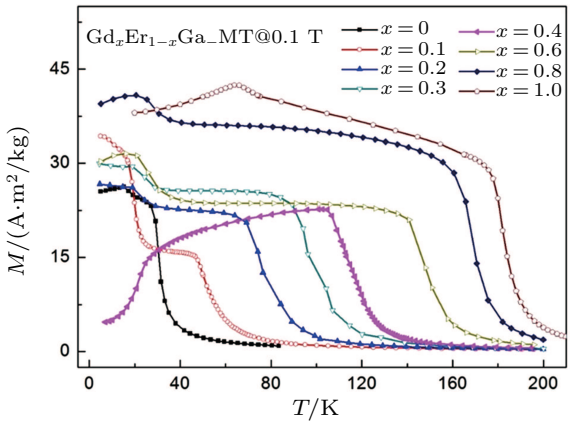

Fig. 9. (color online) The temperature dependences of magnetization curves under a field of 0.1 T for $Gd_xEr_{1-x}Ga$ ($0 \leq x \leq 1$) compounds.

Isothermal magnetization curves up to 5 T at 5 K for $Gd_xEr_{1-x}Ga$ ($0 \leq x \leq 1$) compounds are shown in Fig. 10. The magnetization goes up and comes to its saturation value quickly with magnetic field increasing for $Gd_xEr_{1-x}Ga$ ($x = 0$, 0.1, 0.2, 0.6, 0.8, and 1.0) compounds, and it is the typical characteristic of the FM ground state. For $Gd_{0.3}Er_{0.7}Ga$ and $Gd_{0.4}Er_{0.6}Ga$ compounds, the magnetic exchange interaction is not large enough to counterbalance the crystal field interaction below T_t, and Er and Gd magnetic moment each points to the favorite directions on their own.[34] That is to say, the ground state is AFM below T_t for $Gd_{0.3}Er_{0.7}Ga$ and $Gd_{0.4}Er_{0.6}Ga$ compounds. As a result, the magnetization at 5 K increases linearly with increasing magnetic field in low field ranges (see Fig. 10). Besides, it is found that the magnetization exhibits a sharp increase when the applied field exceeds a certain value, indicating that the field-induced metamagnetic transition from AFM to FM state occurs. The critical field required for metamagnetic transition for $Gd_{0.3}Er_{0.7}Ga$ and $Gd_{0.4}Er_{0.6}Ga$, which is determined from the maximum of dM/dH, is found to be 0.98 T and 1.03 T, respectively.[34] The transition temperatures of $Gd_xEr_{1-x}Ga$ ($0 \leq x \leq 1$) compounds, which are determined from derivative of M–T curves, are all listed in Table 1. We can see that T_C increases from 30 K to 181.9 K as the content of Gd increases from 0 to 1. The reason is that the average value of spin quantum number (S) increases with the content of Gd, and T_C increases with S increasing. The T_{SR} and T_t are listed in the same column, and results show that the change of T_{SR} or T_t is not as large as T_C. The lowest and highest values of T_{SR} are 15 K and 66 K respectively for the $Gd_xEr_{1-x}Ga$ compounds.

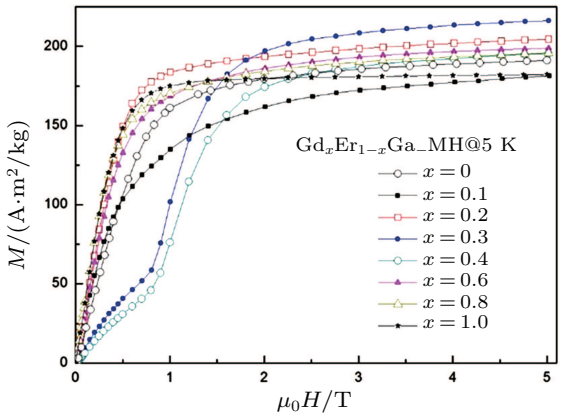

Fig. 10. (color online) The isothermal magnetization curves up to 5 T at 5 K for $Gd_xEr_{1-x}Ga$ ($0 \leq x \leq 1$) compounds.[34]

The SR transition due to the competition between the magnetic exchange interaction and the crystal field interaction has been observed in NdGa, SmGa, HoGa, ErGa, and GdGa compounds by Mössbauer spectrum experiments.[20] With decreasing temperature, the magnetic moments rotate gradually from the bc plane toward the crystallographic a axis. For HoGa compound, the azimuth angle ϕ does not change with temperature and the rotation of the magnetic moments occurs in the ac plane when only the angle θ is changed. For GdGa compound, in the temperature range 5 K To 100 K, the ferromagnetic structure of the GdGa compound is noncollinear. At 5 K the magnetic moments of the Gd^{3+} ions point in two distinct directions with respect to the crystallographic a axis ($\theta_1 = 30^\circ$ and $\theta_2 = 60^\circ$).[20] High-resolution neutron powder diffraction was also employed to study the SR transition of HoGa compound.[29] In the temperature range between T_{SR} and T_C, the magnetic structure comprises ferromagnetic order of the Ho sublattice along the c axis. Upon cooling below T_{SR}, the Ho magnetic moments cant away from the c axis towards the ab plane. At 3 K, the Ho moment is 8.8(2) μ_B and the Ho magnetic moments point in the direction $\theta = 30(2)$ and $\phi = 49(4)$ with respect to the crystallographic c axis. The observation of an ab plane component at around 50 from the a axis is in contrast with the suggested magnetic structure reported on the basis of a ^{119}Sn Mössbauer spectroscopy study

of an Sn-doped HoGa sample.[20,29] The SR transition GdGa compound is also studied by ^{155}Gd Mössbauer spectroscopy and neutron powder diffraction.[30] Between T_C and T_{SR}, the magnetic structure is characterized by ferromagnetic order of the Gd moments along the *b* axis. On cooling below T_{SR}, the Gd 4*c* magnetic moments split into two groups (2:2). At 3.6 K, the Gd moment is 6.7(4) μ_B, and the Gd magnetic moments are in the *bc* plane, canted by 84(3) and 46(4) with respect to the crystallographic *b* axis. This splitting into two magnetically inequivalent sites is confirmed by 5 K ^{155}Gd Mössbauer results.[30]

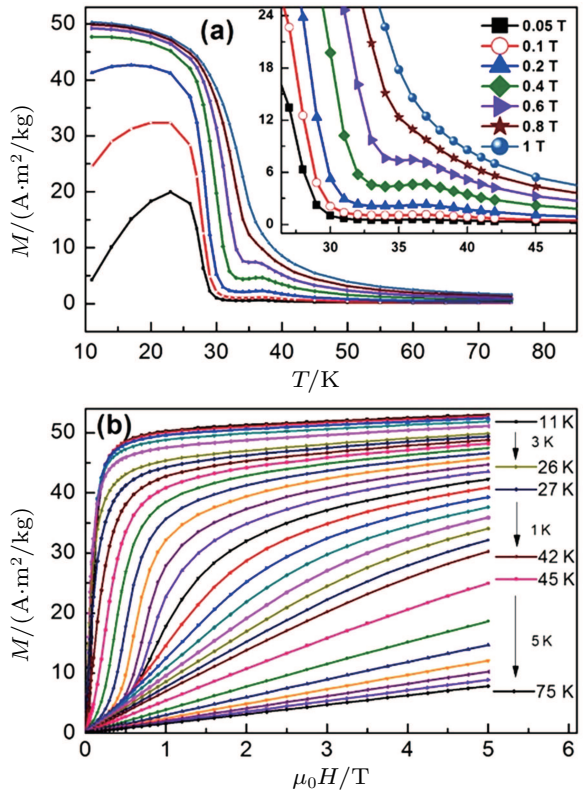

Fig. 11. (color online) (a) The thermal magnetization curves of PrGa compound under the field of 0.05 T, 0.1 T, 0.2 T, 0.4 T, 0.6 T, 0.8 T, and 1 T, respectively. (b) The isothermal magnetization curves up to 5 T at different temperatures in the range from 11 K to 75 K for PrGa compound.[41]

The thermal magnetization curves at different magnetic fields and isothermal magnetization curves are measured for PrGa compound, which are shown in Fig. 11. From *M*–*T* curves at 0.05 T, we can see that the magnetization curve experiences two drops at 28 K and 38 K respectively. The sharp changes are corresponding to two magnetic transition temperatures marked as T_t and T_C. The transition at lower temperature is similar to the FM to AFM transition and it seems to be supported by isothermal magnetization results shown in Fig. 11(b). In the temperature range between T_t and T_C, the magnetization curve shows a linear increase and then a sudden jump with magnetic field increasing, which appears to indicate the ground state is AFM and there is a metamagnetic transition from AFM to FM phase.[41,43] As the applied field is added, T_t moves to higher temperature zone. It indicates that the temperature region of metamagnetic transition gets larger when the applied field increases. To make it clear, partially enlarged view is shown in the inset of Fig. 11(a). When the applied field is high enough, metamagnetic transition occurs in the whole temperature region between T_t and T_C, thus the two drops of magnetization almost become one. The *M*–*T* curves of PrGa are very similar to those of $LaFe_{11.44}Al_{1.56}$.[44] The critical field of metamagnetic transition determined by the maximum value of is also calculated. The result indicates that the critical field increases with temperature. In other words, the temperature zone where metamagnetic transition happens extends with applied field increasing. It is consistent with the conclusion obtained from *M*–*T* curve.

The temperature dependence of heat capacity at different magnetic field for YGa, PrGa, ErGa, and TmGa compounds are measured and the C_H–*T* curves are shown in Fig. 12. The YGa compound is non-magnetic and has the same crystal structure with other *R*Ga compounds. The C_H–*T* curve of the YGa compound obeys the typical heat capacity change rule as temperature increases and there is no peak observed on the curve (see Fig. 12(a)). Unlike the YGa compound, peaks are observed on the C_H–*T* curves of magnetic PrGa, ErGa, and TmGa compounds. The heat capacity results show similar change rules with *M*–*T* curves. Two peaks are clearly shown on the C_H–*T* curve when the applied field is zero for the PrGa compound (Fig. 12(b)). And the two peaks are corresponding to T_t and T_C respectively. The peak at lower temperature moves toward higher zone with applied field increasing. When the applied field exceeds a certain value, the two peaks turn into a large one, such as those in the case of 1, 2, and 5 T.[41] The C_H–*T* curves of the ErGa compound for 0 T, 1 T, 2 T, and 5 T are shown in Fig. 12(c). Two sharp peaks are observed at 15 K and 30 K under zero-field, corresponding to the SR and FM to PM transitions, respectively. With the application of magnetic field, the intensity of the peak at T_{SR} is reduced greatly, and the peak shifts toward higher temperatures with field increasing. On the other hand, the peak at T_C spreads to a broad anomaly with a much lower magnitude when a field larger than 1 T is applied, and it almost disappears under a field of 5 T. It may also be noted from Fig. 12(c) that the values of heat capacity in applied fields above T_C are much larger than those at zero-field in a wide temperature range. The abnormal heat capacity of ErGa may be related to the existence of short-range FM correlations in the PM state T_C.[19] Figure 12(d) displays the heat capacity curves for TmGa under the fields of 0, 1, 2, and 5 T, respectively. It clearly shows two successive magnetic transitions at $T_C = 12$ K and at $T_N = 15$ K, which

is fully consistent with the magnetic measurements.[39] With the increase of magnetic field, the two peaks are not only turn a broader and lower, but also shifts toward higher temperature, which is the typical characteristic of FM material.[2] It is known that the heat capacity peak is caused by the absorption of heat which is utilized in randomization of magnetic moments around transition temperature.[39] With the application of field, the randomization of moments would spread out over a wide temperature region, and the maximum peak moves towards higher temperature.[5] In fact, the performance of C_H–T curve is the inevitable result of thermal magnetization data. Now we discuss the form of the magnetic contribution to heat capacity approximately. The magnetic component of internal energy $(E_{\rm M})$ can be expressed as $E_{\rm M} = -\int H_{\rm tot}\,{\rm d}M$, where M is the magnetic moment of the compound and $H_{\rm tot}$ is the total magnetic field in the compound. According to the theory of mean field, the total magnetic field can be expressed as $H_{\rm tot} = H_{\rm e} + \alpha M$, where $H_{\rm e}$ is the external field, α is the mean field constant, and αM represents the internal field.[31,45] The magnetic contribution to heat capacity can be obtained by $\partial E_{\rm M}/\partial T$, thus we can see that $C_H = -(H_{\rm e} + \alpha M)\partial M/\partial T$. According to this formula, a sudden drop of magnetic moment on the M–T curve can definitely cause a sharp peak on the C_H–T curve. Every magnetic transition is accompanied by a sudden drop of magnetic moment in magnetic RGa compound. As a result, obvious peaks are observed on C_H–T curves near transition temperatures.

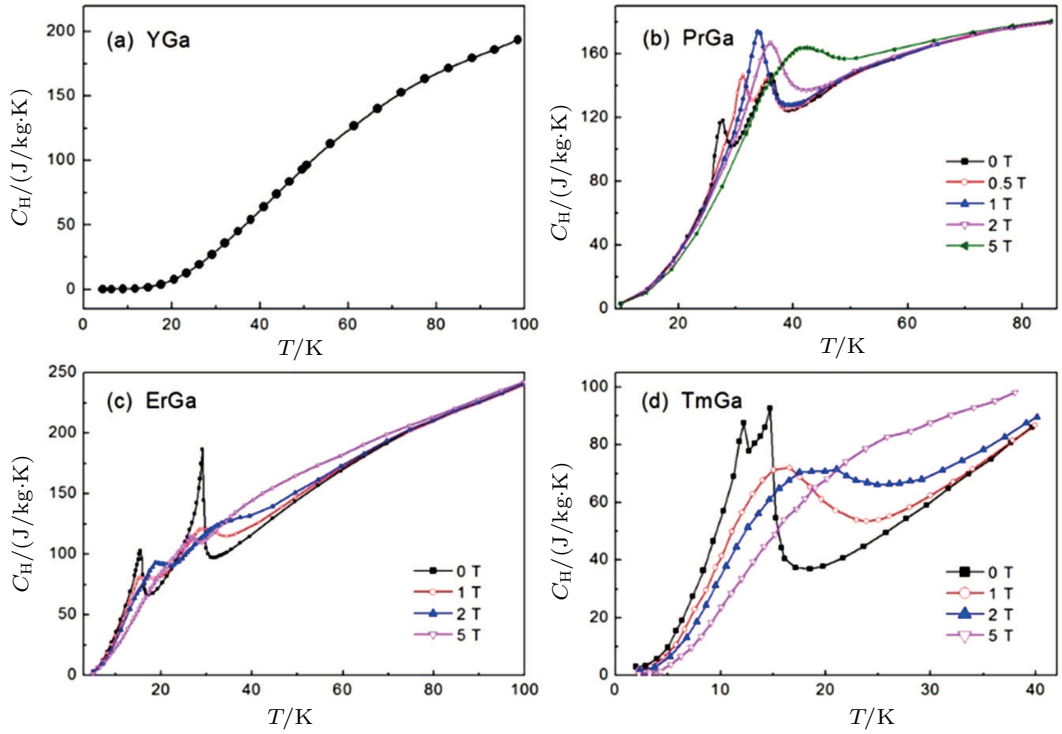

Fig. 12. (color online) (a) The temperature dependence of heat capacity for YGa compound at zero-field. (b) The temperature dependence of heat capacity for PrGa compound at a field of 0 T, 0.5 T, 1 T, 2 T, and 5 T, respectively. (c) The temperature dependence of heat capacity for ErGa compound at a field of 0 T, 1 T, 2 T, and 5 T, respectively. (d) The temperature dependence of heat capacity for TmGa compound at a field of 0 T, 1 T, 2 T, and 5 T, respectively.[19,33,39]

According to the magnetic and heat capacity measurements, ErGa compound undergoes an SR transition and an FM to PM transition as temperature increases.[19] And the SR transition has been confirmed by ^{119}Sn Mössbauer spectroscopy study.[20] Two magnetic transitions are also observed according to magnetic and heat capacity measurements for PrGa compound.[41] However, the no SR transition is observed according to ^{119}Sn Mössbauer spectroscopy experiment.[20] So it is still not clear that what kind of magnetic transition it is at $T_{\rm t}$ and whether the ground state at the temperature range between $T_{\rm t}$ and $T_{\rm C}$ is AFM. High resolution neutron powder diffraction (NPD) is a good way to study the magnetic properties. The magnetic structure of PrGa comound at 4.5 K has been determined in the above section. Then the change of magnetic structure as temperature increasing and magnetic transition of PrGa compound can also be studied by NPD method. All the magnetic structures at different temperatures were solved out. The detailed results including crystal lattice parameters, ordered magnetic moments and errors of refinement are listed in Table 2. The temperature dependence of the ordered magnetic moment and the sketch of the magnetic structures are shown in Fig. 13. As temperature increases, the magnetic moment shows a sudden decrease around $T_{\rm t} \sim 28$ K, whereas the direction of the ordered magnetic moment remains the same. That

is to say, the only change of magnetic structure at T_t is the variation of angle of cone. At $T_C \sim 38$ K the ordered magnetic moment decreases to zero, which indicates an FM to PM transition. Therefore we can conclude that PrGa compound undergoes an FM to FM magnetic transition at T_t and an FM to PM transition at T_C as temperature increases. According to the results of Mössbauer spectroscopy experiments, a magnetic spin reorientation transition from *bc* plane toward the *a* axis with decreasing temperature was observed for NdGa, SmGa, HoGa, and ErGa compounds.[18] But for PrGa compound, there is no such reorientation of the ordered magnetic moments around T_t, though the crystal structure of PrGa compound is almost the same as other *R*Ga compounds. Furthermore, lattice parameters *a*, *b*, and *c* change as temperature increases, but only *c* shows an obvious response to both the FM to FM transition and the FM to PM transition, because the change of magnetic structure at transition temperatures occurs mainly along the *c* axis.

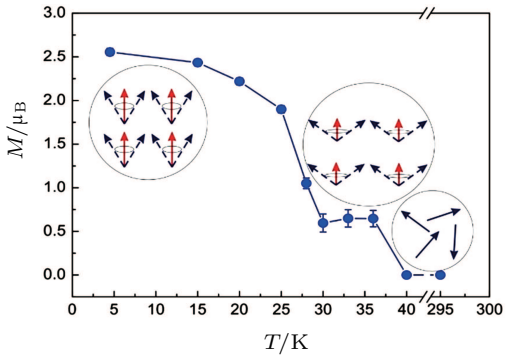

Fig. 13. (color online) Temperature dependence of the ordered magnetic moment obtained from the powder neutron diffraction experiment. The ordered magnetic moments are along the crystallographic *z* axis. M_z and M_{eff} are represented in red and blue arrows, respectively.[33]

Table 2. Refined structural parameters of PrGa compound. Space group *Cmcm*, Atomic positions: Pr (0, *y*, 0.25); Ga (0, *y*, 0.25). *a*, *b*, *c*, and *V* are lattice constant and volume of unit cell. *M*, M_x, M_y, and M_z are the total ordered magnetic moment and the individual component of moment along *a*, *b*, and *c* axes, respectively. ϕ and θ are the angle between the ordered magnetic moment and *x*, *z* axes, respectively. [34]

Atoms	Parameters	4.5 K	15 K	20 K	25 K	28 K	30 K	33 K	36 K	40 K	295 K
	a/Å	4.4545(3)	4.4545(3)	4.4545(3)	4.4538(3)	4.4533(3)	4.4522(3)	4.4515(4)	4.4506(3)	4.4504(4)	4.4494(4)
	b/Å	11.2533(9)	11.2530(9)	11.2527(9)	11.2547(9)	11.259(1)	11.261(1)	11.264(1)	11.265(1)	11.267(1)	11.312(1)
	c/Å	4.1878(3)	4.1880(3)	4.1877(3)	4.1875(3)	4.1865(3)	4.1860(3)	4.1861(3)	4.1862(3)	4.1857(3)	4.1953(4)
	V/Å^3	209.93(4)	209.93(4)	209.91(4)	209.90(4)	209.91(4)	209.87(4)	209.90(5)	209.88(4)	209.89(5)	211.15(5)
Pr	*y*	0.1416(2)	0.1419(2)	0.1418(2)	0.1421(2)	0.1420(2)	0.1425(3)	0.1424(3)	0.1426(3)	0.1429(3)	0.1441(3)
	$(M_x/M_y)/\mu_B$	0	0	0	0	0	0	0	0	0	0
	$(M_z/M)/\mu_B$	2.56(4)	2.43(4)	2.22(4)	1.90(4)	1.05(6)	0.6(1)	0.6(1)	0.65(9)	0	0
	$(\phi/\theta)/(^\circ)$	0	0	0	0	0	0	0	0	0	0
Ga	*y*	0.4301(2)	0.4301(2)	0.4305(2)	0.4302(2)	0.4303(2)	0.4304(2)	0.4306(2)	0.4304(2)	0.4306(2)	0.4304(2)
	R_p/%	6.15	6.01	6.08	5.95	6.08	5.77	6.01	6.07	6.12	5.85
	w_{Rp}/%	7.49	7.26	7.35	7.24	7.44	7.09	7.39	7.29	7.29	7.08
	χ^2	1.363	1.274	1.300	1.281	1.292	1.276	1.313	1.224	1.246	1.458

2.3. The magnetocaloric effects of *R*Ga compounds

The magnetic entropy change of *R*Ga (R = Gd, Tb, Dy, Ho, Er, Tm) compounds was calculated from magnetization isotherms by using the Maxwell relation $\Delta S_M = -\int_0^H (\partial M/\partial T)\mathrm{d}H$. The $-\Delta S_M$ curves calculated from isothermal magnetizations for a field change of 0 T–2 T and 0 T–5 T are presented in Figs. 14(a) and 14(b), respectively. The insets of Fig. 14 are the enlarged view of the curves. Two peaks are found to be centered at T_{SR} and T_C for the *R*Ga (R = Gd, Tb, Dy, Ho, Er) compounds. The two peaks are corresponding to the SR transition and PM to FM transition. The peaks around T_{SR} for TbGa, DyGa, HoGa, and ErGa compounds can be detected clearly in magnetic measurements. Although there are also two magnetic transitions as temperature increases for TmGa compound, only one peak can be observed on the $-\Delta S_M$ curve. The maximal values of $-\Delta S_M$ with a field change of 0 T–5 T for *R*Ga (R = Gd, Tb, Dy, Ho, Er, Tm) compounds are calculated to be 5.3 J/kg·K, 8.3 J/kg·K, 5.8 J/kg·K, 17.1 J/kg·K, 21.3 J/kg·K, and 34.3 J/kg·K, respectively. The refrigerant temperature width is calculated to be 159.4 K, 155.5 K, 112.7 K, 83 K, 30.9 K, and 14.2 K, respectively. The *RC* is 616.1 J/kg, 620.6 J/kg, 381.9 J/kg, 455J /kg, 494 J/kg, and 359.7 J/kg, respectively. All of the MCE parameters with a field change of 0 T–2 T and 0 T–5 T are listed in Table 1. It can be seen that for some compounds the two peaks are far from each other, and for some compounds the two peaks are close to each other. The two magnetic transitions are so near that only one peak can be seen for TmGa compound. Also it is found that the peak value around T_{SR} is comparable to that around T_C for ErGa compound. Figure 15 shows the ΔS_M curves of all the $Gd_xEr_{1-x}Ga$ ($0 \le x \le 1$) compounds for a field change of 0 T–2 T and 0 T–5 T, respectively. Each curve has two peaks, though the peak near T_{SR} is not obvious enough for GdGa. The location of the two peaks is corresponding to T_{SR} or T_t and T_C, respectively. It indicates that both SR transition and PM to FM transition contribute to MCE. As the content of Gd increases, the position of the peak near T_{SR} or T_t changes not much, but the peak near T_C moves to higher temperature obviously. As the content of Gd increases, the value of $|\Delta S_M|$ near T_{SR} or T_t decreases from 16.5 J/kg·K to 3.0 J/kg·K and the value of $|\Delta S_M|$ near T_C decreases from 21.3 J/kg·K to 5.3 J/kg·K. Oesterreicher and Parker[47] have proposed the re-

lationship between $|\Delta S_M|$ near T_C and other magnetic parameters as follows: $\Delta S_M = -1.07R(g_J \mu_B JH/k_B T_C)^{2/3}$. Where R is universal gas constant, g_J is Lande factor, μ_B is Bohr magneton, J is the total angular quantum number, H is external magnetic field, k_B is Boltzmann constant, and T_C is Curie temperature. For $Gd_xEr_{1-x}Ga$ ($0 \le x \le 1$) compounds, the value of J decreases and the value of T_C increases with the content of Gd increasing, so the $|\Delta S_M|$ near T_C shows downtrend. For $Gd_{0.3}Er_{0.7}Ga$ and $Gd_{0.4}Er_{0.6}Ga$, the value of ΔS_M is positive below T_t (inset of Fig. 15), and that is because the magnetic ground state in low temperature zone is AFM. And positive ΔS_M is always observed in that case, which is due to the disordered magnetic sub-lattice antiparallel to the applied magnetic field.[48,49]

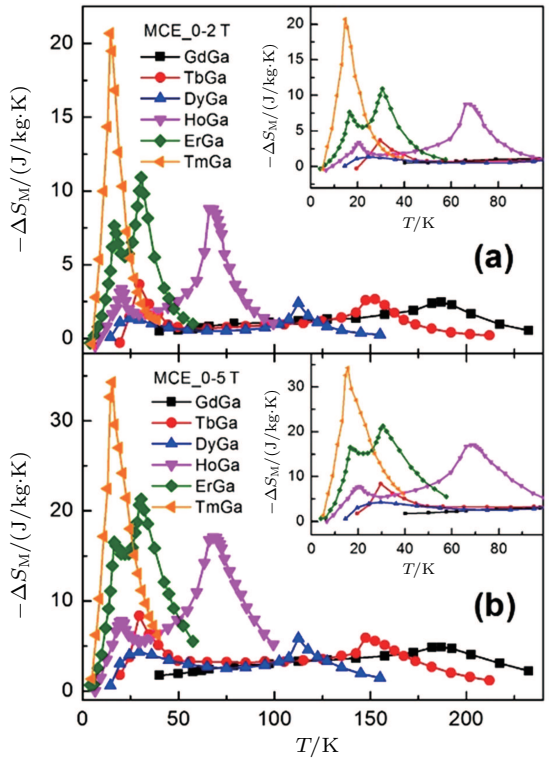

Fig. 14. (color online) (a) The temperature dependence of magnetic entropy with a field change of 0 T–2 T for RGa (R = Gd, Tb, Dy, Ho, Er, Tm) compounds respectively. The inset is the enlarged view of the curves in low temperature range. (b) The temperature dependence of magnetic entropy with a field change of 0 T–5 T for RGa (R = Gd, Tb, Dy, Ho, Er, Tm) compounds respectively. The inset is the enlarged view of the curves in low temperature range.[46]

The value of ΔS_M can be calculated from magnetization data according to the Maxwell relation and from heat capacity data. The ΔS_M–T curves for PrGa, ErGa, and TmGa compounds obtained from the two methods are shown in Fig. 16(a), Fig. 16(b), and Fig. 16(c), respectively. Before we give the details of calculating the ΔS_M of PrGa compound from heat capacity data, we need to review the standard methods to extract ΔS_M from C_H data. Take the $\Delta S_{M,0-5\ T}$ for example, we need three steps to achieve the result:[48]

The first step is to obtain the total entropy at zero-field

$$S(T)_{0\ T} = S(0\ K)_{0\ T} + \int_{0\ K}^{T} \frac{C_{0\ T}}{T} dT. \quad (7)$$

Second step is to have the total entropy at $H = 5$ T

$$S(T)_{5\ T} = S(0\ K)_{5\ T} + \int_{0\ K}^{T} \frac{C_{5\ T}}{T} dT. \quad (8)$$

The last step is to make the difference, that is, $\Delta S_{M,0-5\ T} = S(T)_{5\ T} - S(T)_{0\ T}$ on the assumption that

$$S_M(0\ K)_{0-5\ T} = S(0\ K)_{0\ T} - S(0\ K)_{5\ T} = 0.$$

And the final expression is as follows:

$$\Delta S_M(T)_{0-5\ T} = \int_{0\ K}^{T} \frac{C_{5\ T} - C_{0\ T}}{T} dT. \quad (9)$$

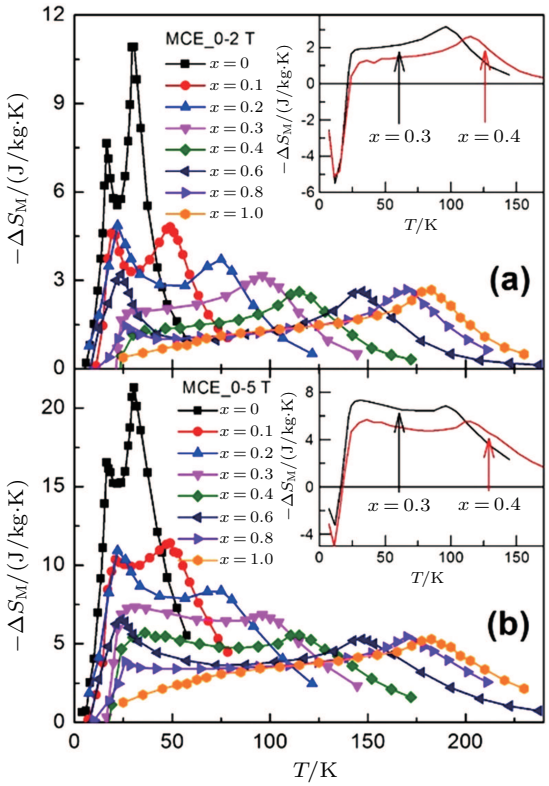

Fig. 15. (color online) (a) The temperature dependence of magnetic entropy with a field change of 0 T–2 T for $Gd_xEr_{1-x}Ga$ ($0 \le x \le 1$) compounds respectively. The inset is the whole curves for $Gd_{0.3}Er_{0.7}Ga$ and $Gd_{0.4}Er_{0.6}Ga$ compounds. (b) The temperature dependence of magnetic entropy with a field change of 0 T–5 T for $Gd_xEr_{1-x}Ga$ ($0 \le x \le 1$) compounds respectively. The inset is the whole curves for $Gd_{0.3}Er_{0.7}Ga$ and $Gd_{0.4}Er_{0.6}Ga$ compounds.[34]

However, heat capacity needs be measured at extremely low temperature, so now the question is whether we may use the above standard method. Considering the fact that the starting temperature of heat capacity measurement for PrGa compound is 10 K and the magnetic structure is complex in low temperature range, the standard method to calculate ΔS_M from C_H data will not hold true in this case anymore. In fact, the problem can be solved as long as we make some modifications to this method. The key point of modification is to replace the reference temperature of 0 K with 72.5 K.[41] In this case, the value of is not zero, but we can acquire its value from the calculations of M–H data. The reason why we choose 72.5 K as the reference temperature is that the magnetic ground state

and magnetic transition are clearly known here far from T_C. And we can see that the curves obtained from the two methods are consistent well with each other above 25 K. Large deviation below 25 K may result from the complex magnetic structure and magnetic transition in PrGa compound.[41] The temperature dependences of ΔS_M for ErGa and TmGa compounds calculated from magnetizations and heat capacity data for field changes of 0–2 and 0 T–5 T are shown in Fig. 16(b) and Fig. 16(c), respectively. The results obtained by using the two techniques are in good agreement with each other.

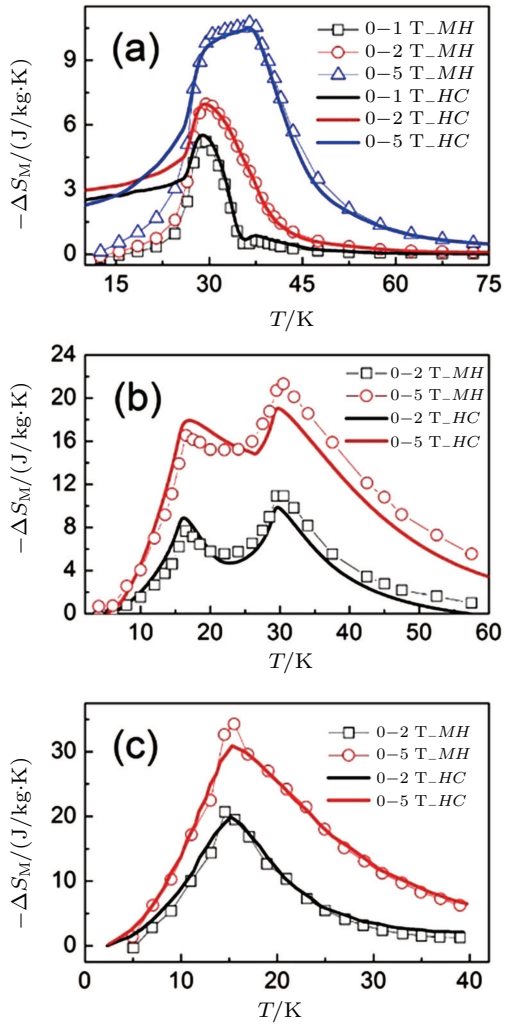

Fig. 16. (color online) (a) Magnetic entropy change curves obtained from heat capacity measurement (solid lines) and magnetic property measurement (empty symbols). (b) Temperature dependences of magnetic entropy change ΔS_M calculated from magnetizations and heat capacity data for field changes of 0 T–2 T and 0 T–5 T, respectively. (c) Temperature dependences of magnetic entropy change in TmGa for different magnetic field changes.[19,39,41]

As another important parameter to evaluate the MCE of magnetocaloric materials, the adiabatic temperature change ΔT was calculated from the C_P versus T curves by using the method suggested by Pecharsky and Gschneidner,[50] and it is summarized below. Firstly, $S(T)_{0\ T}$ is obtained according to formula (7) and $S(72.5\ K)_{0\ T}$ is set to be zero. Secondly, $S(T)_{5\ T}$ is obtained from $S(T)_{0\ T}$ and $\Delta S_{M,0-5\ T}$, which is calculated from M–H data. Thirdly, we can obtain the curves of $T(S)_{0\ T}$ and $T(S)_{5\ T}$, which are the inverse functions of $S(T)_{0\ T}$ and $S(T)_{5\ T}$ respectively. Finally, we make a difference according to the formula $T(S)_{5\ T}$–$T(S)_{0\ T}$ and then the ΔT–T curves are obtained.

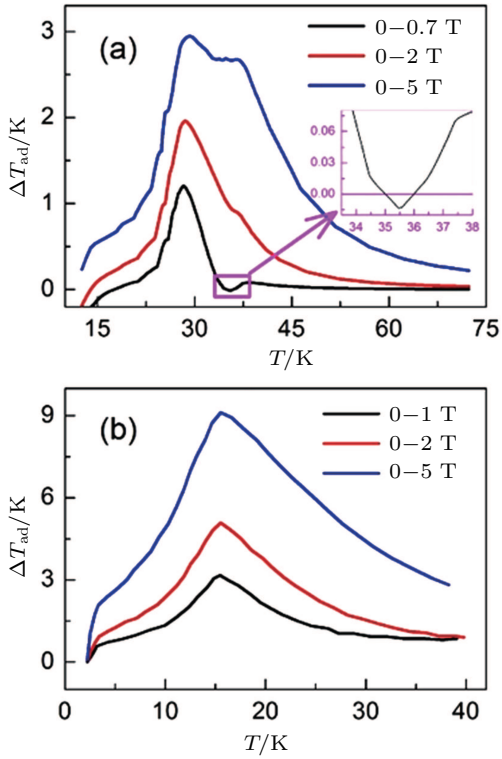

Fig. 17. (color online) (a) Temperature dependence of adiabatic temperature change ΔT_{ad} for PrGa compound under a field change of 0 T–0.7 T, 0 T–2 T and 0-5 T, respectively. The inset is the enlarged view of the curve for 0 T–0.7 T. (b) Temperature dependence of adiabatic temperature change ΔT_{ad} for TmGa compound under a field change of 0 T–1 T, 0 T–2 T and 0 T–5 T, respectively.[39,41]

The ΔT curves of PrGa compound for a field change of 0 T–0.7 T, 0 T–2 T, and 0 T–5 T are shown in Fig. 17(a) and the inset is the enlarge view of the curves. As two most important parameters to characterize MCE, ΔT and ΔS_M curves show similar change rules. When the magnetic field change is small such as 0.7 T, two peaks are observed on the curves near T_t and T_C respectively. That is to say, both the FM to FM transition and the PM to FM transition contribute to MCE. We can also see that the peak near T_t is much higher than that near T_C. That is because the FM to FM transition is of first order and accompanied by volume transition, which always plays an important role in enhancing MCE.[51,52] With the field change increasing, the peak in lower temperature zone shifts towards higher temperature region. That is because the temperature zone where the FM to FM transition occurs extends. When the field change is high enough such as 5 T, the two peaks are merged together and a wide platform is observed on the curve from 29.5 K to 37.5 K. This kind of material with nearly constant ΔT and ΔS_M in a wide temperature range has many practical applications, because people can use as few materials as possible in the limited space of magnetic refrigerator to realize refrigeration. The magnetic property and MCE of PrGa are very similar to those of $LaFe_{11.44}Al_{1.56}$.[44] Some other *R*Ga compounds have the same crystal structures as PrGa compounds,

but no platforms are found on their ΔS_M–T curves.[19,29,32] The main difference is that the transition temperature does not shift toward higher zone obviously with applied field increasing for other *R*Ga compounds. Though the maximum value of ΔS_M and ΔT for PrGa is not large enough ($(\Delta S_M)_{max}$ is 10.7 J/kg·K and $(\Delta T)_{max}$ is 2.9 K for a field change of 5 T), the feature of nearly constant ΔS_M and ΔT is valuable for researches compared with other *R*Ga compounds.[41] Anyway, the future work is still necessary to improve the maximum value of ΔS_M and keep the platform on the curves at the same time. Positive ΔS_M value and negative ΔT value are observed around 35.5 K for the field changes of 0.7 T, and similar results have been reported more than once.[48,49] The maximum values of ΔT for TmGa compound are 3.2, 5, and 9.1 K for the field change of 1, 2, and 5 T, respectively (Fig. 17(b)). The MCE of TmGa, especially under the low magnetic field change, is comparable with or even larger than those of other magnetocaloric materials around the liquid hydrogen temperature. Therefore, TmGa compound appears to be a very attractive candidate material for use in a magnetic refrigerator working in low temperature.

To evaluate the applicability of *R*Ga compounds as magnetic refrigerant materials in a reasonable way, we have estimated the RC by using the approach suggested by Gschneidner *et al*.[53] The *RC* is defined as $RC = \int_{T_1}^{T_2} |\Delta S_M| \, dT$, where T_1 and T_2 are the temperatures corresponding to both sides of the half maximum value of $-\Delta S_M$ peak, respectively. Calculations show that the maximal value of *RC* is 158.7, 616.1, 620.6, 381.9, 455, 494, 359.7 J/kg with a magnetic field change of 0 T–5 T for *R*Ga (*R* = Pr, Gd, Tb, Dy, Ho, Er, Tm) compounds, respectively. Especially, the value of *RC* for TbGa is found to be 900 J/kg with $T_1 = 22.7$ K (temperature of the cold end) and $T_2 = 183$ K (temperature of the hot end) for a field change of 0 T–7 T.[32] Although the TbGa compound has a moderate ΔS_M, its *RC* value is much larger than those of other magnetic refrigerant materials in a wide temperature range. The large *RC* of TbGa originates from the combined contribution from SR and FM–PM transitions, which enlarges the temperature span of the MCE. It is noted that the value of ΔS_M for *R*Ga increases monotonically with the decrease of T_C as the *R* atomic number increases. The results indicate that the working temperature and temperature span of the MCE could be tuned by the substitution between different *R* elements. All the magnetic parameters and MCE results of $Gd_xEr_{1-x}Ga$ ($0 \le x \le 1$) compounds are also listed in Table 1. We can see that though the maximum value of $|\Delta S_M|$ decreases with the content of Gd increasing, the value of *RC* is greatly improved compared with ErGa. Also we find that the T_{width} greatly extends as the content of Gd increases. Since both transitions (PM to FM transition and SR transition) contribute to MCE, there is a positive correlation between T_C–T_{SR} and T_2–T_1. According to the discussions on transition temperatures, T_C increases much faster than T_{SR} with Gd-content increasing; therefore, the increasing of Gd-content enhances T_{width}. And the extending of T_{width} plays an important role in improving the value of *RC* according to the calculation method. The exact value of *RC* fluctuates with the content of Gd increasing, but $Gd_{0.2}Er_{0.8}Ga$ and $Gd_{0.3}Er_{0.7}Ga$ compounds show better performances than others in this series by considering both ΔS_M and *RC*. Another important result is that table-like ΔS_M curves are observed for certain compounds, such as those in the case of $x = 0.1$, 0.2, 0.3, and 0.4. This kind of ΔS_M curves has been observed several times and such a feature of ΔS_M curves is very useful for practical applications of refrigeration.[54,55]

2.4. The physical mechanism of magnetic field controlled magnetocaloric effect and magnetoresistance in PrGa compound

As we mentioned before, the isothermal magnetization curves showed a typical AFM-like characteristics in the temperature range between T_t and T_C. However, neutron diffraction results show that PrGa compound is an FM-ordered state in this temperature zone. We take the representative isothermal magnetization curve at 32 K to reinterpret the magnetizing process in PrGa compound. The isothermal magnetization curve at 32 K is quoted and the magnetic structure sketches in different field zones have been plotted in Fig. 18.

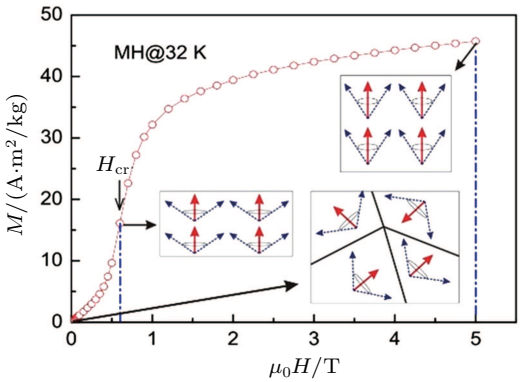

Fig. 18. (color online) Isothermal magnetization curve of PrGa compound at 32 K and the corresponding magnetic structure in every magnetizing stage. M_z and M_{eff} are symbolized in red and blue arrows, respectively. Domain walls under zero-field are represented by the black lines in the inset.[33]

The magnetizing process can be divided into two stages by the critical field (H_{cr}), which is determined by the maximum of dM/dH.[33] For PrGa compound, H_{cr} is the critical field where the metamagnetic transition begins and H_{cr} is calculated to be 0.6 T at 32 K. In the range of $H \le H_{cr}$, there are many magnetic domains with different FM-ordered directions, so the macroscopic magnetization is zero at the beginning. The magnetization increases gradually with increasing magnetic field. In this stage, magnetizing process is mainly achieved by means of domain-wall displacement. Inside of every magnetic domain, the projection of every magnetic moment on z axis does not really change. Since the ordered magnetic moment is rather small at 32 K (see Fig. 13), the magnetization changes slowly in this stage. In the range of $H > H_{cr}$, the domain-wall displacement reaches its limits. As magnetic field continues to increase, the magnetizing process is achieved by means of magnetic moment rotation. That is,

the direction of every magnetic moment tends to align with z axis gradually. The most remarkable difference between the above two stages is that the magnetizing process is irrelevant to the degree of magnetic order in the first stage, but it is closely related in the second stage.

The ΔS_M curves calculated from the Maxwell relation of PrGa compound with a field change of 0 T–0.3 T and 0 T–5 T are shown Fig. 19, respectively. Figure 19 also shows that only for a large field change can we observe the plateau. When $T < T_t$ or $T > T_C$, the value of $-\Delta S_M$ is relatively small no matter the field change is large or small. The temperature range between T_t and T_C is the most important zone for the formation of the plateau. Again we take 32 K data to interpret the cause of the plateau.[33] When the field change is 0 T–0.3 T, the magnetizing process is in the first stage. As we have mentioned before, magnetizing process is achieved by domain-wall displacement, and S_M hardly changes in this stage. The value of $-\Delta S_M$ is almost zero and no plateau is observed for a field change of 0 T–0.3 T. When the magnetic field exceeds H_{cr}, the magnetizing process steps into the second stage and all the magnetic moments begin to rotate toward z axis. ΔS_M changes significantly and thus a large ΔS_M value is observed for a field change of 0 T–5 T. It can be seen that the formation of a plateau is closely related to the magnetic structure, magnetic transition, and magnetizing process in PrGa compound.

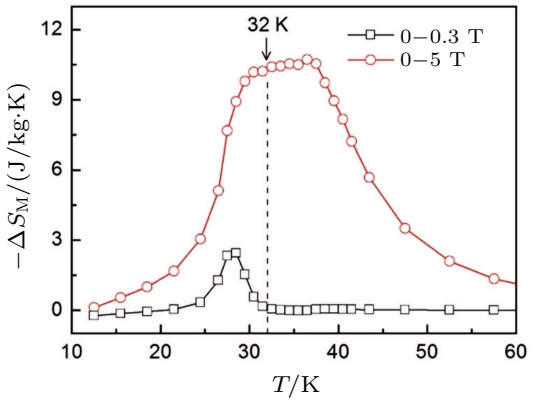

Fig. 19. (color online) The temperature dependence of magnetic entropy change curves for PrGa compound under a field change of 0 T–0.3 T and 0 T–5 T, respectively.[33]

The magnetic field dependence of MR at various temperatures has been measured and calculated (shown in Fig. 20). It is observed that the MR drops significantly with the increase of field when the magnetic field smaller than ~ 1 T around T_t, then retains a large value with the further increase of field. It is worth noting that the MR value is nearly as large as 30% at 28 K when a relatively small field (1 T) is applied, which is beneficial for the potential technology applications of the present sample. For the PrGa compound, the values of MR are found to be $\sim 34\%$ and $\sim 35\%$ at 28 K and 30 K in a magnetic field of 5 T, respectively. The maximal MR in PrGa is comparable to or much larger than those of some best known R-based intermetallic compounds, such as $SmMn_2Ge_2$ (8%),[56] $Ce(FeRu)_2$ (20%),[57] Gd_2In (29%),[58] $Gd_5(Si_2Ge_2)$ (26%),[59] and $Gd_5(Si_{1.8}Ge_{2.2})$ (20%).[60] Theoretical study based on the independent scattering mechanism shows that in metallic systems, the difference in resistivity owing to the magnetic structure modification. The electrical resistivity in magnetic materials includes residual resistivity (ρ_0), resistivity due to electron–electron scattering (ρ_E), resistivity due to electron–phonon scattering (ρ_L) and resistivity due to the electron–magnon interactions (ρ_M).[59] Among them, magnetic field mainly affects the ρ_M term. ρ_M increases with increasing S_M and reaches to its maximum value when the temperature exceeds T_C.[61] Since the FM-ordered magnetic component is along z axis, spin polarization of electrons exists. The component in the xy crystal plane is in the disordered state, therefore the electron motion within the xy plane is almost forbidden. The only motion path of electrons is thus along z axis, and the obstacle of the movement mainly comes from the disordered M_{xy}. Therefore, we assume that the resistance caused by the magnetic moments is proportional to the projected area of the circular cone in the xy crystal plane. The above assumption can be expressed in the following formula:[33]

$$\rho_M = \alpha \cdot M_{xy}^2. \tag{10}$$

Coefficient α is a constant.

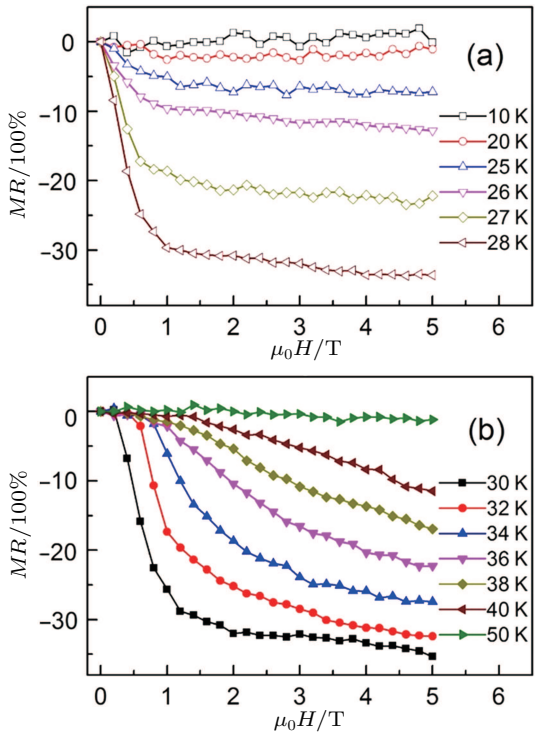

Fig. 20. (color online) (a) The field dependence of magnetoresistance up to 5 T for PrGa compound at the temperatures from 10 K to 28 K. (b) The field dependence of magnetoresistance up to 5 T for PrGa compound at the temperatures from 30 K to 50 K.[33]

Since MR mainly comes from magnetic contribution in PrGa compound, at the fixed temperature of T, the change of electrical resistivity with different magnetic fields can be written as follows:

$$\rho(H,T) - \rho(0,T) = \rho_M(H,T) - \rho_M(0,T). \tag{11}$$

At zero-field, the non-magnetic part of resistivity can be written as the multiple of the magnetic part, and then the total resistivity at zero-field can be written as follows:

$$\rho(0,T) = [1+\mu(T)]\cdot\rho_{\rm M}(0,T), \tag{12}$$

where $\mu(T)$ is a constant related to temperature. MR is usually written in the following formula:[61,62]

$$MR(H,T) = \frac{\rho(H,T)-\rho(0,T)}{\rho(0,T)}. \tag{13}$$

Put Eq. (11) and (12) into Eq. (13), we can get a new form of MR:

$$MR(H,T) = \beta(T)\left[\frac{\rho_{\rm M}(H,T)}{\rho_{\rm M}(0,T)}-1\right]. \tag{14}$$

It should be noted that $\mu(T)$ has been replaced by $\beta(T)$ on the basis of $\beta(T) = 1/[1+\mu(T)]$. Considering Eq. (6) and Eq. (9), we can get the following expression:[33]

$$MR(H,T) = \beta(T)\left[\frac{M_{\rm eff}^2 - M_z(H,T)^2}{M_{\rm eff}^2 - M_z(0,T)^2}-1\right]. \tag{15}$$

Then it is the key question to determine $M_z(H,T)$ and $M_z(0,T)$. $M_z(0,T)$ is the FM-ordered component of magnetic moments at zero magnetic field and it cannot be detected from the macroscopic magnetic measurement because of the existence of magnetic domains. While $M_z(0,T)$ can be determined accurately by NPD results at zero field. The deviation of $M_z(0,T)$ obtained from bulk compound and powder sample has been discussed. In order to study MR in bulk PrGa compound, we revised the $M_z(0,T)$ obtained from NPD experiment by taking M_z (0, 5 K) as a reference. The expression of $M_z(H,T)$ is very complex, because it is not only temperature-dependent but also field-dependent. The whole temperature range is divided into three parts by $T = 17$ K and $T = 38$ K:[33]

Case 1 $T < 17$ K

The magnetizing process is generally realized by domain-wall displacement and magnetic moment rotation sequentially as magnetic field increases. $M(H = 5\ {\rm T}, T)$ is a macroscopic physical quantity, and if $M(H = 5\ {\rm T}, T)$ is no more than $M_0(T)$, we can conclude that the magnetizing process is only in the first stage and M_z does not really change even though the magnetic field is as high as 5 T. There is almost no difference between $M_0(T)$ and $M(H = 5\ {\rm T}, T)$ in this temperature range. So, we have the following expression:

$$M_z(H,T) = M_0(T). \tag{16}$$

Cases 2 17 K$\leq T < 38$ K

In this temperature range, $M(H = 5\ {\rm T}, T)$ is considerably larger than $M_0(T)$, which indicates that the magnetizing process experiences both stages as magnetic field increases from 0 T to 5 T. Also it should be noted that $H_{\rm cr}$ is obtained in this temperature range. As we discussed on the magnetizing process at 32 K, $H_{\rm cr}$ is the field separatrix of the two magnetizing stages. And $M(H,T)$ can be considered as the measure of $M_z(H,T)$, when the magnetic field exceeds $H_{\rm cr}$. So $M_z(H,T)$ can be expressed in the following piecewise function:

$$M_z(H,T) = \begin{cases} M_0(T), & H \leq H_{\rm cr}, \\ M(H,T), & H > H_{\rm cr}. \end{cases} \tag{17}$$

Case 3 $T \geq 38$ K

In this temperature range, PrGa compound is in the PM state and every magnetic moment distributes randomly at zero field. When the magnetic field is applied, the macroscopic magnetization $M(H,T)$ is the ordered component of the magnetic moment along z axis. So, we have the following expression:

$$M_z(H,T) = M(H,T). \tag{18}$$

Putting Eqs. (16)–(18) into Eq. (15), we can obtain $MR(H,T)$. In order to simplify the expression of MR, we make the following variable transformation:

$$X \equiv M(H,T)/M_{\rm eff}, \tag{19}$$

$$X_0 \equiv M_0(T)/M_{\rm eff}, \tag{20}$$

$$X_{\rm cr} \equiv M(H_{\rm cr},T)/M_{\rm eff}. \tag{21}$$

Then, MR can be expressed below:

Case 1) $T < 17$ K

$$MR(X) = 0. \tag{22}$$

Case 2) 17 K$\leq T < 38$ K

$$MR(X) = \begin{cases} 0, & X \leq X_{\rm cr}, \\ \beta(T)\left[\dfrac{1-X^2}{1-X_0^2}-1\right], & X > X_{\rm cr}. \end{cases} \tag{23}$$

Case 3) $T \geq 38$ K

$$MR(X) = -\beta(T)X^2. \tag{24}$$

On one hand, $MR(X)$ can be calculated according to Eq. (22)–(24). On the other hand, the experimental results of $MR(X)$ can be calculated from $MR(H,T)$ and $M(H,T)$. The curves for X dependence of MR at $T = 15$ K, 20 K, 26 K, 27 K, 32 K, and 38 K were plotted in Fig. 21. The dotted lines are the calculated results and the scattered symbols are the experimental results. The experimental results are in good accordance with the calculated results in all three temperature zones. This indicates that the assumption about $\rho_{\rm M}$ expressed in Eq. (10) and the calculation of MR are reasonable. And also we can see that MR is indeed closely related magnetic structure, magnetic transition and magnetizing process in PrGa compound.

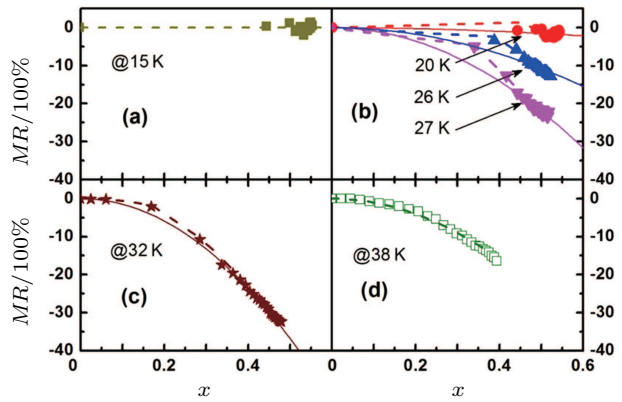

Fig. 21. (color online) Relationships between MR and X at $T = 15$ K, 20 K, 26 K, 27 K, 32 K, and 38 K, respectively. $X = M(H,T)/M_{\text{eff}}$. The scattered symbols are the experimental data. The dotted lines are the calculated results. The quadratic dependence of $MR = \beta(T)X^2$ was plotted in solid lines.[33]

Many works on MR in granular system have been reported, and it indicates that MR and X have the quadratic relationship $MR = -\beta(T)X^2$ in granular materials.[63–65] So it is necessary to discuss whether the quadratic relationship is still appropriate in bulk PrGa compound. From Eqs. (22)–(24) and Fig. 21, it is clear that the MR for $T < 17$ K does not obey the quadratic relationship and the result for $T \geq 38$ K matches the quadratic relationship strictly. The relationship of MR and X has more complex form in the temperature range between 17 K and 38 K according to Eq. (23). The MR results at $T = 20$ K, 26 K, 27 K, and 32 K shown in Fig. 21(b) and Fig. 21(c) are in this temperature range. To make it easy to compare, the function of $MR = -\beta(T)X^2$ is also plotted in Fig. 21(b) and Fig. 21(c) in solid line. It shows that the experimental result for $T = 32$ K can be considered to obey the quadratic relationship approximately. However, the experimental results for $T = 20$ K, 26 K, and 27 K show considerable deviations from the $MR = -\beta(T)X^2$ relation. In order to find out why the approximation is effective in Fig. 21(c) and why the approximation is ineffective in Fig. 21(b), we need to review the derivation formula of MR in the temperature range between 17 K and 38 K.[33] According to the second part of Eq. (23), if $M_0(T)$ can be approximated as zero, MR can be expressed as $MR = -\beta(T)X^2$. It shows that M_0(20 K), M_0(26 K), and M_0(27 K) are 1.7 μ_B, 1.3 μ_B, and 1.0 μ_B, respectively, while M_0(32 K) is only 0.5 μ_B which is relatively smaller than each of the above three. As an approximation, we treat M_0(32 K) as zero, and then obtain the quadratic relationship in the second part of Eq. (23). Further, if the X_{cr} at 32 K is neglected, MR(32 K) can be expressed as $MR = -\beta(T)X^2$ approximately. However, $M_0(T)$ at 20 K, 26 K, and 27 K is relatively large and it cannot be approximated as zero. Therefore, MR curves deviate noticeably from the quadratic relationship shown in Fig. 21(b).

3. *R*Ni compounds

The binary RNi (R = Y, Ce, Pr, Nd, Sm, Gd, Tb, Dy, Ho, Er, Tm) compounds have been fabricated and studied.[66] Results show that DyNi, HoNi, ErNi, TmNi, and YNi compounds crystallize in the FeB structure. But CeNi, PrNi, NdNi, SmNi, GdNi, and TbNi form in the CrB structure. YNi and CeNi compounds exhibit only Pauli paramagnetism according to magnetic measurement above 4.2 K. Other RNi compounds are all magnetic ordered. The Curie temperature is determined to be 22 K, 28 K, 45 K, 71 K, 52 K, 62 K, 37 K, 13 K, and 8 K for PrNi, NdNi, SmNi, GdNi, TbNi, DyNi, HoNi, ErNi, and TmNi, respectively. Nickel appears to be nonmagnetic in the RNi compounds and Curie–Weiss behavior is obeyed in the paramagnetic region for the RNi compounds except TmNi. The saturation moments obtained by extrapolating the measured magnetization to infinite field are less than that of free R ion moment for the RNi compounds except GdNi. This disagreement may be attributed to partial quenching of the orbital angular momentum of the R ion by the crystalline field generated by the surrounding ions although the possibility cannot be excluded that the low moments are merely due to strong magnetic anisotropy. A secondary magnetic transition is observed below Curie temperature for NdNi and HoNi compounds. And little short range exists past the magnetic transition for the RNi compounds.[66]

Neutron diffraction experiment was employed to study the magnetic structure and magnetic transition of single crystal HoNi compound.[67] The magnetic (102) and (201) peaks increase rapidly with decreasing temperature below 35 K, which indicates that there is a magnetic-disorder to magnetic-order transition around 35 K. The intensity of the (100) line is zero at 78 K and very strong at 20 and 4.2 K, indicating that there is a AFM z component exists at the temperature range. The intensity of (200) line increases rapidly below 15 K with decreasing temperature, indicating that there is a formation of y component around 15 K. The results of neutron diffraction confirmed the two magnetic transitions around 15 K and 35 K of HoNi compound. The magnetocaloric effect of PrNi compound has also been studied.[68] Powder x-ray diffraction shows that PrNi compound crystallizes in CrB-type orthorhombic structure. The heat capacity of PrNi was measured at the field of 0 T, 2 T, 5 T, 7.5 T, and 10 T, respectively. PrNi undergoes a second-order phase transition from an FM to PM state as temperature increases. The Curie temperature is determined to be 19 K according to the zero-field heat capacity data. The maximum MCE for PrNi is 4.2 K, which occurs at 19 K for a field change from 0 T to 10 T.[68] The magnetic structure of DyNi compound has also been studied by neutron diffraction technique.[69] From the magnetization measurements at 1.6 K, DyNi compound exhibits narrow domain walls frozen by the anisotropy.

The Pt–Ni substitution on the crystal structure and magnetic behavior of the $PrNi_{1-x}Pt_x$ pseudo-binary compounds has also been studied.[70] The orthorhombic CrB-type structure possessed by PrNi was found to remain conserved for Pt doped compounds. The unit cell volume (and consequently the interatomic distances) linearly increases with increasing

Pt concentration. The MCE was determined consistently from the specific heat and magnetization data. It has the same value in the boundary compounds PrNi and PrPt.[70] The effect of hydrogenation on the structure and magnetic properties of ErNi has also been investigated.[71] Results show that ErNi compound can form crystalline hydrides which remain in the structure of the original compound. There is little change in lattice parameter and magnetic properties of the crystalline hydrides to compare with original compound.[71] The drastic change of the magnetization due to the spin flopping was observed for both single crystal ErNi and DyNi compounds.[72] It has been confirmed that Pr–Pr and Gd–Gd exchange interactions are ferromagnetic, but Pr–Gd exchange interactions are antiferromagnetic in single crystal $Pr_{1-x}Gd_xNi$ compounds.[73] And the case is similar to the $Nd_{1-x}Gd_xNi$ and $Nd_{1-x}Tb_xNi$ system.[74,75]

In this section, we will review the magnetic properties and magnetocaloric effect of binary *R*Ni (R = Gd, Dy, Ho, Er) compounds and pseudo-binary (Ho,Er)Ni compounds. The data for GdNi and DyNi is cited from the work of Suresh *et al*.[77,78] The data for HoNi and ErNi is newly obtained in this work and at the same time we noted that some magnetic measurement has been carried out by Suresh *et al*.[77,78] The data for (Ho,Er)Ni compounds are all newly obtained.[76] The main research content is magnetic transition, magnetic structure, magnetocaloric effect and the main research method is magnetic measurement and powder neutron diffraction experiment.

3.1. The crystal structure and basic magnetic properties of *R*Ni (R = Gd, Dy, Ho, Er) compounds and $Ho_xEr_{1-x}Ni$ compounds

Binary *R*Ni (R = Gd, Dy, Ho, Er) compounds and pseudo-binary $Ho_xEr_{1-x}Ni$ ($0 \le x \le 1$) compounds were fabricated and powder x-ray diffraction was carried out to confirm the phase purity. The XRD patterns of $Ho_xEr_{1-x}Ni$ ($0 \le x \le 1$) compounds are shown in Fig. 22. The patterns of GdNi and DyNi are not shown literature.[77,78] All of the XRD patterns have been fitted and refined. All of the *R*Ni compounds is single phase without any impurity phases. The vertical bars on the bottom of Fig. 22 are Bragg positions. It can be seen that almost all of the peaks can be corresponding to the Bragg positions. Actually, results of refinement show that GdNi compound crystallize in the orthorhombic CrB-type structure (space group *Cmcm*, #63), which is the same with *R*Ga compounds. Both Gd and Ni atoms are in the same crystallographic $4(c)$ sites with the C_{2v} point symmetry.[22,23] While other *R*Ni compounds crystallize in the orthorhombic FeB type structure (space group *Pnma*, #62).[69,77,78] The unit cell of FeB-type crystal structure is shown in Fig. 23. Both *R* and Ni atoms occupy the 4*c* site of the unit cell. The structure is made up of trigonal prisms with *R* at the corners and Ni at the center.[77] The lattice parameters of GdNi are determined to be $a = 3.751 \pm 0.002$ Å, $b = 10.275 \pm 0.006$ Å, $c = 4.232 \pm 0.002$ Å. The lattice parameters of DyNi, HoNi, ErNi are $a = 7.023 \pm 0.001$ Å, 7.018±0.001 Å, 6.992±0.001 Å, $b = 4.173 \pm 0.001$ Å, 4.137±0.001 Å, 4.115±0.001 Å, $c = 5.439 \pm 0.001$ Å, 5.435±0.001 Å, 5.418±0.001 Å, respectively.[77,78] As the *R* atom number increases, the radius of *R* atom decreases. And as a result, the crystal parameters also show a decreasing tendency.

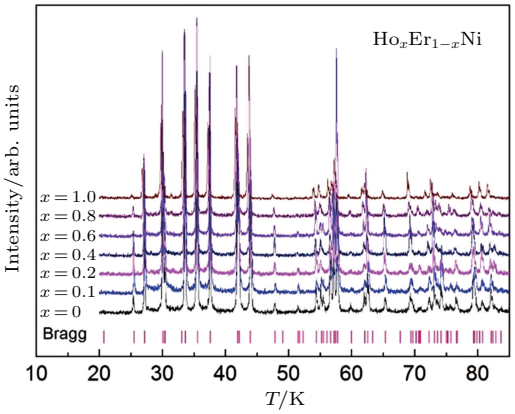

Fig. 22. (color online) The x-ray powder diffraction pattern of pseudo-binary $Ho_xEr_{1-x}Ni$ ($0 \le x \le 1$) compounds. The positions of the Bragg peaks are shown as vertical bars below the observed intensities.[76]

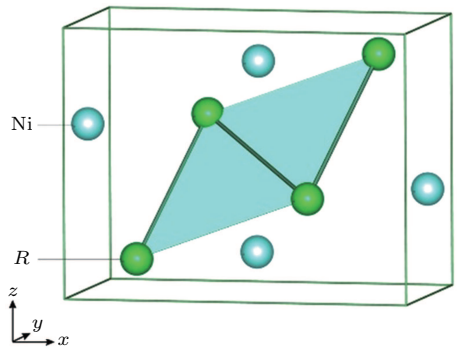

Fig. 23. (color online) The crystal structure and unit cell of *R*Ni compounds.

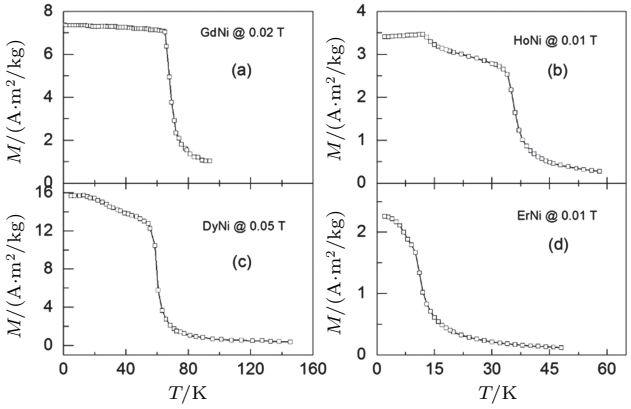

Fig. 24. (a) The temperature dependence of magnetization curve for GdNi compound at a field of 0.02 T. (b) The temperature dependence of magnetization curve for HoNi compound at a field of 0.01 T. (c) The temperature dependence of magnetization curve for DyNi compound at a field of 0.05 T. (d) The temperature dependence of magnetization curve for ErNi compound at a field of 0.01 T.[77,78]

The thermal magnetization curves of RNi (R = Gd, Dy, Ho, Er) compounds were measured and the field-cooling curves of GdNi, HoNi, DyNi, and ErNi are shown in Fig. 24(a), Fig. 24(b), Fig. 24(c), and Fig. 24(d), respectively.[77,78] As the temperature increases, the magnetization of GdNi compound shows a sudden decrease at $T_C = 69$ K, which is determined by the maximum of dM/dT. In the low temperature range, the magnetization of GdNi compound almost keeps a stable value. The above result is in accordance with previous work.[66] From the M–T curve, it can be concluded that GdNi is a simple FM material, and it undergoes an FM to PM transition as temperature increases around T_C. HoNi compound has been known as a multi-phase-transition material, and the magnetic transitions have been observed by magnetic measurements and neutron diffraction technique.[66,67] From Fig. 24(b), it can be seen that as temperature increases the magnetization undergoes drastic change twice at 13.5 K and 35.5 K, respectively. The two temperatures are corresponding to the SR transition and FM to PM transition respectively. The magnetic properties of DyNi and ErNi compounds have been studied before, and drastic change of the magnetization due to the spin flopping was observed for both ErNi and DyNi compounds.[72] The magnetic structure of DyNi compound is non-collinear, and the magnetization of DyNi compound shows several increase due to spin flopping with external field increase.[77] DyNi and ErNi compounds have been treated as simple FM materials in previous work, and only one FM to PM transition has been discussed for DyNi and ErNi compounds.[78] However, from Fig. 24(c) and Fig. 24(d), it is clearly shown that there are two drastic change of magnetization below T_C as temperature increases for DyNi and ErNi compounds, which indicates that SR transition may exist both for DyNi and ErNi compounds. The value of T_{SR} for DyNi and ErNi is determined to be 20 K and 6.5 K, respectively. The T_C for DyNi and ErNi is determined to be 59 K and 11 K, respectively.[77] All of the transition temperatures of RNi compounds (R = Gd, Dy, Ho, Er) are shown in Table 3. As the atom number increases, Curie temperature shows a decrease tendency. That is because the spin angular momentum quantum number (S) increases with atom number for heavy rare earth elements. And S is positively correlated with Curie temperatures of R-based compounds.

Table 3. The transition temperatures and magnetocaloric parameters of RNi (R = Gd, Dy, Ho, Er) compounds and $Ho_xEr_{1-x}Ni$ ($0 \le x \le 1$) compounds.

Materials	T_t/K	T_C/K	MCE_0–2 T			MCE_0–5 T			Ref.
			$-\Delta S_M(T)_{max}$/(J/kg·K)	T_{width}/K	RC/(J/kg)	$-\Delta S_M(T)_{max}$/(J/kg·K)	T_{width}/K	RC/(J/kg)	
GdNi	–	69	8.7	19.9	133.3	16.8	31.7	396.8	[78]
DyNi	20	59	9.7	20.6	150.5	18	31	429.8	[77]
HoNi	13.5	35.5	7.8	33.4	198.7	16.6	41.6	556.7	[76]
$Ho_{0.8}Er_{0.2}Ni$	11	32	7.5	32.7	179.8	16.1	40.1	487.3	[76]
$Ho_{0.6}Er_{0.4}Ni$	9	27	6.9	27.8	145.1	16.1	34.2	431.1	[76]
$Ho_{0.4}Er_{0.6}Ni$	4	20	10.4	16.3	148.8	20.7	26.3	418	[76]
$Ho_{0.3}Er_{0.7}Ni$	5	16.5	12.2	13.2	119.7	25.3	21.3	407.7	[76]
$Ho_{0.2}Er_{0.8}Ni$	6	13.5	15.2	9.3	128.4	28.3	18.2	392.3	[76]
$Ho_{0.1}Er_{0.9}Ni$	9	11	18	7	104.2	34	14.2	366.6	[76]
ErNi	7	11	14.2	10.7	122.4	29.6	15.6	350	[76]

The isothermal magnetization curves of HoNi compound were measured up to 5 T and the curves at 2 K, 12 K, 18 K, 24 K, 30 K, 36 K, 42 K, 48 K, and 55 K are shown in Fig. 25, respectively. For the M–H curve obtained below T_C, the magnetization increases as magnetic field increases, and reaches its saturation values quickly. That is the typical feature of FM materials. The two magnetic transitions HoNi compound undergoes as temperature increases have been confirmed by magnetic measurement and neutron diffraction technique. Then it can be concluded that the transition around T_{SR} is FM to FM transition, because the M–H curves obtained below and above T_{SR} are both FM type. The M–H curve at 36 K shows a nearly linear change feature, which is the characteristic of PM state. So it can be concluded that there is little short range FM order above T_C for HoNi compound.

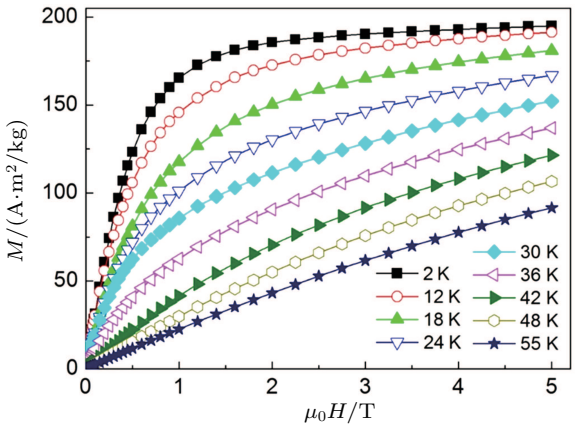

Fig. 25. (color online) The field dependence of magnetization curve for HoNi compound in the temperature range from 2 K to 55 K.

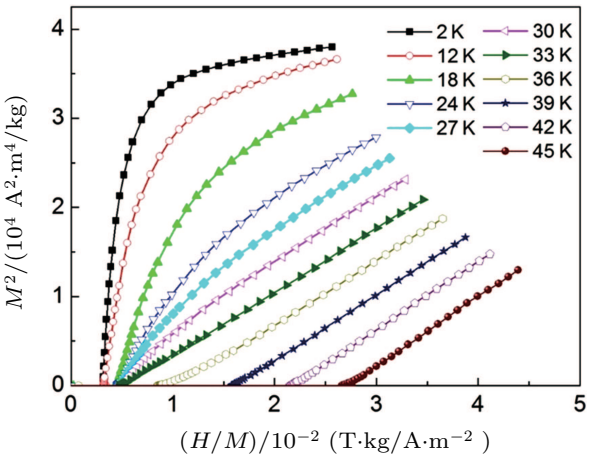

Fig. 26. (color online) The Arrott plots of HoNi compound in the temperature range from 2K to 45 K.

Arrott plot was obtained from the isothermal magnetization curves for HoNi compound and it is shown in Fig. 26. According to the Banerjee criterion a magnetic transition is expected to be of the first-order when the slope of Arrott plot is negative, whereas it will be of the second-order when the slope is positive.[42,79] From the Arrott plots in the temperature range from 2 K to 45 K, it can be seen that none of them show a negative slope. The positive slope of Arrott around T_{SR} and T_C indicates that the SR transition and FM to PM transition are both of second order. Generally to say, the magnetocaloric effect materials of second order are more valuable for actually use, because there are little magnetic hysteresis and heat hysteresis in the process of magnetic transition.[19]

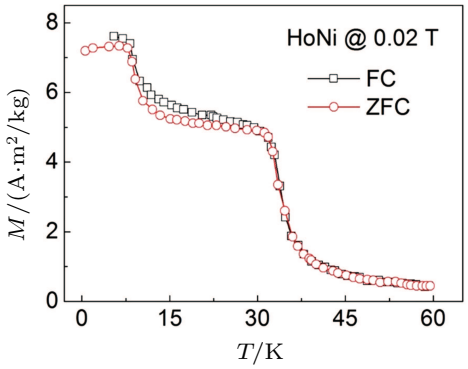

Fig. 27. (color online) The temperature dependence of zero-field-cooling magnetization and field-cooling magnetization curves for HoNi compound under a field of 0.02 T.

Figure 27 shows the ZFC and FC curves of HoNi compound at a field of 0.02 T. It is clearly that HoNi compound show good thermal reversibility both around T_{SR} and T_C. The results of ZFC and FC are in accordance with the results of Arrott plots. In addition, the ZFC and FC curves also clearly show that HoNi compound undergoes two magnetic transitions as temperature increases at $T = 13.5$ K and $T = 35.5$ K, respectively. The magnetic transition of HoNi will be discussed in detail in the following section.

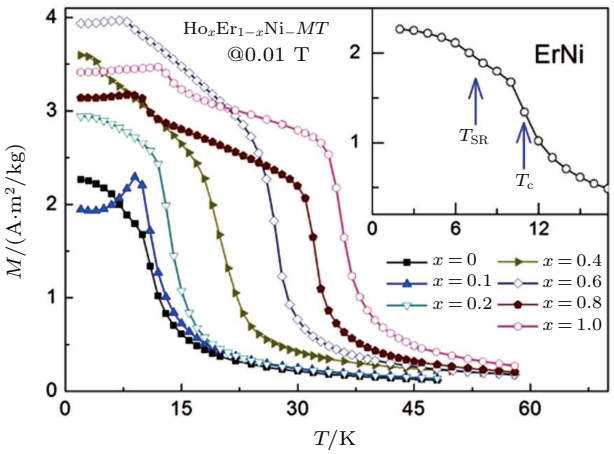

Fig. 28. (color online) The temperature dependence of magnetization curves for $\mathrm{Ho}_x\mathrm{Er}_{1-x}\mathrm{Ni}$ ($0 \le x \le 1$) compounds at a field of 0.01 T. The inset is the enlarged view of M–T curve for ErNi compound.[76]

In order to study the influence of Ho atom on the magnetic property of ErNi compound, $\mathrm{Ho}_x\mathrm{Er}_{1-x}\mathrm{Ni}$ ($0 \le x \le 1$) compounds were fabricated and the thermal magnetization curves at a field of 0.01 T were measured.[76] The M–T curves of $\mathrm{Ho}_x\mathrm{Er}_{1-x}\mathrm{Ni}$ ($0 \le x \le 1$) compounds are shown in Fig. 28. The inset of Fig. 28 is the enlarge view of M–T curve of ErNi compound. The magnetization undergoes a sharp decrease around T_C for all of the $\mathrm{Ho}_x\mathrm{Er}_{1-x}\mathrm{Ni}$ ($0 \le x \le 1$) compounds. And it is clear that there is also another significant decrease in low temperature range for $\mathrm{Ho}_x\mathrm{Er}_{1-x}\mathrm{Ni}$ ($0.4 \le x \le 1$) compounds, which indicates that these compounds undergo another magnetic transition in low temperature zone. Considering of the SR transition of HoNi, the above transitions are probably SR transition as well. Spin slopping was observed with field increasing for ErNi compound, but ErNi compound has been treated as a simple FM material in previous researches.[72,78] But from the enlarge view of M–T curve of ErNi compound, it can be seen that there is also another decrease of magnetization around $T = 7$ K, although the decrease is not so obvious. Actually, the decrease has been observed in work given by Kumar *et al.*[78] So it can be concluded that ErNi compound also under goes an SR transition and an FM to PM transition as temperature increases, which is the same case as HoNi compound. After the detailed study of the ZFC and FC, it found that $\mathrm{Ho}_{0.2}\mathrm{Er}_{0.8}\mathrm{Ni}$ compound also undergoes two magnetic transitions. But for $\mathrm{Ho}_{0.1}\mathrm{Er}_{0.9}\mathrm{Ni}$ compound, no drastic change of magnetization can be observed obviously except for the one at T_C. AC susceptibility measurements show that $\mathrm{Ho}_{0.1}\mathrm{Er}_{0.9}\mathrm{Ni}$ compound also undergoes an SR transition around 9 K.[76] All of the magnetic transition temperatures have been determined by the position of the peak on the $\mathrm{d}M/\mathrm{d}T$ curves. The transition temperatures are shown in Table 3. It can be seen that the Curie temperature increases from 11 K to 35.5 K as the

content of Ho atoms increases, showing a steadily increasing tendency. But the SR transition temperature only changes between 4 K and 13.5 K, which is relatively stable compared with T_C. That is because the Curie temperature is positively correlated with S, and the average S of $Ho_xEr_{1-x}Ni$ compound increases as the content of Ho increases. But for T_{SR}, it is affected by crystal field and crystal structure. Considering that the $Ho_xEr_{1-x}Ni$ compounds crystallize in the identify crystal structure, T_{SR} thus changes not so much for different content of Ho atoms. It can also be seen that 10% of Ho-substitution for Er atoms obviously shortens the temperature interval between SR transition and FM to PM transition. The isothermal magnetization curves up to 5 T at 2 K for $Ho_xEr_{1-x}Ni$ ($0 \le x \le 1$) compounds were also measured and have been shown in Fig. 29. All of the M–H curves show that the magnetization increases as magnetic field adding up and arrives at its stable value quickly, which is the typical feature of FM ground state. It indicates that the ground state of $Ho_xEr_{1-x}Ni$ ($0 \le x \le 1$) compounds in low temperature range is FM and it can be speculated that the SR transitions are FM to FM transition for $Ho_xEr_{1-x}Ni$ ($0 \le x \le 1$) compounds. The saturation magnetization for HoNi compound shows the largest value, because the total angular quantum number of HoNi compound is the largest. The saturation magnetizations for other $Ho_xEr_{1-x}Ni$ compounds show a confused order in value, which indicates the magnetizing process is affected by other factors, such as crystal field.

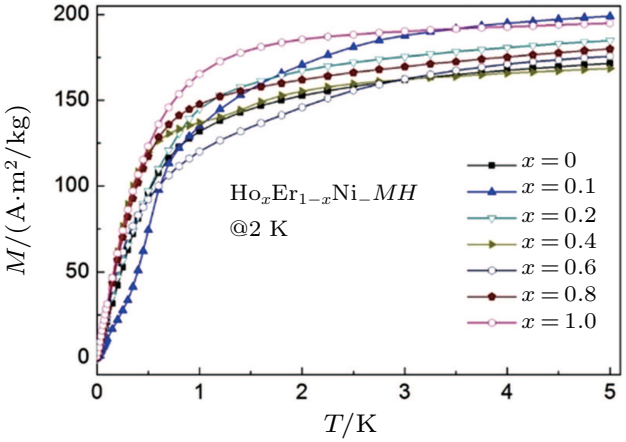

Fig. 29. (color online) The field dependence of magnetization curves up to 5 T at 2 K for $Ho_xEr_{1-x}Ni$ ($0 \le x \le 1$) compounds, respectively.

3.2. The magnetic structure and magnetic transitions of HoNi compound studied by neutron diffraction experiment

The magnetic transition of HoNi compound has been studied according to many kinds of experiments such as magnetic measurements and neutron diffraction technique.[66,67,78,80–82] It indicates that HoNi compound undergoes an SR transition and an FM to PM transition as temperature increases. The neutron diffraction studies show that the magnetic moments in HoNi have ferromagnetic components along the a axis and antiferromagnetic components along the c axis in the temperature range between T_{SR} and T_C.[67,78] Below T_{SR}, a change in symmetry has been observed due to the development of the ferromagnetic component along the b axis which grows with decreasing temperature.[78] From the behavior of the M–T curve of HoNi, the presence of a canted structure below T_{SR} can be inferred.[78] But the magnetic and magnetic transition of HoNi compound still needs to be studied further. In the following section the magnetic structure and magnetic transition of HoNi compound will be studied systemically by employing powder neutron diffraction experiments.[76]

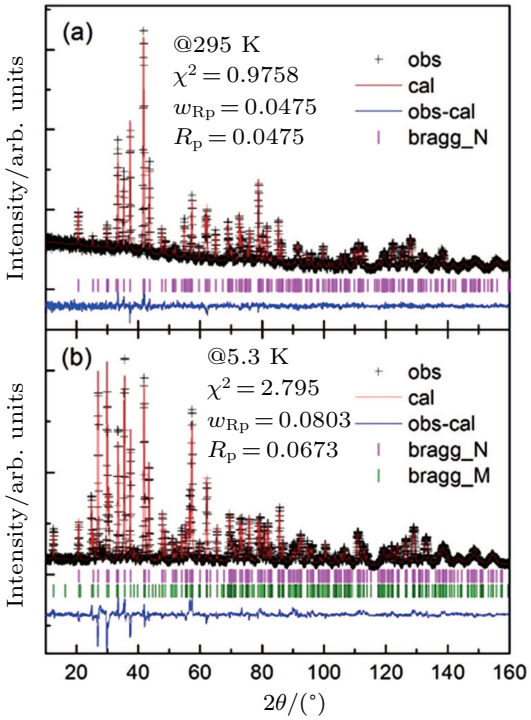

Fig. 30. (color online) The neutron powder diffraction pattern of HoNi at 295 K (a) and 5.3 K (b), respectively. The observed data and the calculated patterns are plotted in cross and solid line, respectively. The solid line at the bottom is the difference between the observed and calculated data. The Bragg positions for the nuclear and magnetic structure are marked as short vertical lines. Only nuclear model is considered in the refinement at 295 K and both nuclear model and magnetic model are considered in the refinement at 5.3 K.[76]

Firstly, the magnetic structure of HoNi compound at low temperature needs to be determined. And before determining the magnetic structure, the crystal structure was analyzed and determined. The powder neutron diffraction pattern of HoNi compound at 295K is shown in Fig. 30(a). The fitted lines, differences and Bragg positions are also shown there. Since the Curie temperature is around 35 K, HoNi compound is in PM state at 295 K. Thus only nuclear model is considered in the process of refining and fitting. All of the peaks

can be indexed to the FeB-type orthorhombic crystal structure (space group *pnam*, #62). The crystal structure has been shown in Fig. 23 and the related parameters are as follows: $a = 7.0162(2)$ Å, $b = 4.1405(1)$ Å, $c = 5.4359(1)$ Å, $\chi^2 = 0.9759$, $w_{Rp} = 0.0476$, $R_p = 0.0384$. The powder neutron diffraction pattern at 5.3 K is shown in Fig. 30(b). The fitted lines, differences and Bragg positions are also shown in the figure. At 5.3 K, HoNi compound is in FM-ordered magnetic state. Thus nuclear and magnetic structures are both considered. The Bragg positions for nuclear structure and magnetic structure are marked in Fig. 30(b), respectively. The related parameters are as follows: $a = 6.9765(1)$ Å, $b = 4.15480(3)$ Å, $c = 5.4004(1)$ Å, $\chi^2 = 2.795$, $w_{Rp} = 0.0803$, $R_p = 0.0673$. Results indicate that the only Ho atoms are magnetic ordered, and the Ni atoms contribute nothing to the magnetic moment. According to the refined magnetic structure at 5.3 K, Ho atoms are FM-ordered along *a* axis and *b* axis, and they are AFM-ordered along *c* axis. The component of ordered magnetic moment for *x*, *y*, *z* is determined to be 7.66(7) μ_B, 4.4(1) μ_B, and 3.80(5) μ_B, respectively. And the total ordered magnetic moment is calculated to be 9.63(8) μ_B, which is close to the effective moment of Ho^{3+} ion. It indicates that almost no magnetic component is quenched for Ho ion in HoNi compound. The magnetic structure of HoNi compound is presented in Fig. 31, where it is viewed from *b* axis. Since it is viewed from *b* axis, the *y* component of ordered magnetic moment cannot be plotted.

From Fig. 31 it can be seen that the Ho atoms are connected in the form of six-member ring and the Ni atoms are in the center of the six-member ring. Half of the Ho atoms point to one direction with a positive *x* component and a positive *z* component, and the other half of Ho atoms point to another direction with a positive *x* component and negative *z* component. The *x* component is the same for all the Ho atoms, which indicates that Ho atoms are FM ordered in HoNi compound. The absolute value of *z* component of all the Ho atoms is also uniform, which means that AFM order of Ho atoms exists in HoNi compound. Just as what has been mentioned before, there is also an FM order of Ho atoms along *b* axis in HoNi compound, which cannot be presented in Fig. 31.

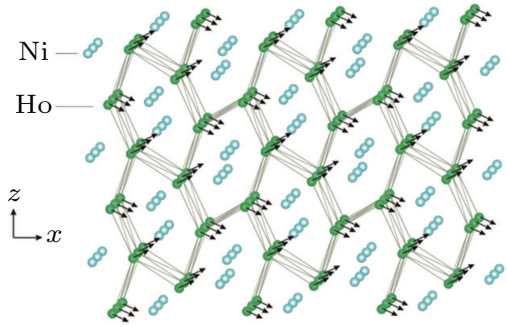

Fig. 31. (color online) The magnetic structure of HoNi compound viewed from the crystal *y* direction. The black arrows are corresponding to the ordered magnetic moments of Ho atoms.

Secondly, the neutron powder diffraction patterns at different temperatures were also obtained and the magnetic structures at different temperatures were determined according to the refinement and fitting. The specific parameters of crystal structure, ordered magnetic moments, and error information are all listed in Table 4.

Table 4. (a) Refined structural parameters of HoNi compound. Space group *Pnma*, Atomic positions: Ho (*x*, 0.25, *z*); Ni (*x*, 0.25, *z*). *a*, *b*, *c*, and *V* are lattice constant and volume of unit cell. *M*, M_x, M_y, and M_z are the total ordered magnetic moment and the individual component of moment along *a*, *b*, and *c* axes, respectively. ϕ and θ are the angle between the ordered magnetic moment and *x*, *z* axes, respectively.

Atoms	Parameters	5.3 K	8 K	10 K	12 K	13 K	15 K	20 K	25 K
	a/Å	6.9765(1)	6.9763(2)	6.9765(2)	6.9768(2)	6.9765(2)	6.9769(2)	6.9764(1)	6.9766(2)
	b/Å	4.15480(3)	4.15477(4)	4.15481(3)	4.15486(4)	4.15482(4)	4.15490(4)	4.15478(3)	4.15482(4)
	c/Å	5.4004(1)	5.4008(1)	5.4007(1)	5.4010(2)	5.4010(2)	5.4015(2)	5.4016(1)	5.4019(2)
	V/Å^3	156.534(5)	156.542(6)	156.545(5)	156.562(6)	156.556(6)	156.582(6)	156.566(5)	156.582(6)
Ho	*x*	0.1820(3)	0.1816(3)	0.1817(3)	0.1813(4)	0.1818(3)	0.1812(3)	0.1814(3)	0.1808(4)
	z	0.1313(6)	0.1327(7)	0.1327(6)	0.1332(7)	0.1318(7)	0.1307(8)	0.1332(6)	0.1336(7)
	M_x/μ_B	7.66(7)	7.63(8)	7.73(6)	7.58(7)	7.57(8)	7.42(7)	6.98(5)	5.93(7)
	M_y/μ_B	4.4(1)	3.9(1)	2.7(1)	1.5(3)	1.9(2)	1.3(3)	0	0
	M_z/μ_B	–3.80(5)	–3.74(6)	–3.69(5)	–3.70(6)	–3.73(6)	–3.65(6)	–3.39(4)	–3.06(6)
	M/μ_B	9.63(8)	9.34(9)	8.99(7)	8.57(9)	8.65(9)	8.38(8)	7.76(6)	6.67(7)
	θ/(°)	113.2(2)	113.6(3)	114.2(3)	115.6(3)	115.6(3)	115.8(3)	115.9(3)	117.3(5)
	ϕ/(°)	30.1(6)	27.0(8)	19.6(9)	11(2)	14(2)	10(2)	0	0
Ni	*x*	0.0358(3)	0.0354(3)	0.0355(3)	0.0357(3)	0.0364(3)	0.0857(3)	0.0362(2)	0.0362(3)
	z	0.6282(5)	0.6268(5)	0.6261(5)	0.6257(5)	0.6271(6)	0.6287(6)	0.6269(4)	0.6261(5)
	R_p/%	0.0673	0.0816	0.0705	0.0854	0.0838	0.0793	0.0609	0.0796
	w_{Rp}/%	0.0803	0.0982	0.0837	0.1016	0.0996	0.0957	0.0736	0.0967
	χ^2	2.795	1.346	1.984	1.396	1.364	1.335	2.271	1.262

Table 4. (b) Refined structural parameters of HoNi compound. Space group *Pnma*, Atomic positions: Ho (x, 0.25, z); Ni (x, 0.25, z). a, b, c, and V are lattice constant and volume of unit cell. M, M_x, M_y, and M_z are the total ordered magnetic moment and the individual component of moment along a, b, and c axes, respectively. ϕ and θ are the angle between the ordered magnetic moment and x, z axes, respectively.

Atoms	Parameters	30 K	32 K	34 K	36 K	38 K	40 K	42 K	45 K	295 K
	a/Å	6.9769(2)	6.9774(2)	6.9760(2)	6.9758(2)	6.9767(2)	6.9768(2)	6.9779(2)	6.9784(2)	7.0162(2)
	b/Å	4.15490(4)	4.15500(4)	4.1559(1)	4.1557(1)	4.1555(1)	4.1552(1)	4.1546(1)	4.1536(1)	4.1405(1)
	c/Å	5.4022(2)	5.4011(2)	5.3999(2)	5.4003(2)	5.4003(2)	5.4008(2)	5.4011(2)	5.4019(2)	5.4359(1)
	V/Å^3	156.601(6)	156.584(6)	156.552(6)	156.553(6)	156.565(6)	156.570(6)	156.580(6)	156.578(6)	157.916(5)
Ho	x	0.1804(3)	0.1797(3)	0.1802(3)	0.1797(3)	0.1797(3)	0.1797(3)	0.1798(3)	0.1803(3)	0.1800(2)
	z	0.1315(8)	0.1316(7)	0.1316(7)	0.1332(7)	0.1340(7)	0.1318(7)	0.1329(7)	0.1334(6)	0.1313(5)
	M_x/μ_B	4.27(6)	3.08(7)	0	0	0	0	0	0	0
	M_y/μ_B	0	0	0	0	0	0	0	0	0
	M_z/μ_B	–2.00(7)	–1.33(9)	0	0	0	0	0	0	0
	M/μ_B	4.71(7)	3.36(7)	0	0	0	0	0	0	0
	$\theta/(^\circ)$	115.1(8)	113(1)	0	0	0	0	0	0	0
	$\phi/(^\circ)$	0	0	0	0	0	0	0	0	0
Ni	x	0.0367(3)	0.0360(3)	0.0367(3)	0.0365(3)	0.0364(3)	0.0364(3)	0.0364(3)	0.0363(3)	0.0372(2)
	z	0.6277(6)	0.6285(6)	0.6291(5)	0.6286(5)	0.6276(5)	0.6282(5)	0.6271(5)	0.6275(5)	0.6285(4)
	R_p/%	0.0667	0.0671	0.0642	0.0677	0.0639	0.0632	0.0609	0.0660	0.0384
	w_{Rp}/%	0.0816	0.0811	0.0797	0.0832	0.0787	0.0783	0.0755	0.0804	0.0475
	χ^2	1.087	0.9613	0.9177	0.8818	0.9514	0.8915	0.8803	0.9041	0.9758

Results show that the x component of ordered magnetic moment exists in the temperature range from 5.3 K to 32 K, and it changes from 7.66(7) μ_B to 3.08(7) μ_B. The z component shows the similar case to the x component and it changes from 3.80(5) μ_B to 1.33(9) μ_B as temperature increases from 5.3 K to 32 K. So the temperature around 32 K is corresponding to magnetic order to disorder temperature point, which is known as Curie temperature. Also it is found that the y component of ordered magnetic moment changes from 4.4(1) μ_B to 1.3(3) μ_B as temperature increases and it disappears from $T = 20$ K. It indicates that the there is a magnetic transition and the transition temperature is around 15 K. As a matter of fact, the magnetic transition of HoNi compound in low temperature range has been observed according to magnetic measurements.[66,78]

Figure 32(a) shows the thermal magnetization curve of HoNi compound at a field of 0.01 T. As temperature increases, the magnetization shows drastic decrease at T_{SR} and T_C, respectively. The value of T_{SR} and T_C is determined to be 13.5 K and 35.5 K, respectively, according to the maximum of dM/dT (see the inset of Fig. 32(a)). The results of ordered magnetic moments and the components along different axis according to NPD fitting are also shown in Fig. 32(b). It is clear that the FM x component and AFM z component both undergo an order to disorder transition around 32 K, and the FM y component decreases as temperature increases and falls down to zero at 20 K. As the total ordered magnetic moment, M shows sudden decrease both at T_{SR} and T_C.

The angle between the x axis and the xy component of the ordered magnetic moment was also calculated for every temperature and it was marked as ψ. The temperature dependence of the ψ curve is shown in Fig. 32(c). As temperature increases, ψ decreases from 30° at 5.3 K to 10° at 15 K, and it falls down to zero at 20 K, which means that the y component disappears. From the change tendency of the three components of ordered magnetic moment and the value of ψ as temperature increases, it can be seen that the HoNi compound undergoes a spin reorientation process at T_{SR} except for the ferromagnetic to paramagnetic transition at T_C as temperature increases. Besides, an obvious change of crystal lattice parameters was also observed according to the neutron powder diffraction experiments. The temperature dependences of parameters a, b, c, and V are shown in Fig. 33. Parameters a, b, c, and V all show a change corresponding to the spin reorientation transition around 15 K, which means that the disappearing of the y component affects the crystal structure from three directions. As temperature increases, all of the above parameters show sharp variation at the temperature T_C, which indicates that the ferromagnetic to paramagnetic transition affects the crystal structure more than the spin reorientation transition does. Although the spin reorientation transition has been observed and studied before, the present work shows a more complete sketch of that magnetic transition for the HoNi compound.

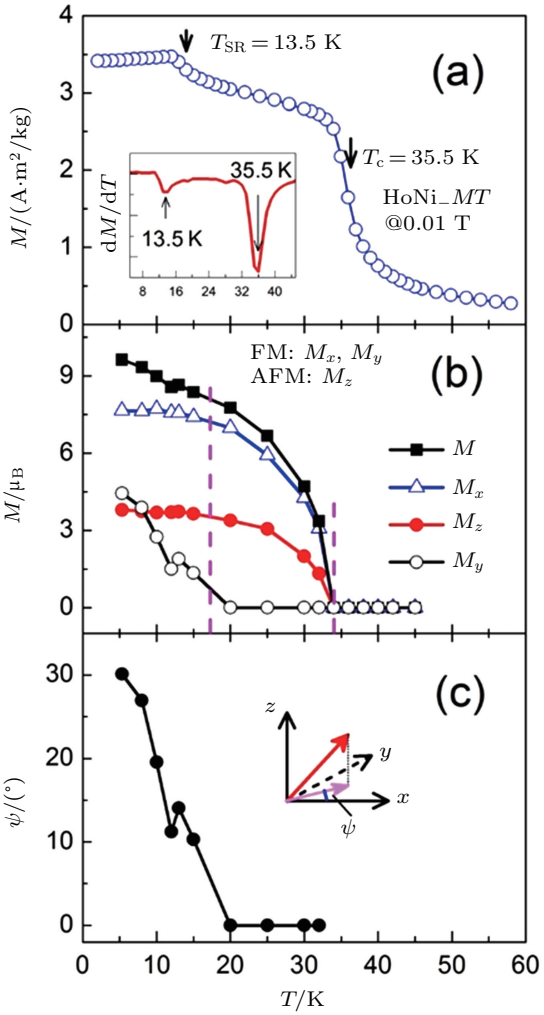

Fig. 32. (color online) (a) The field dependence of magnetization curve for HoNi compound at a field of 0.01 T. The inset is the plot of first order derivation of M–T curve. (b) The x component, y component, z component and total value of ordered magnetic moment in HoNi compound. (c) The temperature dependence of the angle between x axis and the projection of ordered magnetic moment in xy plane.[76]

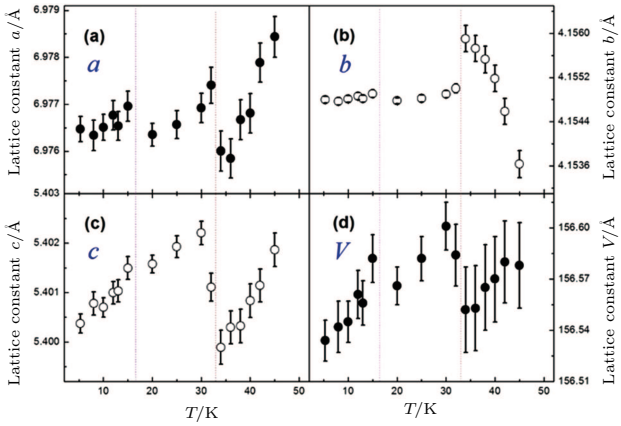

Fig. 33. (color online) (a) The temperature dependence of lattice constant a. (b) The temperature dependence of lattice constant b. (c) The temperature dependence of lattice constant c. (d) The temperature dependence of the volume of unit cell.

3.3. The magnetocaloric effect of *R*Ni compounds

The ΔS_M of RNi (R = Gd, Dy, Ho, and Er) compounds was calculated based on the isothermal magnetization data (not shown here) by using the Maxwell relation $\Delta S_M = -\int_0^H (\partial M/\partial T)\,dH$. The ΔS_M curves as a function of temperature for RNi (R = Gd, Dy, Ho, Er) compounds with a field change of 0 T–2 T and 0 T–5 T are shown in Fig. 34(a) and Fig. 34(b), respectively. The data for GdNi and DyNi compounds are cited from literatures.[77,78] and the data for HoNi and ErNi compounds are newly obtained in this work. The MCE curve obtained for GdNi shows a steady increase in the $-\Delta S_M$ value with temperature and attains maximum value around its T_C.[78] The maximum value of ΔS_M, T_{width}, and RC for a field change of 0 T–5 T for DyNi compound are estimated to be 18 J/kg·K, 31 K, and 429.8 J/kg, respectively. The large MCE values in DyNi can be attributed to its metamagnetic nature.[77] It is possible that the gradual flopping of moments towards the direction of the applied field is responsible for the reduction in magnetic entropy, which results in MCE.[77] Spin-flop process has indeed been found to be responsible for the anomalous magnetoresistance observed along the c axis in single crystals of DyNi compound.[77,83] The curve for ErNi shows a sharp increase in the $-\Delta S_M$ value near its T_C exhibiting the character of a typical ferromagnet whereas there is another peak around 15 K in the case of HoNi. The difference in the MCE behavior of ErNi and HoNi implies that though these compounds are non-collinear, they have different arrangements of moments in the magnetic sub-lattice.[78] The peak in low temperature range in HoNi compound is corresponding to the SR transition. It also can be seen that the maximum value at T_{SR} is comparable to that at T_C, which indicates that there is a very large change of magnetic entropy in the process of spin reorientation for HoNi compound. The two peaks on the ΔS_M curve for HoNi compound are corresponding to the two transition temperatures. As is discussed based on the thermal magnetization curves, there are also two magnetic transitions for DyNi and ErNi compounds. But no obvious magnetic entropy change is observed on the ΔS_M curve around T_{SR} for DyNi and ErNi compounds, which indicates that the SR transition is very weak for the DyNi and ErNi compounds. All of the MCE parameters are listed in Table 3. It is also clear that the maximum ΔS_M for ErNi compound shows the largest value among the RNi compounds.

The isothermal magnetization curves at different temperatures were measured and the ΔS_M was calculated for all of the $Ho_xEr_{1-x}Ni$ ($0 \le x \le 1$) compounds by using Maxwell relation $\Delta S_M = -\int_0^H (\partial M/\partial T)_H\,dH$.[84] The temperature dependence of ΔS_M is shown in Fig. 35. It is found that the $(\Delta S_M)_{max}$ of $Ho_{0.1}Er_{0.9}Ni$ is the largest among $Ho_xEr_{1-x}Ni$ ($0 \le x \le 1$) compounds. The value of $(\Delta S_M)_{max}$ for ErNi and $Ho_{0.1}Er_{0.9}Ni$ compound is 29.6 J/kg·K and 34 J/kg·K, respectively, i.e., 10% of Ho-substitution brings as high as $\sim$ 14.9% ((34–29.6)/29.6 = 0.149) enhancement on $(\Delta S_M)_{max}$. The refriger-

ant capacity (*RC*) of $Ho_xEr_{1-x}Ni$ ($0 \le x \le 1$) compounds were also calculated by using the approach suggested by Gschneidner *et al.*[53] The *RC* is defined as $RC = \int_{T_1}^{T_2} |\Delta S_M| \, dT$, where T_1 and T_2 are the temperatures corresponding to both sides of the half-maximum value of $(\Delta S_M)_{max}$, respectively. The refrigerant temperature width (T_{width}) is defined as the temperature span of the full width at half maximum value of $(\Delta S_M)_{max}$. Then T_{width} can be obtained by T_2–T_1.

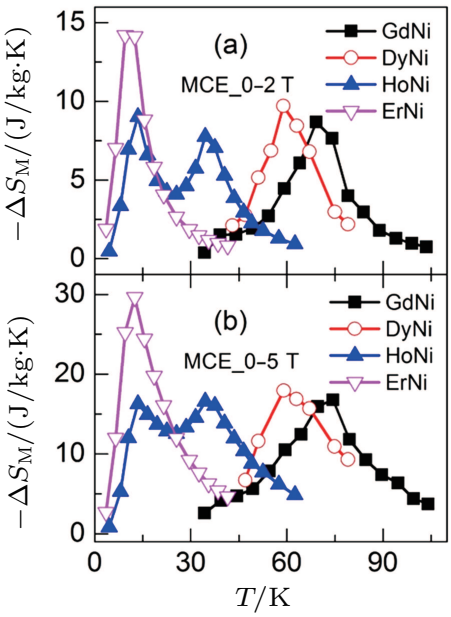

Fig. 34. (color online) (a) The temperature dependence of magnetic entropy change curves under a field change of 0 T–2 T for *R*Ni (*R* = Gd, Dy, Ho, Er) compounds, respectively. (b) The temperature dependence of magnetic entropy change curves under a field change of 0 T–5 T for *R*Ni (*R* = Gd, Dy, Ho, Er) compounds, respectively.

All the MCE parameters including $(\Delta S_M)_{max}$, T_{width}, and *RC* for $Ho_xEr_{1-x}Ni$ ($0 \le x \le 1$) compounds are listed in Table 3. As the content of Ho increases, the $(\Delta S_M)_{max}$ first increases and then decreases. Among all the $Ho_xEr_{1-x}Ni$ ($0 \le x \le 1$) compounds, $Ho_{0.1}Er_{0.9}Ni$ compound shows the largest $(\Delta S_M)_{max}$. $Ho_{0.1}Er_{0.9}Ni$ compound has proved to be a second-order-transition material according to Arrott plots, but the $(\Delta S_M)_{max}$ (34 J/kg·K for 0 T–5 T) is comparable to the representative low temperature first-order-transition MCE material $ErCo_2$ compound (36.8 J/kg·K for 0 T–5 T).[85] The changing trend of T_{width} is opposite to $(\Delta S_M)_{max}$. Among all the $Ho_xEr_{1-x}Ni$ ($0 \le x \le 1$) compounds, $Ho_{0.1}Er_{0.9}Ni$ compound shows the smallest T_{width}. As for *RC*, it increases monotonously from 350 J/kg to 556.7 J/kg as the content of Ho changes from 0 to 1. For Ho–Er–Ni compounds, $Ho_{0.1}Er_{0.9}Ni$ exerts ideal $(\Delta S_M)_{max}$ but with ordinary T_{width} and *RC*. But it is valuable to discuss the MCE enhancement (peak value) with 10% of Ho-substitution compared with ErNi.

In fact, the MCE enhancement in Ho–Er–Ni compounds is closely related to the temperature interval between SR transition and FM to PM transition. Magnetic materials are in the non-steady magnetic state around transition temperatures. When a field is applied around transition temperature, obvious MCE can be observed, because the magnetic entropy is easy to change in this state. As a result, more than one S_M peaks can be observed in multi-phase-transition MCE materials, such as ErGa.[19] and Ho_2In.[86] compounds. According to thermal magnetization and ac susceptibility measurements, all of the $Ho_xEr_{1-x}Ni$ ($0 \le x \le 1$) compounds undergo two magnetic transitions as temperature increases: SR transition and FM to PM transition. More specially, the temperature interval between the two transitions is only 2 K for $Ho_{0.1}Er_{0.9}Ni$, which is the smallest value among the $Ho_xEr_{1-x}Ni$ ($0 \le x \le 1$) compounds. When the temperature interval between the magnetic transitions is large, the corresponding two ΔS_M peaks are separate, such as HoNi, $Ho_{0.8}Er_{0.2}Ni$ and $Ho_{0.6}Er_{0.4}Ni$ compounds (see Fig. 35). But for other samples, the two peaks are hard to distinguish, because they overlap and merge together, which is similar to $Ho_{12}Co_7$ compound with large field change.[18] In this case, T_{width} can also be used to evaluate the level of overlap. It is conspicuous that the T_{width} is the smallest for $Ho_{0.1}Er_{0.9}Ni$ compound, indicating the two ΔS_M peaks are almost entire-overlapping. Therefore, $Ho_{0.1}Er_{0.9}Ni$ compound shows the largest $(\Delta S_M)_{max}$.

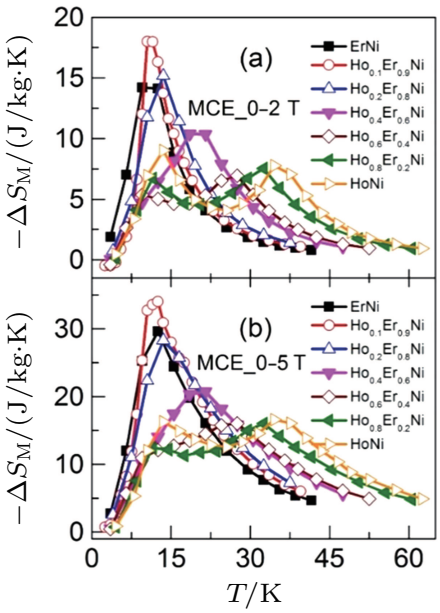

Fig. 35. (color online) (a) The temperature dependence of magnetic entropy change curves under a field change of 0 T–2 T for $Ho_xEr_{1-x}Ni$ ($0 \le x \le 1$) compounds, respectively. (b) The temperature dependence of magnetic entropy change curves under a field change of 0 T–5 T for $Ho_xEr_{1-x}Ni$ ($0 \le x \le 1$) compounds, respectively.

4. $R_{12}Co_7$ compounds

It was reported that there are eight intermetallic compounds existing in the Co–*R* system, and $R_{12}Co_7$ is among them.[87] Although $R_{12}Co_7$ (*R* = Gd, Tb, Dy, Ho, Er) compounds have identical monoclinic structures, they exhibit dif-

ferent magnetic properties.[88] $R_{12}Co_7$ (R = Gd–Er) compounds crystallize in a monoclinic $Ho_{12}Co_7$-type structure ($P2_1/c$).[88] There are four different types of Co-centered R polyhedral in the unit cell: trigonal prism, cube, Archimedian antiprism, and truncated Archimedian antiprism.[88] The crystal structure of $R_{12}Co_7$ compound is shown in Fig. 36. If the crystal structure is viewed from (100) direction, there are three types of Co-centered rare-earth polyhedral. Co(1) is at the center of a trigonal prism, Co(2) is surrounded by an Archimedian antiprism and Co(4) is at the center of a cube.[88]

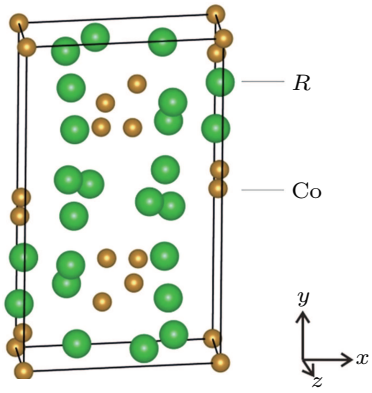

Fig. 36. (color online) The crystal structure of $R_{12}Co_7$ compounds.

It has been reported that $Gd_{12}Co_7$, $Tb_{12}Co_7$, $Gd_4Tb_8Co_7$, $Gd_8Tb_4Co_7$, and $Dy_{12}Co_7$ undergo only one ferromagnetic (FM) to paramagnetic (PM) transition as temperature increases.[89–92] But a spin reorientation transition was observed at 123 K in $Gd_{12}Co_7$ compound according to literature.[92] According to our previous work, $Ho_{12}Co_7$ compound undergoes an antiferromagnetic (AFM) to AFM transition, an AFM to FM transition and an FM to PM transition at 9 K, 17 K, and 30 K, respectively.[18] According to the calculation and analysis of effective magnetic moments of R ions, Co atoms are considered to contribute to the magnetic moments in $Ho_{12}Co_7$ and $Dy_{12}Co_7$ compounds.[18,91] The magnetocaloric effect of $R_{12}Co_7$ (R = Gd, Tb, Dy, Ho) compounds are studied in detail, and the value of RC is 555 J/kg for a field change of 0 T–5 T for $Ho_{12}Co_7$ compound with two ΔS_M peaks close to each other on the ΔS_M curves.[18] Recently, the magnetic property and magnetocaloric effect of $Ho_xEr_{12-x}Co_7$ (x = 0, 4, 6, 8, 10, 12) compounds are studied in detail.[93]

In the following section, we will review the property and magnetocaloric effect of binary $R_{12}Co_7$ (R = Gd, Tb, Dy, Ho) and pseudo-binary $Ho_xEr_{12-x}Co_7$ (x = 0, 4, 6, 8, 10, 12) and $Gd_{12-x}Tb_xCo_7$ (x = 0, 4, 8) compounds. The related data for $Gd_{12}Co_7$, $Tb_{12}Co_7$ and $Gd_{12-x}Tb_xCo_7$ (x = 0, 4, 8) compounds is cited from the literatures.[89,90,92]

4.1. The magnetic transition of $R_{12}Co_7$ compounds

The temperature (T) dependence of magnetization (M) was measured in both zero field-cooled (ZFC) and field-cooled (FC) processes in order to determine the thermal hysteresis and the magnetic transition temperature.

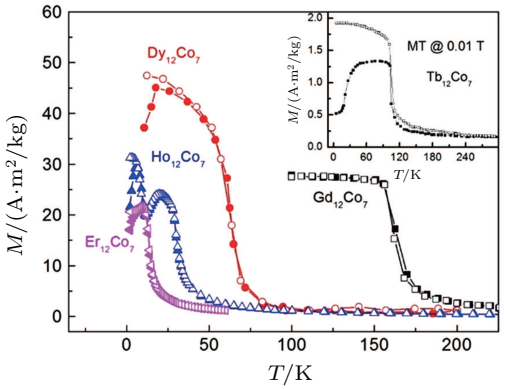

Fig. 37. (color online) The temperature dependence of zero-field-cooling and field-cooling magnetization curves at a field of 0.1T for $R_{12}Co_7$ (R = Gd, Dy, Ho, Er) compounds. The inset is the temperature dependence of zero-field-cooling and field-cooling magnetization curves at a field of 0.01 T for $Tb_{12}Co_7$ compounds.[18,89–92]

Figure 37 shows the thermomagnetic M–T curves of $R_{12}Co_7$ (R = Gd, Dy, Ho, Er) compounds measured under an external magnetic field of 0.1 T. The inset of the Fig. 37 is the ZFC and FC curves of $Tb_{12}Co_7$ compound under a field of 0.01 T. Apparently, the ZFC and FC magnetization curves are almost same for $Gd_{12}Co_7$ compound. The large drop of M–T curves corresponds to ferromagnetic to paramagnetic phase transition. The T_C of the compound is defined as the temperature where dM/dT reached the peak point. In this work, T_C of $Gd_{12}Co_7$ is about 163 K, the compound shows soft-ferromagnetic behavior below 163 K.[90] The ZFC and FC magnetization curves of $Tb_{12}Co_7$ compound are separated from each other below 100 K and there is a cusp in the ZFC curve, which is due to the temperature-dependent coercivity.[89] The compound shows ferromagnetic behavior. The Curie temperature T_C of $Tb_{12}Co_7$ is about 100 K, as obtained from the minimum of the first derivative of the FC M–T curve in a magnetic field of 0.01 T.[89] One can find that $Dy_{12}Co_7$ experiences an FM–PM transition around the Curie temperature T_C = 64 K, defined as the minimum value of dM/dT curve.[91] It can also be seen from Fig. 37 that the ZFC and FC curves are completely reversible in the vicinity of T_C as shown usually in magnetic materials with a second-order magnetic transition. Meanwhile, a significant thermal irreversibility between the ZFC and FC branches is clearly observed below T_C under 0.1 T. Like many rare earth-metal compounds,[94] $Dy_{12}Co_7$ may have strong anisotropy due to its large Dy content. It has been reported that in materials with high anisotropy energy and low exchange energy, the domain wall width could be comparable to that of lattice spacing, thus leading to a large pinning effect.[94] Considering the magnetic anisotropy and low T_C for $Dy_{12}Co_7$, the thermomagnetic irreversibility is likely attributed to the narrow domain wall pin-

ning effect.[91] When the sample is cooled under a zero field, it freezes in an irregular domain structure where the direction of the spontaneous magnetization is only determined locally by the magnetic anisotropy.[91] When a small field is switched on and the sample is warmed up, the walls begin to move and in every domain the direction of magnetization turns into the energetically most favorable direction which now also depends on the direction of the applied field.[95] So we can see that the ZFC magnetization is low below T_C and reaches a maximum at low temperature. Whereas in FC mode, the magnetic field during the cooling prevents the pinning effect, and therefore the magnetization at low temperature is higher than that in ZFC mode and gradually reaches saturation.[91] According to the M versus T characteristics, it is suggested that the $Ho_{12}Co_7$ compound undergoes three magnetic transitions in sequence with decreasing temperature. The transition at the highest temperature corresponds to a change from paramagnetic state to ferromagnetic state at $T_C = 30$ K. The rest two phase transitions are ferromagnetic to antiferromagnetic transition at $T_2 = 17$ K and antiferromagnetic to antiferromagnetic transition at $T_1 = 9$ K, which will be confirmed by the isothermal magnetization curves.[18] The transition temperatures for $Er_{12}Co_7$ compound is determined to be 6.5 K and 13.5 K, respectively. All of the transition temperatures of $R_{12}Co_7$ compounds are listed in Table 5.

Table 5. The transition temperatures and magnetocaloric parameters of $R_{12}Co_7$ (R = Gd, Tb, Dy, Ho) and $Ho_xEr_{12-x}Co_7$ ($x = 0, 4, 6, 8, 10, 12$) and $Gd_{12-x}Tb_xCo_7$ ($x = 0, 4, 8$) compounds.

Materials	T_t/K	T_C/K	MCE_0–2 T			MCE_0–5 T			Ref.
			$-\Delta S_M(T)_{max}$/(J/kg·K)	T_{width}/K	RC/(J/kg)	$-\Delta S_M(T)_{max}$/(J/kg·K)	T_{width}/K	RC/(J/kg)	
$Gd_{12}Co_7$	123	163/160.8	4.6	37.4	123.3	8.8	71.7	462.8	[90,92]
$Gd_8Tb_4Co_7$	–	140.8	–	–	–	8.2	51.8	316	[92]
$Gd_4Tb_8Co_7$	–	118.9	–	–	–	7.1	38.5	202.2	[92]
$Tb_{12}Co_7$	–	100	3.1	8.7	20.5	–	–	–	[89]
$Dy_{12}Co_7$	–	64	5	21.7	81.5	10	42.1	303.7	[91]
$Ho_{12}Co_7$	9/17	30	9.2	29.4	206.2	19.2	37.4	555	[18]
$Ho_{10}Er_2Co_7$	9/19	26.3	6.2	20.9	94.8	16.1	32.5	396	[93]
$Ho_8Er_4Co_7$	11	22	7.8	22.8	137.8	17.0	31.8	422	[93]
$Ho_6Er_6Co_7$	12	18	9.7	19.7	150.5	18.6	28.5	411	[93]
$Ho_4Er_8Co_7$	8.6	15	9.6	16.5	122.6	18.0	24.7	342	[93]
$Er_{12}Co_7$	6.5	13.5	10.2	14.5	103.6	18.3	22.8	317	[93]
$Ho_6Er_6Co_7$ 42% $Ho_{12}Co_7$ 58%	–	–	–	–	–	16.7	38.0	553	[93]

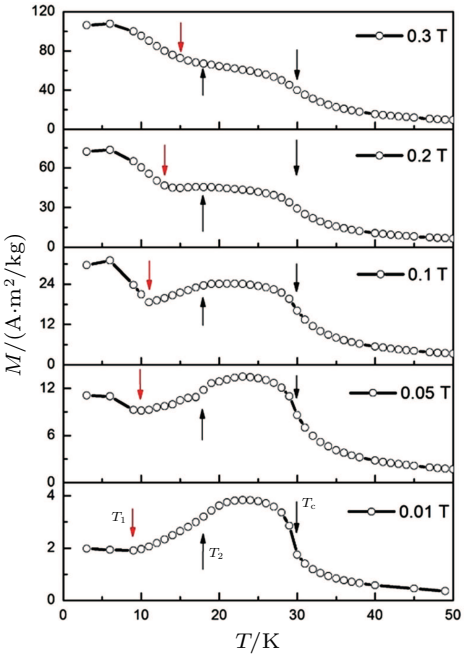

Fig. 38. (color online) The temperature dependence of magnetization curves for $Ho_{12}Co_7$ compound at a field of 0.01 T, 0.05 T, 0.1 T, 0.2 T, and 0.3 T, respectively.[18]

The M–T curves of $Ho_{12}Co_7$ compound under different external magnetic field are shown in Fig. 38. One can find that T_1 increases monotonically with magnetic field increasing from 0.01 T to 0.3 T. However, almost no change is observed for T_2 and T_C with magnetic field change. It indicates that a field-induced metamagnetic transition from AFM to FM state occurs below T_2, and T_1 is pushed towards higher temperature with the applied magnetic field increasing. Similar phenomenon has been observed in PrGa compound.[43] Figure 39(a) shows the isothermal magnetization curves of $Ho_{12}Co_7$ in a temperature range of 3 K–50 K under the magnetic fields up to 7 T. The isothermal magnetization curves in some selected temperature ranges at low magnetic fields are shown in Figs. 39(b), 39(c), and 39(d), respectively. One can find that the isothermal magnetization curves between $T_2 = 17$ K and $T_C = 30$ K, show FM characters (Fig. 39(d)). The magnetization remains a linear dependences of the magnetic field at low field range below $T_2 = 17$ K (Figs. 39(b) and 39(c)), indicating the existence of AFM ground state.[18] Now we can confirm the transition around T_2 is corresponding to FM to AFM transition, and the one around T_1 is corresponding

to AFM to AFM transition. The magnetization curves deviate from the linear relationship, when the applied field exceeds a certain value, showing a field-induced metamagnetic transition from AFM to FM state. The critical field determined from the maximum of dM/dH for $Ho_{12}Co_7$ is found to be 0.12 T at 6 K and 0.28 T at 16 K.[18] The result indicates that the $Ho_{12}Co_7$ compound is a weak antiferromagnetic material below T_2, and a small magnetic field can destroy the AFM structure. One can also find that the isothermal magnetization curves obtained well above T_C show strong curvatures at low fields from Fig. 39(a). Similar results have been observed in some other intermetallic compounds.[19,96,97] It may result from the existence of short-range ferromagnetic correlations in the PM state.

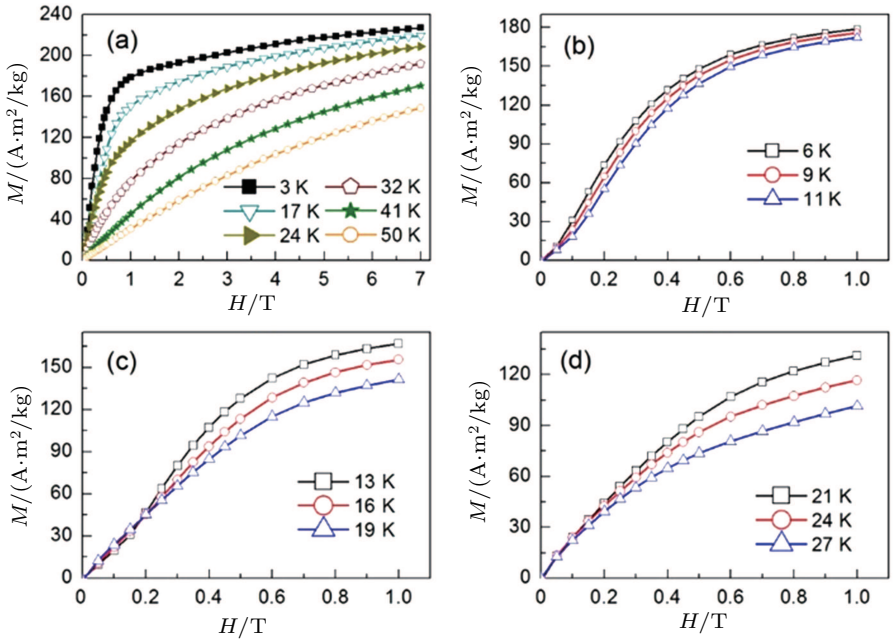

Fig. 39. (color online) (a) The field dependence of magnetization curves up to 7 T for $Ho_{12}Co_7$ compound at the temperatures from 3 K to 50 K. (b) The isothermal magnetization curves in the low field range at 6 K, 9 K, and 11 K. (c) The isothermal magnetization curves in the low field range at 13 K, 16 K, and 19 K. (d) The isothermal magnetization curves in the low field range at 21 K, 24 K, and 27 K.[18]

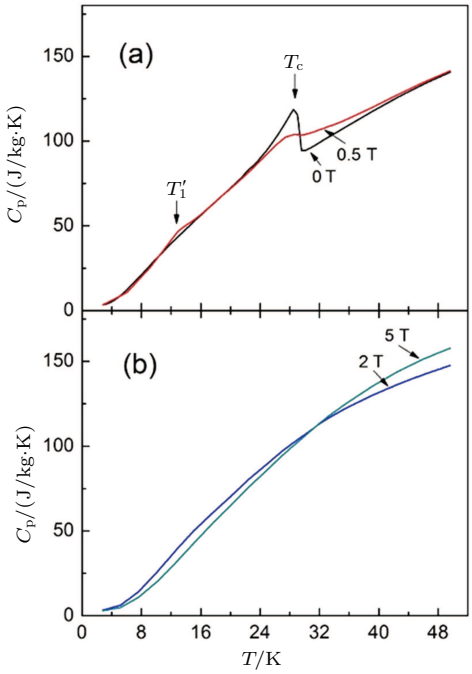

Fig. 40. (color online) (a) The temperature dependence of heat capacity curves for $Ho_{12}Co_7$ compound at a field of 0 T and 0.5 T, respectively. (b) The temperature dependence of heat capacity curves for $Ho_{12}Co_7$ compound at a field of 2 T and 5 T, respectively.[18]

The S-shaped Arrott plots (not shown here) below T_2 confirm the existence of the field-induced first-order AFM–FM transition. The positive slope of the Arrott plot above T_C indicates a characteristic of a second-order PM–FM transition. The temperature dependences of the heat capacity in different magnetic fields are shown in Fig. 40. The peaks around 30 K, which are obvious for $H = 0$ T and 0.5 T, are corresponding to T_C. It is found that there are obvious differences of heat capacity below T_2 for different magnetic field. The reason why the applied magnetic field affects heat capacity so greatly is that a magnetic transition from the weak AFM ground state to the FM state occurs. There is no obvious peak related to the AFM to AFM transition temperature for zero-field heat capacity curve, but an obvious peak around 13 K appears on the heat capacity curve for an applied field of 0.5 T.[18] As is illustrated in the M–T curves, the peak is corresponding to AFM to AFM transition and it has been pushed by the applied field from T_1 ($= 9$ K) to higher temperature (~ 13 K). In the temperature range between T_2 and T_C, the differences of heat capacity for different magnetic fields are not as clear as those in lower temperature range. That is because $Ho_{12}Co_7$ compound is FM state in this range, and the influence of applied field on heat capacity is small. The heat capacity data demonstrates that the statement of magnetic transition on the basis of M–T and

M–H curves is reasonable.

$Tb_{12}Co_7$ compound has been treated as a simple ferromagnetic material and it shows typical soft ferromagnetic features below T_C=100 K. But from the isothermal magnetization (*M–H*) curves up to 5 T at 5 K and 80 K, which is shown in Fig. 41, it seems that $Tb_{12}Co_7$ compound shows weak AFM ground state at 5 K, which is very different from the FM type curve obtained at 80 K. Considering that $Ho_{12}Co_7$ compound with the same structure with $Tb_{12}Co_7$ compound undergoes complex magnetic transition as temperature increases, it is possible that $Tb_{12}Co_7$ compound undergoes another magnetic transition in low temperature range besides the FM to PM transition at T_C. The reason why the low-temperature transition was not observed according to *M–T* curves may be the AFM ground state in low temperature range is too weak. The temperature (T) dependences of magnetization (M) of $Gd_{12-x}Tb_xCo_7$ ($x = 0$, 4, and 8) alloys under a 0.05-T applied field in zero-field cooling (ZFC) and field cooling (FC) modes are shown in Fig. 42. The Curie temperature T_C, which is defined as the temperature at the maximum of dM/dT versus T plot, for $Gd_{12}Co_7$, $Gd_8Tb_4Co_7$, and $Gd_4Tb_8Co_7$ are 160.8, 140.8, and 118.9 K, respectively. All alloys undergo an FM to PM order transition. The magnetization changes rapidly with the change of temperature in the vicinity of T_C, indicating that a large entropy change may be observed near Curie temperature. Furthermore, a spin reorientation behavior with T_{SR}=123 K is observed for the $(Gd_{12-x}Tb_x)Co_7$ alloy with $x = 0$, which should result from the competition between magnetic exchange and the crystalline electric field.[98] It should be noted that no SR transition is observed on the *M–T* curve of $Gd_{12}Co_7$ compound according to Chen *et al.*[90] The FC and ZFC data branch out from each other in the vicinity of Tc, indicating thermomagnetic irreversibility for this alloy.

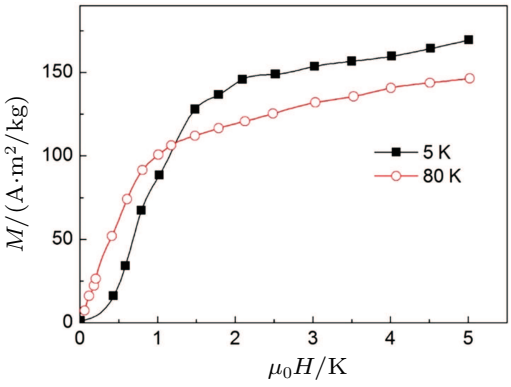

Fig. 41. (color online) The field dependences of magnetization curve up to 5 T for $Tb_{12}Co_7$ compound at 5 K and 80 K, respectively.[89]

The zero-field-cooled (ZFC) and field-cooled (FC) magnetization curves for $Ho_xEr_{12-x}Co_7$ ($x = 0$, 4, 6, 8, 10, 12) compounds were measured[93] and the ZFC curves are shown in Fig. 43. The field dependence of magnetization (*M–H*) curves were also measured in detail for $Ho_xEr_{12-x}Co_7$ ($x = 0$, 4, 6, 8, 10, 12) compounds. For the $Ho_xEr_{12-x}Co_7$ ($x = 0$, 4, 6, 8) compounds, two drastic changes are observed at different temperature range on the *M–T* curves, which indicates that there are two magnetic transitions. *M–H* measurements show that the magnetic ground state of the three temperature zones divided by the two transition temperatures is antiferromagnetic (AFM), ferromagnetic (FM), and paramagnetic (PM), respectively. That is, $Ho_xEr_{12-x}Co_7$ ($x = 0$, 4, 6, 8) compounds undergo an AFM to FM transition and an FM to PM transition in sequence as temperature increases. The transition temperature (T_1) of AFM to FM transition is 6.5 K, 8.6 K, 12 K, and 11 K and the Curie temperature (T_C) is 13.5 K, 15 K, 18 K, and 22 K for $Ho_xEr_{12-x}Co_7$ ($x = 0$, 4, 6, 8) compounds, respectively. All of the transition temperatures of $Ho_xEr_{12-x}Co_7$ ($x = 0$, 4, 6, 8, 10, 12) compounds are listed in Table 5. From the results of transition temperature, it is found that as the content of Ho atoms increases, the number of transitions grows from two to three and the magnetic property becomes more and more complex. The transition at T_1, whether the AFM to FM transition for $Ho_xEr_{12-x}Co_7$ ($x = 0$, 4, 6, 8) compounds or the AFM to AFM transition for $Ho_xEr_{12-x}Co_7$ ($x = 10$, 12) compounds, means the competition of two ordered magnetic states. From Table 5, the value of T_1 fluctuates not more than 5.5 K as the content of Ho atoms changes. That is because the competition is affected by crystal structure and crystal field, and the crystal structure of $Ho_xEr_{12-x}Co_7$ ($x = 0$, 4, 6, 8, 10, 12) compounds is consistent with one another. The results are similar to the changing characteristics of spin reorientation transition temperature in $Gd_xEr_{1-x}Ga$ compounds.[34] However, the Curie temperature of $Ho_xEr_{12-x}Co_7$ ($x = 0$, 4, 6, 8, 10, 12) compounds shows a steadily increasing trend as the content of Ho atoms increases. That is because the Curie temperature and spin angular number (S) are positively correlated. Since the S of Ho is larger than Er, more Ho atoms means larger average S and thus the Curie temperature increases step by step as the content of Ho goes up.

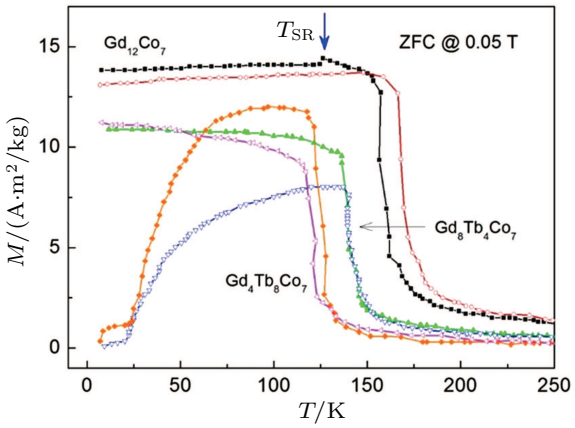

Fig. 42. (color online) Temperature dependencies of magnetization curves for $Gd_{12-x}Tb_xCo_7$ ($x = 0$, 4, and 8) compounds under a field of 0.05 T.[92]

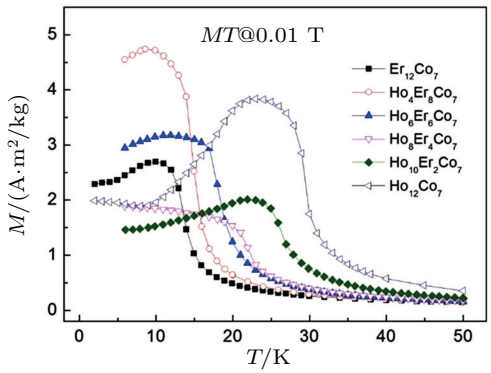

Fig. 43. (color online) The temperature dependence of magnetization curves at a field of 0.01 T for $Ho_xEr_{12-x}Co_7$ ($x = 0$, 4, 6, 8, 10, 12) compounds, respectively.[93]

4.2. The magnetocaloric effect of $R_{12}Co_7$ compounds

The magnetic entropy change ΔS_M of $R_{12}Co_7$ (R = Gd, Tb, Dy, Ho, Er) compounds can be calculated from isothermal magnetization data by using Maxwell relation $\Delta S_M(T) = -\int_0^H (\partial M/\partial T)\,dH$.

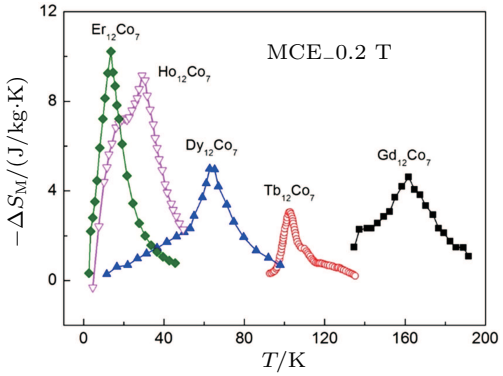

Fig. 44. (color online) The temperature dependence of magnetic entropy change curves under a field change of 0 T–2 T for $R_{12}Co_7$ (R = Gd, Tb, Dy, Ho, Er) compounds, respectively.

Figure 44 displays the values of ΔS_M for $R_{12}Co_7$ (R = Gd, Tb, Dy, Ho, Er) compounds as a function of temperature for a field change of 0 T–2 T. The maximum value of $|\Delta S_M|$ for a field change of 0 T–2 T is calculated to be 4.6 J/kg·K, 3.1 J/kg·K, 5J/kg·K, 9.2 J/kg·K, and 10.2 J/kg·K for $R_{12}Co_7$ (R = Gd, Tb, Dy, Ho, Er) compounds, respectively. The maximum value of $|\Delta S_M|$ nearly shows an increase tendency as the R atom number increases. The change tendency of T_{width} is not as obvious as maximum of $|\Delta S_M|$. All of the MCE parameters including MCE for 0 T–5 T are all listed in Table 5. For $Dy_{12}Co_7$ compound, the distinct "λ"-type of ΔS_M–T curves as well as the immovable position of the peak of ΔS_M with the increase of field change further confirms the SOPT (second-order phase transition) nature of $Dy_{12}Co_7$. The maximum values of ΔS_M reach 5 J/kg·K and 10.0 J/kg·K for the field changes of 0 T–2 T and 0 T–5 T, respectively. These values are comparable with or larger than those of some magnetocaloric materials with a SOPT in a similar temperature range under the same field change. For example, for the field change of 0 T–5 T, the maximum values of TbCoAl (T_C = 70 K) compound and $Er(Co_{0.85}Si_{0.15})_2$ (T_C = 60 K) compound are 10.5 J/kg·K and 8 J/kg·K, respectively.[99,100] In addition, refrigerant capacity (RC), another important parameter to quantify the heat transferred between the hot and cold sinks in an ideal refrigeration cycle, is estimated by using the approach $RC = \int_{T_1}^{T_2} |\Delta S_M|\,dT$, where T_1 and T_2 are the temperatures corresponding to the both sides of half maximum value of ΔS_M peak.[53] Thus, the RC values of $R_{12}Co_7$ compounds are obtained for the field changes of 0 T–2 T and 0 T–5 T, respectively.

The ΔS_M of $Ho_{12}Co_7$ was calculated from isothermal magnetization data by using the Maxwell relation $\Delta S_M = \int_0^H (\partial M/\partial T)_H\,dH$ and from heat capacity data through the expression $\Delta S_M = \int_0^H \{[C(T,H) - C(T,0)]/T\}\,dT$ as well.[50] Figure 45(a) shows the ΔS_M as a function of temperature for different magnetic field changes. Figure 45(b) shows the comparison of ΔS_M curves obtained from the two different ways. The curves obtained using magnetization data are not in good agreement with the corresponding curves obtained using heat capacity. Considering that the actual combined relative error in the ΔS_M calculated from magnetization data can reach ~ 20% and that from heat capacity data can be ~ 4%,[3,50] the deviations between the value of ΔS_M calculated from the two methods are in the error range with the maximal error being ~17% and ~11%, for the field change of 0 T–2 T and 0 T–5 T, respectively. Although there are differences between the curves obtained from the two methods, the shape of the curves matches well with each other. It is clear that there are two peaks on the ΔS_M–T curves, which indicates that both AFM–FM and PM–FM transitions contribute to MCE. Figure 45(c) shows that when the field change is small, for example 0 T–0.2 T, the value of ΔS_M is positive in certain temperature range, and as the field change increasing, the value of ΔS_M changes into negative. That results from the occurrence of metamagnetic transition, because the positive or negative value of ΔS_M is related to AFM or FM state. Besides, with the field change increasing, the first peak corresponding to AFM–FM transition moves towards higher temperatures, while the second peak related to PM–FM transition almost centers at ~ 30 K, which is in accordance with the results of M–T and C_p–T measurements. When the field change is high enough, for example 0 T–2 T and 0 T–5 T, the first peak is so close to the second one that they almost change into a larger peak. On the basis of magnetization measurement, the maximal value of $-\Delta S_M$ for $Ho_{12}Co_7$ is found to be 19.2 J/kg·K around T_C for a field change 0 T–5 T. Compared with the refrigerant materials in a similar temperature range, the value of $Ho_{12}Co_7$ compound is smaller than that of ErGa (21.3 J/kg·K at 30 K),[19] DyCuAl (20.4 J/kg·K at 28 K),[16] and $ErCo_2$ (33 J/kg·K at 36 K)[101]

compounds, but it is larger than that of DyNiAl (19 J/kg·K at 32 K),[102] TbCoC_2 (15.3 J/kg·K at 30 K),[103] and $GdNi_5$ (11.5 J/kg·K at 32 K).[104]

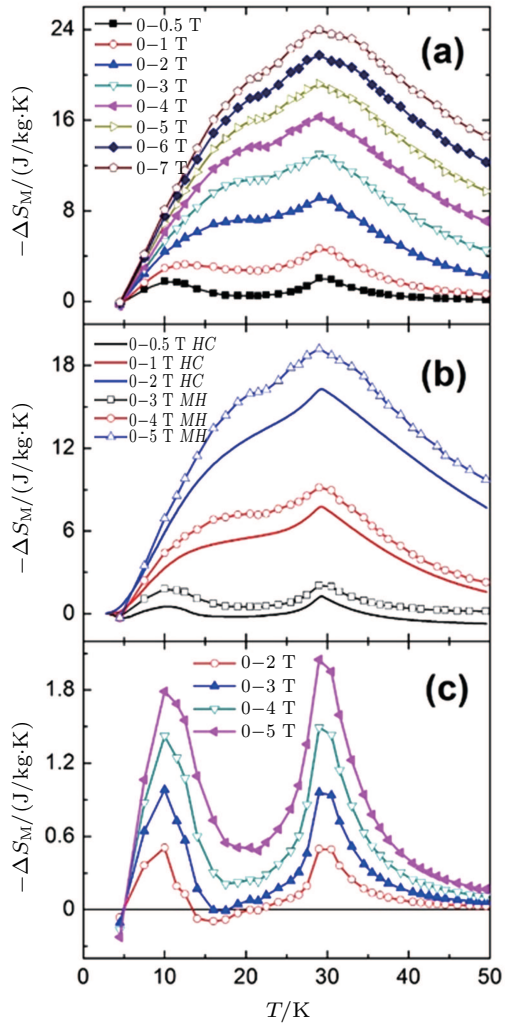

Fig. 45. (color online) (a) The temperature dependence of magnetic entropy change curves for $Ho_{12}Co_7$ compound under a field change of 0 T–0.5 T, 0 T–1 T, 0 T–2 T, 0 T–3 T, 0 T–4 T, 0 T–5 T, 0 T–6 T, and 0 T–7 T, respectively. (b) Temperature dependences of magnetic entropy change calculated from magnetization and heat capacity data for field changes of 0–0.5 T, 0 T–2 T, and 0 T–5 T, respectively. (c) Temperature dependences of magnetic entropy change calculated from magnetization only for field changes of 0–0.2 T, 0–0.3 T, 0–0.4 T, and 0–0.5 T, respectively.[18]

One can also see from Fig. 45(b) that both the peak value and peak width of ΔS_M–T curves depend on the magnetic field change. When the field change is 0 T–0.5 T, the maximum value of the two peaks are small and they are far apart from each other. However, when the applied field increases to 2 T and 5 T, the two peaks become one large peak. That is to say, both of the maximal value and the width of the peak have an obvious increase. The peak shape is very helpful to improvement of the value of *RC* in $Ho_{12}Co_7$ compound. The *RC* value of $Ho_{12}Co_7$ is estimated to be 206.2 J/kg with $T_1 = 10.4$ K (temperature of the cold reservoir) and $T_2 = 39.8$ K (temperature of the hot reservoir) for a field changing from 0 T to 2 T. And the *RC* value is estimated to be 554.9 J/kg with $T_1 = 12.3$ K and $T_2 = 49.8$ K for a field changing from 0 T to 5 T. As a result, $Ho_{12}Co_7$ compound has an outstanding refrigerant capacity among the magnetocaloric materials in a similar temperature range, such as ErGa (*RC* = 494 J/kg with $T_1 = 14.3$ K and $T_2 = 45.2$ K),[19] DyCuAl (*RC* = 427 J/kg with $T_1 = 17$ K and $T_2 = 45$ K),[16] $ErCo_2$ (*RC* = 273 J/kg with $T_1 = 33$ K and $T_2 = 43$ K),[101] DyNiAl (*RC* = 492 J/kg with $T_1 = 19$ K and $T_2 = 53$ K),[102] TbCoC_2 (*RC* = 354 J/kg with $T_1 = 23.5$ K and $T_2 = 50$ K),[103] and $GdNi_5$ (*RC* = 198 J/kg with $T_1 = 21$ K and $T_2 = 45$ K),[104] although ErGa, DyCuAl, and $ErCo_2$ exhibit larger ΔS_M values. Here, the *RC* values of some compounds are estimated from the temperature dependence of ΔS_M in the literatures, respectively. The large value of ΔS_M and *RC* suggests that $Ho_{12}Co_7$ can be an appropriate candidate for magnetic refrigerant in low temperature ranges.

Figure 46 shows the temperature dependencies of ΔS_M under the applied magnetic field change from 0 T to 5 T. And the inset of Fig. 46 shows the ΔS_M curves of $Tb_{12}Co_7$ compound under the field change of 0 T–1 T and 0 T–2 T, respectively. The peak values of ΔS_M are found to be 8.8, 8.2, and 7.1 J/kg·K for the alloys with $x = 0$, 4, and 8, respectively.[92] The *RC* values are calculated to be 478.4 J/kg, 327.2 J/kg, and 160.2J/kg for $Gd_{12-x}Tb_xCo_7$ alloys with $x = 0$, 4, and 8, respectively.[92] It should be noted that no obvious peak is found around the T_{SR} of $Gd_{12}Co_7$ compound. There are two possible reasons for the absence of the peak in low temperature range: firstly, the magnetic measurement was not carried out as low as possible; secondly, the SR transition is too weak.

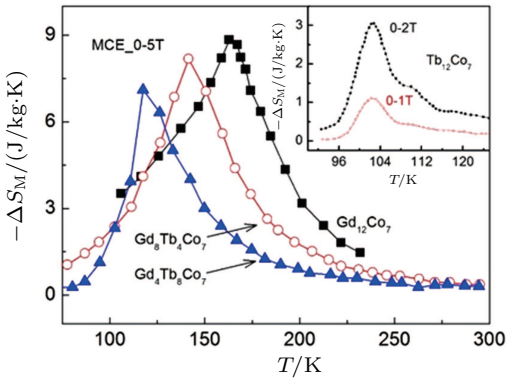

Fig. 46. (color online) The temperature dependence of magnetic entropy change curves under a field change of 0 T–5 T for $Gd_{12}Co_7$, $Gd_8Tb_4Co_7$, and $Gd_4Tb_8Co_7$ compounds, respectively. The inset is the temperature dependence of magnetic entropy change curves for $Tb_{12}Co_7$ compound under a field change of 0 T–1 T and 0 T–2 T, respectively.[92]

The ΔS_M (T) curves of $Ho_xEr_{12-x}Co_7$ ($x = 0$, 4, 6, 8, 10, 12) compounds for a field change of 0 T–2 T and 0 T–5 T are shown in Fig. 47, respectively.[93] The maximum value of ΔS_M for each $Ho_xEr_{12-x}Co_7$ ($x = 0$, 4, 6, 8, 10, 12) compounds is listed in Table 5. Two peaks are observed obviously on the ΔS_M curve of $Ho_{12}Co_7$ compound. Actually, this kind

of multi-peaks ΔS_M curves has been observed in many magnetocaloric materials with several transitions, such as ErGa, HoNi, TbGa, DyGa, etc.[19,32,78] For other $Ho_xEr_{12-x}Co_7$ compounds, only one peak around T_C can be observed and in low temperature zone there is a small convex instead of a peak. For $Er_{12}Co_7$ compound the small convex can even hardly be observed.

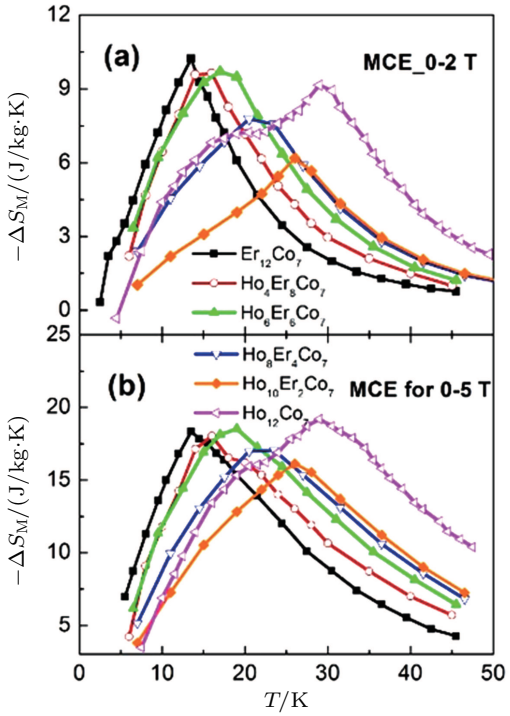

Fig. 47. (color online) (a) The temperature dependence of magnetic entropy change curves under a field change of 0 T–2 T for $Ho_xEr_{12-x}Co_7$ ($x = 0$, 4, 6, 8, 10, 12) compounds, respectively. (b) The temperature dependence of magnetic entropy change curves under a field change of 0 T–5 T for $Ho_xEr_{12-x}Co_7$ ($x = 0$, 4, 6, 8, 10, 12) compounds, respectively.[93]

Another important parameter to evaluate the magnetocaloric materials is refrigerant capacity (*RC*) and it has been also calculated. All of the parameters, $-(\Delta S_M)_{max}$, *RC*, and T_{width}, are listed in Table 5. As the content of Ho atoms goes up, the T_{width} of $Ho_xEr_{12-x}Co_7$ ($x = 0$, 4, 6, 8, 10, 12) compounds increases steadily. The change characteristics of T_{width} are closely related to the transition temperatures. According to the analysis of transition temperatures, T_1 changes slightly and T_C increases rapidly as the content of Ho atoms goes up. Therefore, T_{width} shows an increase with the content of Ho atoms. The *RC* shows a similar changing trend to T_{width}, but $Ho_{10}Er_2Co_7$ compound is an exception. Though the maximum of ΔS_M is not so large, the T_{width} and *RC* show good performance for $Ho_xEr_{12-x}Co_7$ ($x = 0$, 4, 6, 8, 10, 12) compounds.

For the actual application of magnetocaloric materials in refrigerators, the materials with table-like ΔS_M curves have more important value. That is because a much wider temperature range of cooling can be realized by this kind of magnetocaloric materials. The magnetocaloric materials with a plateau on ΔS_M curve are so useful that people have made efforts to design them by mixing different kinks of materials, such as R_3Ni_2 and RFeSi.[105,106] Considering that each $Ho_xEr_{12-x}Co_7$ ($x = 0$, 4, 6, 8, 10, 12) compound shows advantages on MCE at different temperature zones, the $Ho_xEr_{12-x}Co_7$ compounds are mixed at different weight proportions with each two as one group. It is found that when $Ho_{12}Co_7$ and $Ho_6Er_6Co_7$ compounds are combined at the weight ratio of 58:42, the mixed magnetocaloric material shows the best performance (Fig. 48). The maximum of ΔS_M is 16.7 J/kg·K, and the T_{width} and *RC* are as high as 38 K and 553 J/kg, respectively. The *RC* of newly obtained material is comparable to $Ho_{12}Co_7$ compound and the T_{width} is even better. The most important is that there is a plateau on the ΔS_M curve, which means that the mixed compounds of $Ho_{12}Co_7$ and $Ho_6Er_6Co_7$ with a weight ratio of 58:42 has a larger using value. The excellent MCE performance indicates its potential use for cooling in the temperature range around 20 K–30 K.

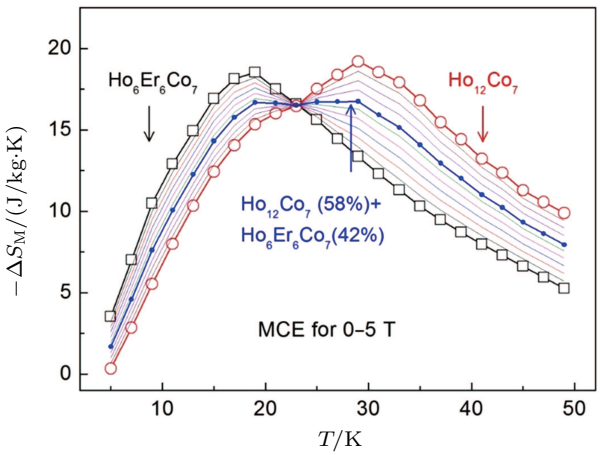

Fig. 48. (color online) The temperature dependence of magnetic entropy change curves under a field change of 0 T–5 T for the $Ho_{12}Co_7$ compound, $Ho_6Er_6Co_7$ compound and the mixture of the two compounds with different ratio.[93]

5. The R_3Co compounds

In recent years, much attention has been paid to the rare-earth (*R*)-based intermetallic compounds with a low temperature phase transition for the purpose of magnetic refrigerant application.[18,107–109] Among the *R*-based compounds, the binary R_3T (T = Co and Ni) series with the highest rare-earth content is a subject of special attention. Although these compounds have identical crystallographic structures, they exhibit complex magnetic structures and possess different magnetic-phase transitions, which will induce interesting magnetocaloric properties.[49] The magnetic properties of R_3Co (R = Gd, Tb, Dy, Ho, Er) compounds were also studied by the magnetization, electrical resistivity, and NMR measurements.[110] The magnetic ordering temperatures were obtained from the electrical resistivity measurement and the complex magnetic susceptibilities were explained by the metamagnetic transition under an applied field.[110] Specific heat measurements were performed in wide temperature range

$T = 2$ K–300 K for the R_3Co (R = Er–Gd, Y) compounds. Using values of the Sommerfeld coefficient and Debye temperature estimated for Y_3Co compound, the Debye temperatures, phonon and conduction electron contributions as well as magnetic contribution to the specific heat were estimated for all other R_3Co compounds.[111]

Based on magnetization, magnetoresistance, a.c. susceptibility, and specific heat, magnetic phase diagrams of the compound Dy_3Co were obtained for the main crystallographic axis.[112] The different AFM structures exist below $T_N = 44$ K: AFM1 exists at $T < T_t = 32$ K and AFM2 exists at the temperatures between T_t and T_N.[112] The field-induced magnetic phase transitions observed along the three main axes are associated with a complex non-collinear AFM structure and are accompanied by a significant change in the electrical resistivity.[112] Electrical resistivity and calorimetric measurements on single crystal Dy_3Co show that below $T_N = 44$ K the non-collinear antiferromagnetic structure exhibits field-induced magnetic phase transitions of a first-order type along all principal axes, accompanied by a strongly anisotropic giant magnetoresistance and by a change of the Sommerfeld coefficient of the specific heat.[113] The neutron elastic scattering experiments were used to determine the structural parameters and comparative analysis of the possible magnetic structures in the ground state of Dy_3Co.[114]

The single crystal Er_3Co compound has been investigated by means of magnetic susceptibility, magnetization, electrical resistivity, and heat capacity measurements.[115] Complex non-collinear ferromagnetic structure was observed below 13.8 K. Using the magnetization and magnetoresistance measurements along the main crystallographic directions, a complicated and anisotropic magnetization process was revealed.[115] Magnetic and magnetocaloric properties of polycrystalline samples of Gd_3Co have been studied. The Gd_3Co compound is antiferromagnets with $T_N = 128$ K and it undergoes metamagnetic transition in the AFM phase. The maximum values of isothermal magnetic entropy change are 11 J/kg·K.[116] The magnetic and transport properties of single crystal Tb_3Co compound were studied. The orthorhombic Tb_3Co compound exhibits both FM and AFM behaviors below the critical temperature $T_t \approx 72$ K as evidenced by metamagnetic transitions along the a and b axes and ferromagnetic magnetization process along the c axis.[117] Field-induced transitions along all three axes are observed between T_t and T_N (82 K).[117] And the metamagnetic transitions are accompanied by a significant magnetoresistance effect.[117] The measurements of the magnetization in high steady and pulsed fields together with neutron diffraction measurements on a powder sample and on a single crystal have been performed to study the magnetic state of the Tb_3Co compound.[118] It has been shown that the modulated antiferromagnetic structure which exists in Tb_3Co below $T_{Na} = 82$ K transforms to the incommensurate magnetic structure with a strong ferromagnetic component along the c axis with further cooling below the critical temperature $T_t \approx 72$ K. The phase transition from the high-temperature to the low-temperature magnetic state at T_t is of the first order.[118]

A large reversible magnetocaloric effect has been observed in Tb_3Co compound. Under a magnetic field change of 5 T, the maximum value of magnetic entropy change ΔS_M is -18 J/kg·K at 84 K and the relative cooling power is 738 J/kg with no hysteresis loss.[119] Magnetic properties and magnetocaloric effect of the Dy_3Co compound are studied. The maximal value of magnetic entropy change ΔS_M is -13.9 J/kg·K with a refrigerant capacity (RC) of 498 J/kg around T_N for a field change of 0 T–5 T.[49] And the magnetic properties and magnetocaloric effects of Ho_3Co, Er_3Co, Tm_3Co, and $Er_{3-x}Gd_x$Co compounds have also been studied in detail.[120–124] In the following section, the above contents especially MCEs will be reviewed. And the data of Tb3Co compound is cited from literature.[119]

5.1. The magnetic properties of R_3Co compounds and $Er_{3-x}Gd_x$Co compounds

Polycrystalline R_3Co (R = Gd, Tb, Dy, Ho, Er, Tm) and $Er_{3-x}Gd_x$Co ($0 \leq x \leq 3$) compounds were prepared by arc melting in a high-purity argon atmosphere. The purities of starting materials were 99.9% for R and Co. The sample was turned over and remelted several times to ensure its homogeneity. The ingot obtained by arc melting was wrapped by molybdenum foil, sealed in a quartz tube of high vacuum, annealed at 873 K for 4–8 days and then quenched to room temperature.[49,119] X-ray diffraction (XRD) measurements on powder samples were performed by using CuKα radiation to identify the crystal structure. Magnetizations were measured as functions of temperature and magnetic field by using a superconducting quantum interference device (SQUID) magnetometer and vibrate sample magnetometer (VSM). Both the ac susceptibility and the specific heat were measured by using a physical property measurement system (PPMS) from Quantum Design. The powder XRD patterns of R_3Co (R = Gd, Tb, Dy, Ho, Er, Tm) and $Er_{3-x}Gd_x$Co ($0 \leq x \leq 3$) compounds obtained at room temperature were refined by the Rietveld method. The refinement shows that the prepared sample is of single phase, crystallizing in the orthorhombic Fe_3C-type crystal structure (space group *Pnma* #62). The crystal structure of R_3Co compounds is shown in Fig. 49. R atoms occupy two nonequivalent positions [4c (R4c) and 8d (R8d)] and Co atoms are located at the 4c position within the trigonal prisms formed by Tm atoms. Results of all the structural parameters are determined by the Rietveld technique using GSAS program.[123] For $Er_{3-x}Gd_x$Co ($0 \leq x \leq 3$) compounds, with increasing Gd concentration, the diffraction peaks move to the left and the unit cell volume increases linearly. It is attributed to the contraction law of rare-earth intermetallic compound (the bigger atomic radius of the Gd atom than Er).[122]

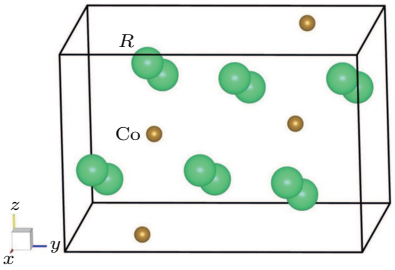

Fig. 49. (color online) The crystal structure of R_3Co compounds.

The temperature dependences of zero-field-cooling (ZFC) and field-cooling (FC) magnetization (M) for Tb_3Co, Ho_3Co, Er_3Co, and Tm_3Co compounds were measured and they are shown in Fig. 50(b), Fig. 50(d), Fig. 50(e), and Fig. 50(f), respectively. The applied field is different and the field is 0.005 T, 0.01 T, 0.05 T, and 0.01 T for Tb_3Co, Ho_3Co, Er_3Co, and Tm_3Co compounds, respectively. The ZFC curves of Gd_3Co and Dy_3Co compounds are shown in Fig. 50(a) and Fig. 50(c), respectively and the applied field is 0.01 T. Although the crystal structure of R_3Co (R = Gd, Tb, Dy, Ho, Er, Tm) compounds is the same, the magnetic properties of them differs from each other a lot. Results show that Gd_3Co is a simple AFM material and it undergoes an AFM to PM transition at $T_N = 129$ K as temperature increases.[122] According to neutron diffraction investigation by Baranov *et al.*,[118] Tb_3Co undergoes two successive transitions at temperatures T_t=72 K (FM to AFM transition) and T_N=82 K (AFM to PM transition), corresponding to the maximum slopes in the M–T curve (Fig. 50(b)). The neutron diffraction investigation suggested that the incommensurate FM state, at T_t for a first-order magnetic phase transition, develops to a modulated AFM state that exists below T_N.[118] On the other hand, reversible behavior above 50 K in ZFC and FC curves at a magnetic field of 1 T (not shown here) indicates that Tb_3Co experiences a second-order FM to PM phase transition at $T_C = 82$ K.[119] Arrott plots also confirm its second-order nature. It can be deduced that a small magnetic field, less than 1 T, can induce a metamagnetic transition from AFM to FM state.[119] It is found that the Ho_3Co compound undergoes two successive magnetic phase transitions at low temperatures (see Fig. 50(d)), corresponding to the two maximal values of M–T curve. As revealed by the neutron diffraction studies,[125] the Ho_3Co compound exhibits a PM to AFM transition at $T_N = 21$ K, followed by a spin–reorientation transition at $T_{SR} = 8.5$ K. The anomaly at about 30 K in the M–T curve may be attributed to the existence of a minor amount of impurity phase, because no anomaly of

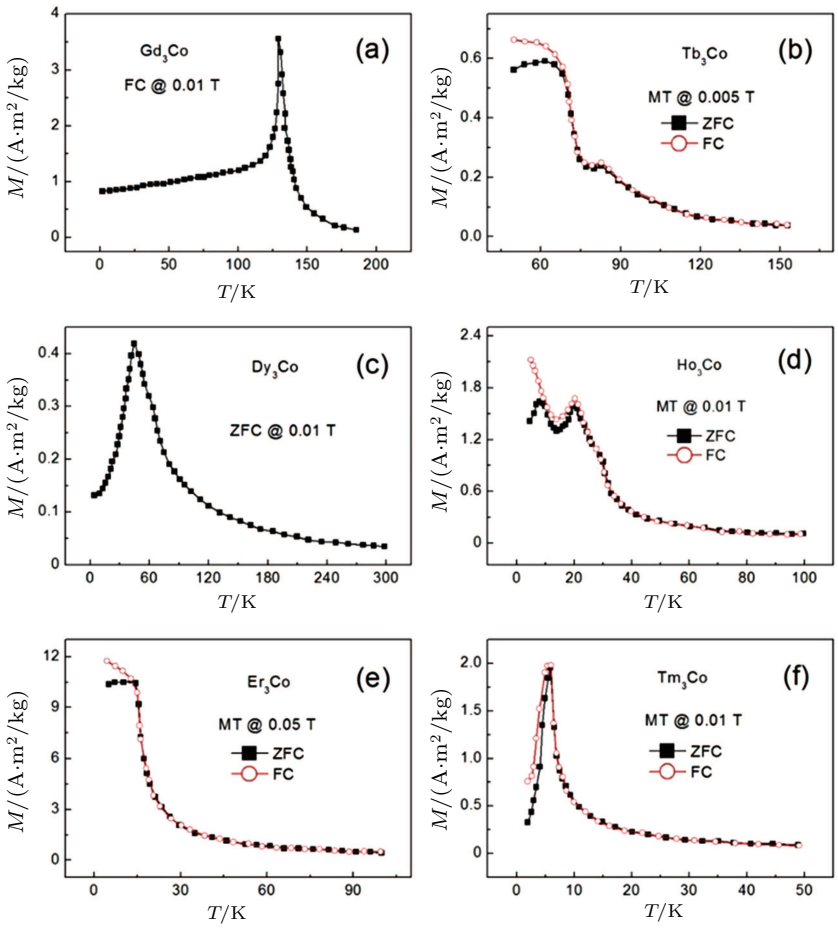

Fig. 50. (color online) (a) The temperature dependence of magnetization curve for Gd_3Co compound under the field of 0.01 T. (b) The ZFC and FC curves for Tb_3Co compound under the field of 0.005 T. (c) The temperature dependence of magnetization curve for Dy_3Co compound under the field of 0.01 T. (d) The ZFC and FC curves for Ho_3Co compound under the field of 0.01 T. (e) The ZFC and FC curves for Er_3Co compound under the field of 0.05 T. (f) The temperature dependence of magnetization curve for Tm_3Co compound under the field of 0.01 T.[49,119–123]

magnetization at the same temperature was observed based on the results reported by Baranov *et al.*[126] and Nagai *et al.*[110]

It can be seen from Fig. 50(e) that Er_3Co undergoes a magnetic transition from FM to PM states, and its Curie temperature T_C is determined to be 13 K, which is in good agreement with the value reported by Saito *et al.*[127] In addition, it is also observed that there is no hysteresis in ZFC and FC curves above T_C. Below T_C, the difference between the ZFC and FC curves may be related to the domain-wall pinning effect.[121] It can be seen that there is almost no thermal hysteresis between the ZFC and FC curves for Tm_3Co compound when the temperature increases above 6.5 K from Fig. 50(f). The small bifurcation may be related to the domain-wall pinning effect below 6.5 K. The dM/dT versus T curve reveals that the Tm_3Co undergoes an AFM to FM transition at $T_N = 4.5$ K and an FM to PM transition at $T_C = 6.5$ K, which is corresponding to the minimum value of dM/dT.[123] The temperature dependence of specific heat (C_p) in a zero-field for Dy_3Co was measured and is shown in Fig. 51. The magnetic property and magnetic transition of Dy_3Co compound will be discussed based on Fig. 50(c) and Fig. 51. The results show that Dy_3Co has two successive magnetic transitions as reported by Baranov *et al.* previously.[112] The anomaly at lower temperature may be associated with the phase transition from one AFM to another AFM state.[112] The transition temperature ($T_{AF} = 29$ K), determined by the position of the low-temperature peak on the specific heat curve, is fully consistent with the value derived from the (dM/dT)–T curve.[49] The transition at higher temperature corresponds to a change from AFM to PM state as temperature increases. The Neel temperature T_N is determined to be 44 K, which is in good agreement with the previous results.[112,113] The temperature dependences of the magnetization at different magnetic fields have also been measured. It is observed that the magnetic fields can drive magnetic transition temperatures T_{AF} and T_N to lower temperature and a field-induced metamagnetic transition from AFM to FM state is present below T_N.[49] When the applied magnetic field is higher than about 1.2 T, the magnetization as a function of temperature for Dy_3Co exhibits step-like behavior above T_N, which corresponds to the FM to PM transition.[49]

The temperature (T) dependences of magnetization (M) data measured in an applied field of 0.01 T under zero-field-cooling (ZFC) and field-cooling (FC) conditions for $Er_{3-x}Gd_xCo$ ($x = 0$, 0.5, 1, 1.5, 2, 2.5, 3) compounds are shown in Fig. 52. The compound Er_3Co shows an FM-like transition at 13 K due to the thermomagnetic irreversibility between ZFC and FC curves.[122] It is obvious that the compound with $x = 0.5$ shows two successive magnetic transitions at $T_{N1} = 28$ K which shows the transition from PM to AFM, and $T_{N2} = 13$ K which coincides to the transition from AFM to FM-like order.[122] However, two transition behaviors seem to disappear instead of a magnetic plateau emerges below T_N for the compounds with $x > 0.05$. Only a sharp AFM transition is observed and T_N linearly shifts to higher temperature with x.[122] No thermal hysteresis is observed between ZFC and FC curves around T_N for the compounds with $x > 0.05$, which is a characteristic of the second-order magnetic transition.[122]

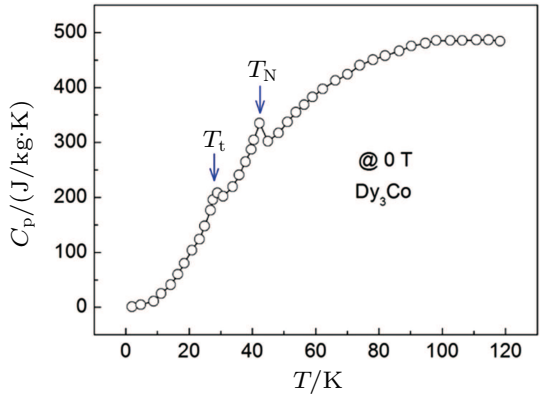

Fig. 51. (color online) The temperature dependence of heat capacity at zero-field for Dy_3Co compound.[49]

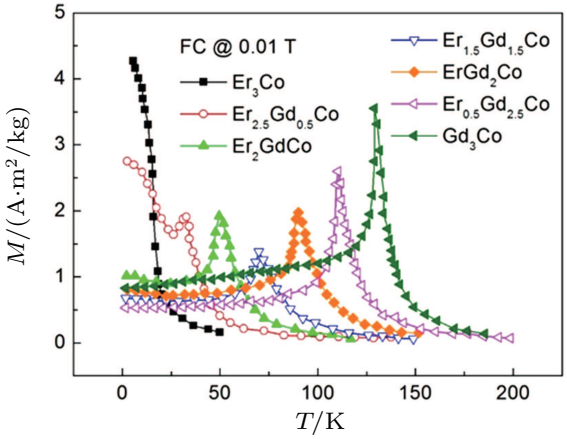

Fig. 52. (color online) The temperature dependences of magnetization curves at a field of 0.01 T for $Er_{3-x}Gd_xCo$ ($x = 0$, 0.5, 1, 1.5, 2, 2.5, 3) compounds, respectively.[122]

All of the magnetic transition temperatures of R_3Co ($R =$ Gd, Tb, Dy, Ho, Er, Tm) and $Er_{3-x}Gd_xCo$ ($x = 0$, 0.5, 1, 1.5, 2, 2.5, 3) compounds have been listed in Table 6. From the table it can be seen that the magnetic property and magnetic transition for R_3Co compound are different from each other. It undergoes two magnetic transitions as temperature increases for Tb_3Co, Dy_3Co, Ho_3Co, Tm_3Co, and $Er_{2.5}Gd_{0.5}Co$ compounds. It undergoes only one magnetic transition as temperature increases for Gd_3Co, Er_3Co, Er_2Gd_1Co, $Er_{1.5}Gd_{1.5}Co$, Er_1Gd_2Co, and $Er_{0.5}Gd_{2.5}Co$ compounds. The Curie temperature or Neel temperature decreases as the rare earth atom number increases for R_3Co ($R =$ Gd, Tb, Dy, Ho, Er, Tm) compounds. That is because the spin angular moment quantum number (S) decreases as atom number increases for Lanthanum series and S is positively correlated with order-disorder transition temperature. With the same reason, it is found that the order–disorder transition temperature increases as the content of Gd atoms in $Er_{3-x}Gd_xCo$ ($x = 0$, 0.5, 1, 1.5, 2, 2.5, 3) compounds.

Table 6. The transition temperatures and magnetocaloric parameters of R_3Co (R = Gd, Tb, Dy, Ho, Er, Tm) and $Er_{3-x}Gd_xCo$ ($0 \le x \le 3$) compounds.

Materials	T_t/K	(T_C/T_N)/K	MCE_0–2 T			MCE_0–5 T			Ref.
			$-\Delta S_M(T)_{max}$/(J/kg·K)	T_{width}/K	RC/(J/kg)	$-\Delta S_M(T)_{max}$/(J/kg·K)	T_{width}/K	RC/(J/kg)	
Gd_3Co	–	129	–	–	–	11.1	60	505.4	[122]
Tb_3Co	72	82	8.5	26.2	177.1	18	39.3	532	[119]
Dy_3Co	29	44	5	33.3	111	13.9	45	498	[49]
Ho_3Co	8	21	6.5	29.3	151.6	14.5	38.5	440	[120]
Er_3Co	–	13/13	12.5/–	16.5/–	163/–	24.5/24.6	24.8/25.1	476/480	[121]
Tm_3Co	4.5	6.5	11.6	8.1	72	19.9	15.3	230.9	[123]
$Er_{2.5}Gd_{0.5}Co$	13	28	–	–	–	13.1	44.6	472	[122]
Er_2Gd_1Co	–	50	–	–	–	11.1	68.7	619.5	[122]
$Er_{1.5}Gd_{1.5}Co$	–	70.2	–	–	–	9.8	83.2	624.5	[122]
Er_1Gd_2Co	–	90	–	–	–	10.3	77.4	591.4	[122]
$Er_{0.5}Gd_{2.5}Co$	–	110.7	–	–	–	11	63.2	518.3	[122]

5.2. The magnetocaloric effects of R_3Co compounds and $Er_{3-x}Gd_xCo$ compounds

The temperature dependences of ΔS_M for R_3Co (R = Gd, Tb, Dy, Ho, Er, Tm) compounds calculated by using Maxwell relation formula under a magnetic field change of 0 T–2 T and 0 T–5 T are shown in Fig. 53(a) and Fig. 53(b), respectively.

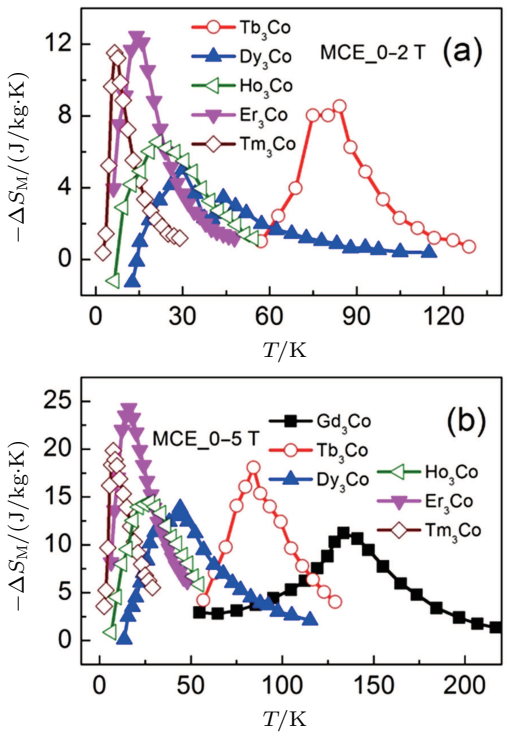

Fig. 53. (color online) (a) The temperature dependences of magnetic entropy change under a field change of 0 T–2 T for R_3Co (R = Tb, Dy, Ho, Er, Tm) compounds, respectively. (b) The temperature dependences of magnetic entropy change under a field change of 0 T–5 T for R_3Co (R = Gd, Tb, Dy, Ho, Er, Tm) compounds, respectively.[46]

For Tb_3Co compound, the maximum of ΔS_M is −8.5, −12.3, −18, and −22.6 J/kg·K, respectively, for the magnetic field changes of 2, 3, 5, and 7 T.[119] The large ΔS_M, −8.5 J/kg·K achieved for a low magnetic field change of 2 T, is beneficial to application.[119] The peaks of ΔS_M at 84 K are just corresponding to the FM to PM phase transition. It is clearly observed that the ΔS_M–T curves of Dy_3Co exhibit two maximum values at 29 K and 44 K, respectively, which corresponds to the two transitions at T_{AF} and T_N. The maximum value of ΔS_M for Dy_3Co is found to be −13.9 J/kg·K around T_N for a magnetic-field change from 0 T to 5 T.[49] It is apparent that the large ΔS_M in Dy_3Co is associated with the field-induced metamagnetic transition below T_N. The refrigerant capacity (RC) of Dy_3Co compound has been also calculated by numerically integrating the area under the ΔS_M–T curve, with the temperatures at half maximum of the peak used as the integration limits.[53] The RC value thus obtained for Dy_3Co is 498 J/kg with T_{cold} = 23.5 K (temperature of the cold reservoir) and T_{hot} = 68.5 K (temperature of the hot reservoir) for a field changing from 0 T to 5 T.[49] The large RC originates from the combined contribution of two successive magnetic transitions, which enlarge the temperature span of large MCE. The full width at half maximum of the ΔS_M peak under a magnetic field of 5 T attains ΔT = 45 K ($\Delta T = T_{hot} - T_{cold}$) for Dy_3Co due to the superposition of the AFM-to-AFM and AFM-to-PM phase transitions.[49]

The values of ΔS_M for Ho_3Co are positive at temperatures below 7 K and at lower magnetic field, but they change to a negative value with the increase of applied field due to the field-induced magnetic transition from AFM to FM state.[120] The positive ΔS_M (negative MCE) is often observed in magnetocaloric materials with the first order magnetic transitions,[9] which results from the mixed exchange interaction, and the applied magnetic field leads to a further spin-disordered state near the transition temperature, thereby increasing the entropy.[10] A small positive value of ΔS_M also indicates a weak AFM coupling in Ho_3Co at low temperatures. It can be seen from Fig. 53 that the peak of the ΔS_M–T curve of Ho_3Co shows a broad distribution due to its successive magnetic transitions. The maximal values of ΔS_M for Ho_3Co are found to be −6.5 J/kg·K and −14.5 J/kg·K for field changes of

0 T–2 T and 0 T–5 T, respectively.[120] The large ΔS_M results from the high saturation magnetization and is caused by the field-induced AFM-to-FM metamagnetic transition.

For Er_3Co compound, both the peak and the width of ΔS_M depend on the applied magnetic field, and increase obviously with increasing field. The temperature dependences of ΔS_M exhibit a λ-shape profile as shown usually in magnetic materials with a second-order magnetic transition. A giant ΔS_M, which results from a second-order FM-to-PM transition, is observed in Er_3Co around T_C. The maximal value of ΔS_M for Er_3Co is found to increase monotonously with applied magnetic field and reaches a value of 24.5 J/kg·K at 16 K for a field change of 0 T–5 T.[121] It is interesting to note that a large reversible ΔS_M for Er_3Co is as high as 12.5 J/kg·K for a field change of 0 T–2 T, which is beneficial to the practical applications because a magnetic field of 2 T can be supplied by a permanent magnet.[121] Calculations show that the maximal value of *RC* for Er_3Co is 476 J/kg for a magnetic field change of 0 T–5 T. In particular, a high value of *RC* is also obtained to be 163 J/kg for a relatively low field change of 0 T–2 T.[121] This is attributed to the appreciably large values of ΔS_M obtained at T_C for Er_3Co.

The maximum value of ΔS_M for Tm_3Co compound is found to increase monotonically with the increase of applied magnetic field and reaches a value of 19.9 J/kg·K for a magnetic field change from 0 T to 5 T. In particular, the maximum value of ΔS_M is found to be 11.6 J/kg·K under a low magnetic change of 2 T, which can be realized by permanent magnet and be advantageous for applications.[123] The large ΔS_M of Tm_3Co compound origins from the field-induced metamagnetic transition from AFM to FM. Moreover, the ΔS_M does not die out even at temperatures well above T_C, possibly due to the presence of spin fluctuations.[124] All of the MCE parameters for R_3Co (R = Gd, Tb, Dy, Ho, Er, Tm) compounds are listed in Table 6.

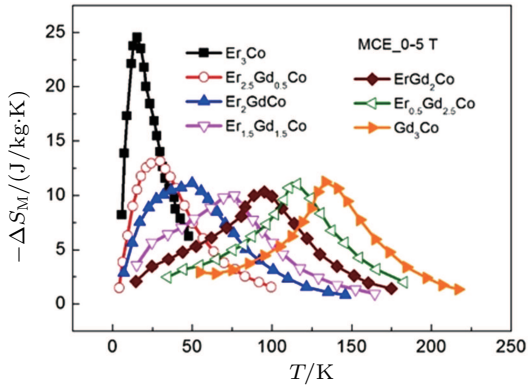

Fig. 54. (color online) The temperature dependences of magnetic entropy change under a field change of 0 T–5 T for $Er_{3-x}Gd_xCo$ (x = 0, 0.5, 1, 1.5, 2, 2.5, 3) compounds, respectively.[122]

The ΔS_M–T curves of $Er_{3-x}Gd_xCo$ (x = 0–3) compounds under magnetic field changes of 0 T–5 T are calculated and shown in Fig. 54. And the related MCE parameters are also listed in Table 6. It can be noted from the ΔS_M–T curves that ΔS_M does not die out even at temperature well above the T_N. This may be attributed to the short range magnetic correlations associated with spin fluctuations.[124] Since the Er_3Co compound undergoes a magnetic transition from PM to FM state, and at the same situation, the Gd_3Co undergoes a magnetic transition from PM to AFM state, the interaction between the Er_3Co and Gd_3Co results in a spin-reorientation transition at lower temperature.[122] Therefore, two obvious peaks of Er_2Gd_1Co can be clearly visualized. The values of ΔS_M for $Er_{3-x}Gd_xCo$ are negative at relative low temperatures and low magnetic field, and the values are changed to positive with the increase of applied field.

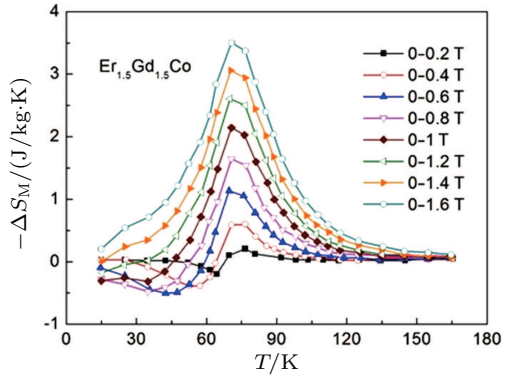

Fig. 55. (color online) The temperature dependences of magnetic entropy change under low field change for $Er_{1.5}Gd_{1.5}Co$ compound.[122]

Take the $Er_{1.5}Gd_{1.5}Co$ for instance, figure 55 shows that the ΔS_M curve of $Er_{1.5}Gd_{1.5}Co$ is negative below the transition temperature for a low magnetic field change. When the value of ΔS_M is negative, the negative value first decreases and then increases with the increase of magnetic field. It indicates the magnetic transition from AFM to FM states.[122] The ΔS_M changes to a positive value with the magnetic field increasing, which is corresponding to the magnetic transition from FM to PM states. A large magnetic entropy change results from the field-induced metamagnetic transition of FM to PM for $Er_{1.5}Gd_{1.5}Co$.[122] This phenomenon results from the mixed exchange interaction, and the applied magnetic field leads to a further spin-disordered state near the transition temperature, thereby enlarges entropy.[10,122] It is observed that the ΔS_M decreases from 24.6 J/kg·K (x = 0) to 9.8 J/kg·K (x = 1.5) with x, then increases from 9.8 J/kg·K (x = 1.5) to 11.1 J/kg·K (x = 3) for a field change of 0 T–5 T.[122] However, the *RC* shows a contrasting behavior. The *RC* value increases with x showing a maximum value of 624.5 J/kg for 0 T–5 T at intermediate content of x = 1.5, which is 30% and 23.6% higher than that of Er_3Co and Gd_3Co, respectively.[122] Then, the *RC* value decreases with x above 1.5. This phenomenon is attributed to the trend of temperature span with x based on the definition of *RC*. It shows a widest temperature span of 83.2 K of ΔS_M

in $Er_{1.5}Gd_{1.5}Co$ compound due to the most preferred chemical proportion with intermediate substitution of $x = 1.5$.[122]

6. The RCu_2 compounds

In recent years, the rare-earth (R) based intermetallic compounds with a low temperature phase transition have drawn much attention for the applications in low-temperature magnetic refrigeration. RCu_2 series are one of the important categories of R-based intermetallic compounds and the magnetic properties of RCu_2 (R = Ce, Pr, Nd, Sm, Eu, Gd, Tb, Dy, Ho, Er, Tm, Yb, and Lu) compounds have been investigated by Sherwood *et al.*[128] Especially, the magnetic properties of the single crystal samples have been studied in detail.[129–132] Much work has also been done on the specific heat, magnetoresistance, magnetostriction in RCu_2 compounds.[132–137] The magnetic structures of some RCu_2 compounds were determined by employing Neutron diffraction experiments.[138–140] The ground state for most RCu_2 compounds is AFM state and field-induced metamagnetic transition was observed with a critical magnetic field.[128] More than one magnetic transitions were observed in $HoCu_2$ compounds, and the transition temperatures were determined to be 7.4 K and 10.5 K, respectively.[133,136,138] The MCE of $HoCu_2$ and $DyCu_2$ compounds have been studied. A large effective refrigerant capacity of 194 J/kg below 44 K was obtained in $DyCu_2$ compound, and a maximum magnetic entropy change of 19.3 J/kg·K with a relative cooling power of 268 J/kg was found in $HoCu_2$ compound.[97,141] In this work, the RCu_2 (R = Gd, Tb, Dy, Ho, Er) compounds were synthesized successfully.[142] The magnetic properties and magnetocaloric effect were investigated in detail. Though the MCEs of $DyCu_2$ and $HoCu_2$ compounds have been studied, the two compounds are still fabricated and investigated newly.

6.1. The crystal structure and magnetic properties of RCu_2 compounds

Binary polycrystalline RCu_2 (R = Gd, Tb, Dy, Ho, Er) compounds were fabricated by arc-melting method and powder x-ray diffraction (XRD) was performed to confirm their phase purity. The room temperature XRD patterns of RCu_2 (R = Gd, Tb, Dy, Ho, Er) compounds are all shown in Fig. 56. Almost all of the diffraction peaks can be indexed to an orthorhombic crystal structure (space group *Imma* #74). The result is in accord with previous work.[140] The Bragg positions are marked at the bottom of the figure. It can also be seen that there is a small impure peak at 31.7° for $ErCu_2$ compound, which indicates that small amount of impurity may exist. However, that does not affect the discussion in the following section because the purity is negligible. That is to say, almost all the obtained RCu_2 (R = Gd, Tb, Dy, Ho, Er) compounds are pure single phase.

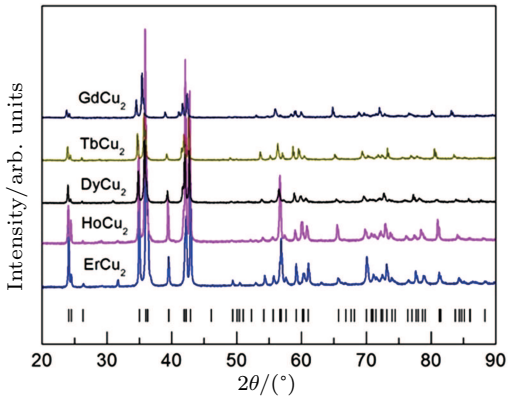

Fig. 56. (color online) The XRD patterns of RCu_2 (R = Gd, Tb, Dy, Ho, Er) compounds measured at room temperature. The vertical bars are corresponding to the Bragg positions.[142]

The lattice parameters were determined by using Rietveld refinement method. For example, the lattice constant of $HoCu_2$ compound is calculated as follows: $a = 4.2865(3)$ Å, $b = 6.7766(6)$ Å, and $c = 7.2754(6)$ Å. As the atom number of R increases, the position of peak moves towards higher angle range. It indicates that the lattice constant becomes smaller and smaller from $GdCu_2$ to $ErCu_2$ compound. It has been described as follows: the RCu_2 compounds crystallize in orthorhombic $CeCu_2$-type structure, which can be considered as a stacking of alternating layers of R and Cu atoms along c axis of crystal.[140] The crystal structure of RCu_2 compounds is shown in Fig. 57. There are four R atoms in form of one parallelogram along with two triangles and eight Cu atoms in form of two triangular prisms in the unit cell.

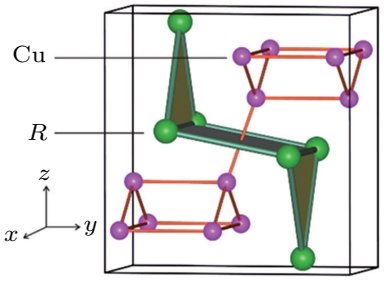

Fig. 57. (color online) The crystal structure of RCu_2 (R = Gd, Tb, Dy, Ho, Er) compounds.[142]

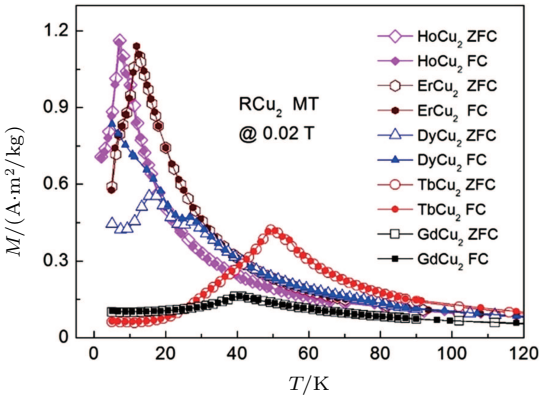

Fig. 58. (color online) The zero-field-cooled and field-cooled magnetization curves of RCu_2 (R = Gd, Tb, Dy, Ho, Er) compounds under a field of 0.02 T.

The temperature dependences of zero-field-cooled (ZFC) and field-cooled (FC) magnetization were measured under a field of 0.02 T for the RCu$_2$ (R = Gd, Tb, Dy, Ho, Er) compounds.[142] And the ZFC and FC curves are shown in Fig. 58. As temperature increases, GdCu$_2$ compound undergoes only one AFM to PM magnetic transition and the Neel temperature is determined to be 40.5 K. As temperature increases, TbCu$_2$ compound undergoes an AFM to AFM transition and an AFM to PM transition at 23.5 K and 49.5 K, respectively. DyCu$_2$ compound undergoes an AFM to AFM transition and an AFM to PM transition at 18.5 K and 31.5 K, respectively. HoCu$_2$ compound undergoes an AFM to AFM transition and an AFM to PM transition at 7 K and 10 K, respectively. ErCu$_2$ compound undergoes an AFM to AFM transition and an AFM to PM transition at 6 K and 12 K, respectively. The transition temperatures are in accord with previous reports.[128,136,138,141] All the transition temperatures for RCu$_2$ (R = Gd, Tb, Dy, Ho, Er) compounds are shown in Table 7. It can be seen that the magnetic property and magnetic transition for RCu$_2$ (R = Gd, Tb, Dy, Ho, Er) compounds is very complex and interesting. Firstly, the magnetic transition shows its multiformity for RCu$_2$ (R = Gd, Tb, Dy, Ho, Er) compounds. GdCu$_2$ compound shows only one magnetic transition, while others show two magnetic transitions. Secondly, the Neel temperatures seems not correlated to spin or atom number. From Gd to Er, the atom number increases monotonously. But the Neel temperature does not change monotonously from GdCu$_2$ to ErCu$_2$. Thirdly, all the ground states of RCu$_2$ (R = Gd, Tb, Dy, Ho, Er) compounds are AFM ordered, and this property may bring special magnetic performances on other aspects.

Table 7. The transition temperatures and magnetocaloric effect parameters of RCu$_2$ (R = Gd, Tb, Dy, Ho, Er) compounds.

Materials	T_t/K	T_N/K	M_{eff}/μ_B	M_{ion}/μ_B	MCE_0–7 T			Ref.
					$-\Delta S_M(T)_{max}$/(J/kg·K)	T_{width}/K	RC/(J/kg)	
GdCu$_2$	–	40.5	8.2	7.9	–	–	–	[142]
TbCu$_2$	23.5	49.5	9.5	9.7	11.5	39.2	339	[142]
DyCu$_2$	18.5	31.5	10.2	10.6	14.8	33	365	[142]
HoCu$_2$	7	10	10.5	10.6	21.5	20.1	330	[142]
ErCu$_2$	6	12	10.1	9.6	13.7	21.8	226.5	[142]

The relationship between the reciprocal magnetic susceptibility (χ^{-1}) and temperature was also obtained from M–T curves. All of the magnetic susceptibility of RCu$_2$ (R = Gd, Tb, Dy, Ho, Er) compounds can be fitted to the Curie–Weiss law. The effective magnetic moment M_{eff} per R atom was calculated by the linear fitting of χ^{-1}–T. The specific value of M_{eff} for each RCu$_2$ compound is shown in Table 7. And for comparison, the theory value is listed as well. It can be seen that the M_{eff} is in good accord with theory value of R ions. It can also be seen that the ZFC and FC curves overlap for most RCu$_2$ (R = Gd, Tb, Dy, Ho, Er) compounds except DyCu$_2$ compound. It indicates that RCu2 series exhibit good heat reversibility. And the divarication between ZFC and FC in DyCu$_2$ compound may result from domain wall pinning effect.[19] It has been mentioned that the ground state is AFM for the most RCu$_2$ (R = Gd, Tb, Dy, Ho, Er) compounds. However, the AFM coupling is weak for some compounds but strong for others. The isothermal magnetization at low temperature up to 7 T is shown in Fig. 59 for GdCu$_2$ and TbCu$_2$, respectively. As magnetic field increases, both GdCu$_2$ and TbCu$_2$ compounds undergo metamagnetic transition. And the critical field (H_{cr}) can be calculated by the maximum of dM/dT. The H_{cr} of GdCu$_2$ and TbCu$_2$ compounds is determined to be 2 T and 5.6 T, respectively. Considering that the available magnetic field in regular lab conditions is 2 T or so, GdCu$_2$ compound has little research value in magnetocaloric effect. Therefore, the magnetocaloric effect will be investigated on TbCu$_2$, DyCu$_2$, HoCu$_2$ and ErCu$_2$ compounds.

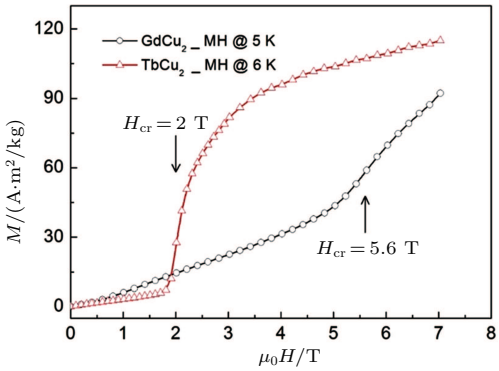

Fig. 59. (color online) The isothermal magnetization of GdCu$_2$ and TbCu$_2$ compounds measured at low temperatures.

6.2. The magnetocaloric effect of RCu$_2$ compounds

The ΔS_M of RCu$_2$ (R = Tb, Dy, Ho, Er) compounds was calculated based on the isothermal magnetization data (not shown here) by using the Maxwell relation.[142] The ΔS_M curves as a function of temperature for RCu$_2$ (R = Tb, Dy, Ho, Er) compounds with a field change of 0 T–7 T are shown in Fig. 60. The inset of Fig. 60 is the low-temperature part of ΔS_M curve for TbCu$_2$ compound. The position of ΔS_M peaks are closely correlated to the disorder–order transition temperatures of each RCu$_2$ (R = Tb, Dy, Ho, Er) compound. Thus the ΔS_M curves for HoCu$_2$ and ErCu$_2$ center at lower temperature

and the ΔS_M curves for $TbCu_2$ and $DyCu_2$ center at higher temperatures. Among all the RCu_2 (R = Tb, Dy, Ho, Er) compounds, the maximum of ΔS_M for $HoCu_2$ compound shows the largest value and that for $TbCu_2$ compound shows the smallest value. Though $ErCu_2$, $HoCu_2$, $DyCu_2$, and $TbCu_2$ compounds all undergo two magnetic transitions, only $TbCu_2$ compound shows more than one peaks on the ΔS_M curve. It should be noted that the secondary peak for $TbCu_2$ compound is positive ΔS_M. Positive ΔS_M has been observed in many AFM MCE materials and the positive value in AFM ordering is considered to be due to disordered magnetic sublattices antiparallel to the applied magnetic field.[48,49] All the RCu_2 (R = Tb, Dy, Ho, Er) compounds are AFM ordered, but most of them does not show positive ΔS_M because AFM ordering is so weak that a field of 7 T has destroyed it. The ΔS_M of $TbCu_2$ compound for a field change of 0 T–7 T showing positive value means that the AFM ordering here is very strong. Furthermore, the positive refrigerant temperature width (T_{width}) is so large that, the secondary peak is higher than the main peak. For $TbCu_2$ compound, the maximum of negative ΔS_M is 11.5 J/kg·K, but the maximum of positive ΔS_M is 13.9 J/kg·K.

Refrigeration capacity (RC) and refrigerant temperature width (T_{width}) are important parameters for MCE materials as well. The RC can be calculated on the basis of, where T_1 and T_2 are the two ends of the half-maximum width of the ΔS_M–T curve, and T_{width} is defined as T_2–T_1. The maximum of ΔS_M for $TbCu_2$, $DyCu_2$, $HoCu_2$, and $ErCu_2$ compounds is calculated to be 11.5 J/kg·K, 14.8 J/kg·K, 21.5 J/kg·K, and 13.7 J/kg·K, respectively. The T_{width} for $TbCu_2$, $DyCu_2$, $HoCu_2$, and $ErCu_2$ compounds is calculated to be 39.2 K, 33 K, 20.1 K, and 21.8 K, respectively. The RC for $TbCu_2$, $DyCu_2$, $HoCu_2$, and $ErCu_2$ compounds is calculated to be 339 J/kg, 365 J/kg, 330 J/kg, and 226.5 J/kg, respectively. All of the MCE parameters are also listed in Table 7. It should be noted that the RC for $TbCu_2$ compound is determined only by the negative ΔS_M part. Since the complex magnetic properties of RCu_2 compounds, $(\Delta S_M)_{max}$, T_{width}, and RC all show no monotonous change trend as the atom number increases. As for $(\Delta S_M)_{max}$, $HoCu_2$ compound shows the best performance. As for T_{width}, $TbCu_2$ compound shows the best performance. As for RC, $DyCu_2$ compound shows the best performance.

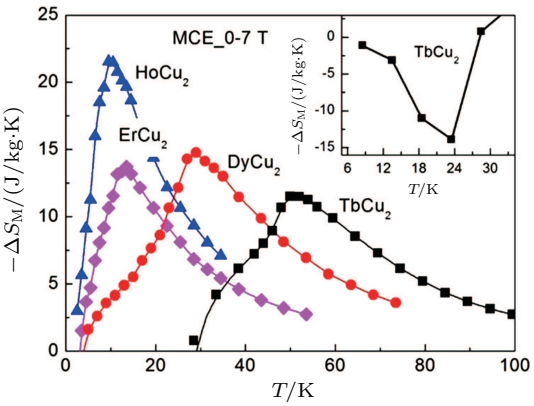

Fig. 60. (color online) The temperature dependence of magnetic entropy change at a field change of 0 T–5 T for RCu_2 (R = Tb, Dy, Ho, Er) compounds.

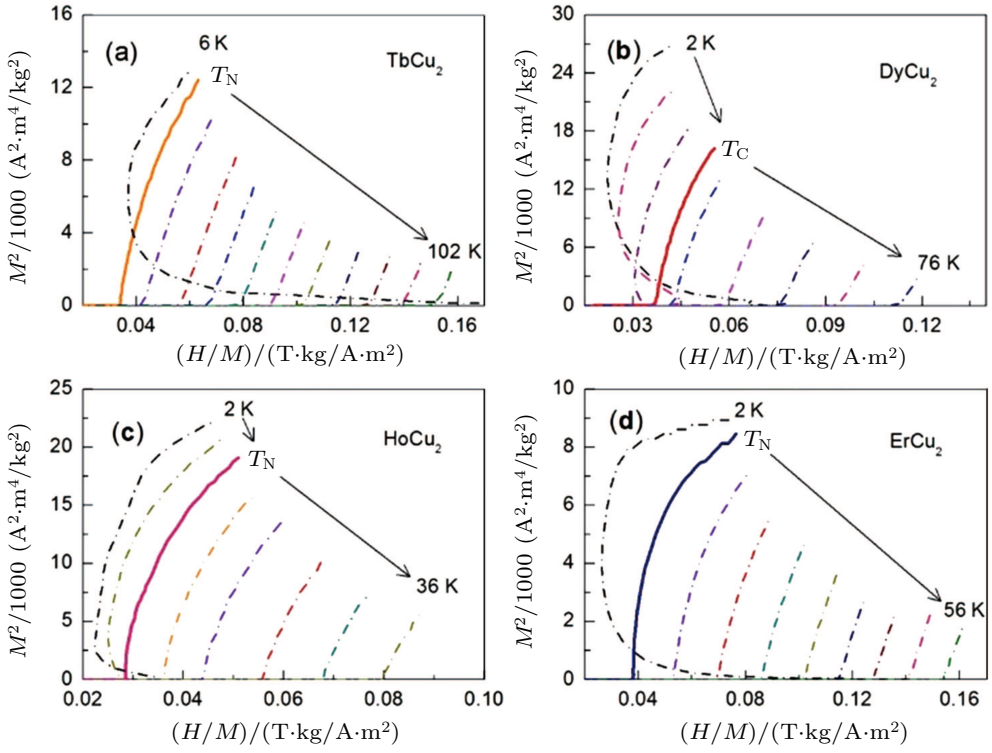

Fig. 61. (color online) The Arrott plots of RCu_2 (R = Tb, Dy, Ho, Er) compounds.

The Arrott plots of RCu$_2$ (R = Tb, Dy, Ho, Er) compounds at different temperatures are calculated from isothermal magnetization data and they are shown in Fig. 61. A magnetic transition is expected to be of the first order when the slope of the Arrott plot is negative, whereas it will be of the second order when the slope is positive. It can be seen that the slope around T_N for each RCu$_2$ compound is positive, which indicates that RCu$_2$ (R = Tb, Dy, Ho, Er) compounds are second order materials. The result is in accord with the heat reversibility observed before because heat and magnetic hysteresis are usually negligible for second order materials. And the MCE materials with small heat and magnetic hysteresis are more valuable for applications.

7. Conclusions

The MCE of binary or pseudo binary R–T (R = Pr, Gd, Tb, Dy, Ho, Er, Tm; T = Ga, Ni, Co, Cu) intermetallic compounds (including RGa series, RNi series, R_{12}Co$_7$ series, R_3Co series, and RCu$_2$ series) have been reviewed, and it is found that these compounds exhibit various magnetic properties and different MCE in low temperature range. Generally, most of the compounds crystallize in orthorhombic structure (space group *Cmcm* #63, space group *Pnma* #62 or space group *Imma* #74), but the R_{12}Co$_7$ series crystallize in monoclinic structure. The magnetic properties of binary R–T (R = Pr, Gd, Tb, Dy, Ho, Er, Tm; T = Ga, Ni, Co, Cu) intermetallic compounds (including RGa series, RNi series, R_{12}Co$_7$ series, R_3Co series, and RCu$_2$ series) are complex and interesting. The ground state is FM or AFM, the number of magnetic transitions is one, two or three, and the magnetocaloric effect is positive or negative. The Curie temperature or Neel temperature of R–T compounds is very low, and order–disorder temperature is negatively correlated with the maximum of ΔS_M according to Oesterreicher *et al.*[47] Thus large value of ΔS_M was usually observed in the compounds with large total angular moment quantum number J, such as Ho series, Er series, and Tm series. Since several magnetic transitions exist for some compounds, multi-peaks are observed on the MCE curves. In some cases, several peaks change to one wide and high peak, which is very useful for actual application as magnetic refrigerant materials. Rare earth atoms are also substituted by other R atoms with different S (spin angular moment) or J (total angular moment), and thus several compounds with better MCE performance are obtained. Those binary and pseudo-binary R–T compounds showing good MCE performance especially under low magnetic field change, may be promising candidates for magnetic refrigeration materials in low temperature range in the future, such as the application in liquefaction of helium, hydrogen, and nitrogen.

Although the MCE of many binary R–T compounds (including RGa series, RNi series, R_{12}Co$_7$ series, R_3Co series, and RCu$_2$ series) have been investigated systematically in the past decades, a lot of important problems, such as the influence of volume transition on MCE, the mechanism of positive MCE in the AFM materials, and the reason of the enhancement of MCE for substituted compounds, have not been addressed well. In fact, some work connected with physical mechanism has been done by employing powder neutron diffraction technique. And more and further investigations are necessary to do. In conclusion, previous studies have revealed that the binary or pseudo-binary R–T (R = Pr, Gd, Tb, Dy, Ho, Er, Tm; T = Ga, Ni, Co, Cu) intermetallic compounds (including RGa series, RNi series, R_{12}Co$_7$ series, R_3Co series, and RCu$_2$ series) exhibit good performance on MCE in low temperature range, suggesting the promising application in low-temperature magnetic refrigeration. However, there is still a lot of work to be done.

References

[1] Zimm C, Jastrab A, Sternberg A, Pecharsky V, Gschneidner K, Osborne M and Anderson I 1998 *Adv. Cryog. Eng.* **43** 1759
[2] Tishin A M and Spichkin Y I 2003 *The magnetocaloric effect and its applications* (London: Institute of Physics Publishing)
[3] Pecharsky V K and Gschneidner K A Jr 1999 *J. Magn. Magn. Mater.* **200** 44
[4] Gschneidner K A Jr, Pecharsky V K and Tsokol A O 2005 *Rep. Prog. Phys.* **68** 1479
[5] Pecharsky V K and Gschneidner K A 1997 *Phys. Rev. Lett.* **78** 4494
[6] Hu F X, Shen B G, Sun J R, Cheng Z H, Rao G H and Zhang X X 2001 *Appl. Phys. Lett.* **78** 3675
[7] Wada H and Tanabe Y 2001 *Appl. Phys. Lett.* **79** 3302
[8] Tegus O, Brück E, Buschow K H J and de Boer F R 2002 *Nature* **415** 150
[9] Tegus O, Brück E, Zhang L, Dagula, Buschow K H J and de Boer F R 2002 *Physica B* **319** 174
[10] Krenke T, Duman E, Acet M, Wassermann E F, Moya X, Mañosa L and Planes A 2005 *Nat. Mater.* **4** 450
[11] de Campos A, Rocco D L, Carvalho A M G, Caron L, Coelho A A, Gama S, da Silva L M, Gandra F C G, dos Santos A O, Cardoso L P, von Ranke P J and de Oliveira N A 2006 *Nat. Mater.* **5** 802
[12] Du J, Cui W B, Zhang Q, Ma S, Xiong D K and Zhang Z D 2007 *Appl. Phys. Lett.* **90** 042510
[13] Hu F X, Shen B G, Sun J R and Wu G H 2001 *Phys. Rev. B* **64** 132412
[14] Korte B J, Pecharsky V K and Gschneidner K A 1998 *J. Appl. Phys.* **84** 5677
[15] Giguere A, Foldeaki M, Schnelle W and Gmelin E 1999 *J. Phys.: Condens. Matter* **11** 6969
[16] Dong Q Y, Shen B G, Chen J, Shen J and Sun J R 2009 *J. Appl. Phys.* **105** 113902
[17] Chen J, Shen B G, Dong Q Y, Hu F X and Sun J R 2010 *Appl. Phys. Lett.* **96** 152501
[18] Zheng X Q, Shao X P, Chen J, Xu Z Y, Hu F X, Sun J R and Shen B G 2013 *Appl. Phys. Lett.* **102** 022421
[19] Chen J, Shen B G, Dong Q Y, Hu F X and Sun J R 2009 *Appl. Phys. Lett.* **95** 132504
[20] Delyagin N N, Krylov V I and Rozantsev I N 2007 *J. Magn. Magn. Mater.* **308** 74
[21] Baenziger N C and Moriarty J L 1961 *Acta Cryst.* **14** 946
[22] Shohata N 1977 *J. Phys. Soc. Jpn.* **42** 1873
[23] Schob O and Parthe E 1961 *Acta Cryst.* **14** 946
[24] Fujii H, Shohata N, Okamoto T and Tatsumoto E 1971 *J. Phys. Soc. Jpn.* **31** 1592

[25] Cable J W, Koehler W C and Wollan E O 1964 *Phys. Rev.* **136** A240
[26] Barbara B, Nguyen V N and Siaud E 1972 *CR Acad. Sci.* **274** 1053
[27] Barbara B, Becle C, Nguyen V N and Siaud E 1971 in *Durham Conf.*
[28] Nesterov V I, Reiman S I and Rozantsev I N 1992 *Fiz. Tverd. Tela* **34** 1270
[29] Susilo R A, Pérez S M, Cobas R, Cadogan J M and Avdeev M 2012 *J. Phys.: Conf. Ser.* **340** 012071
[30] Susilo R A, Cadogan J M, Ryan D H, Lee-Hone N R, Cobas R and Muñoz-Pérez S 2013 *Hyperfine. Interact.* **226** 257
[31] Zhang J Y, Luo J, Li J B, Liang J K, Wang Y C, Ji L N, Liu Y H and Rao G H 2009 *J. Alloys Compd.* **469** 15
[32] Zheng X Q, Chen J, Shen J, Zhang H, Xu Z Y, Gao W W, Wu J F, Hu F X, Sun J R and Shen B G 2012 *J. Appl. Phys.* **111** 07A917
[33] Zheng X Q, Wu H, Chen J, Zhang B, Li Y Q, Hu F X, Sun J R, Huang Q Z and Shen B G 2015 *Sci. Rep.* **5** 14970
[34] Zheng X Q, Chen J, Wang L C, Wu R R, Hu F X, Sun J R and Shen B G 2014 *J. Appl. Phys.* **115** 17A905
[35] von Ranke P, Nóbrega E, de Oliveira I, Gomes A and Sarthour R 2001 *Phys. Rev. B* **63** 184406
[36] von Ranke P J, Pecharsky V K and Gschneidner K A 1998 *Phys. Rev. B* **58** 12110
[37] Tishin A M 1999 *Handbook of Magnetic Materials*, Vol. 12 (Amsterdam: North Holland)
[38] Chen J, Shen B G, Dong Q Y and Sun J R 2010 *Solid State Commun.* **150** 157
[39] Mo Z J, Shen J, Yan L Q, Tang C C, Lin J, Wu J F, Sun J R, Wang L C, Zheng X Q and Shen B G 2013 *Appl. Phys. Lett.* **103** 052409
[40] Gao T, Nishimura K, Matsumoto T, Namiki T and Isikawa Y 2013 *Solid State Commun.* **158** 1
[41] Zheng X Q, Chen J, Xu Z Y, Mo Z J, Hu F X, Sun J R and Shen B G 2014 *J. Appl. Phys.* **115** 17A938
[42] Banerjee S K 1964 *Phys. Lett.* **12** 16
[43] Chen J, Zheng X Q, Dong Q Y, Sun J R and Shen B G 2011 *Appl. Phys. Lett.* **99** 122503
[44] Hu F X, Shen B G, Sun J R, Pakhomov A B, Wong C Y, Zhang X X, Zhang S Y, Wang G J and Cheng Z H 2001 *IEEE. T. Magn.* **37** 2328
[45] Dinesen A R, Linderoth S and Mørup S 2002 *J. Magn. Magn. Mater.* **253** 28
[46] Zheng X Q, Shen J, Hu F X, Sun J R and Shen B G 2016 *Acta Phys. Sin.* **65** 217502 (in Chinese)
[47] Oesterreicher H and Parker F T 1984 *J. Appl. Phys.* **55** 4334
[48] Samanta T, Das I and Banerjee S 2007 *Appl. Phys. Lett.* **91** 152506
[49] Shen J, Zhao J L, Hu F X, Rao G H, Liu G Y, Wu J F, Li Y X, Sun J R and Shen B G 2010 *Appl. Phys. A* **99** 853
[50] Pecharsky V K and Gschneidner K A 1999 *J. Appl. Phys.* **86** 565
[51] Zou J D, Shen B G and Sun J R 2007 *Chin. Phys.* **16** 1817
[52] Fujieda S, Fujita A and Fukamichi K 2002 *Appl. Phys. Lett.* **81** 1276
[53] Gschneidner K A Jr, Pecharsky V K, Pecharsky A O and Zimm C B 1999 *Mater. Sci. Forum* **315–317** 69
[54] Hu F X, Wang G J, Wang J, Sun Z G, Dong C, Chen H, Zhang X X, Sun J R, Cheng Z H and Shen B G 2002 *J. Appl. Phys.* **91** 7836
[55] Biswas A, Samanta T, Banerjee S and Das I 2008 *J. Appl. Phys.* **103** 013912
[56] van Dover R, Gyorgy E, Cava R, Krajewski J, Felder R and Peck W 1993 *Phys. Rev. B* **47** 6134
[57] Kunkel H P, Zhou X Z, Stampe P A, Cowen J A and Williams G 1996 *Phys. Rev. B* **53** 15099
[58] Stampe P A, Zhou X Z, Kunkel H P, Cowen J A and Williams G 1997 *J. Phys.: Condens. Matter* **9** 3763
[59] Levin E M, Pecharsky V K and Gschneidner K A 1999 *Phys. Rev. B* **60** 7993
[60] Morellon L, Stankiewicz J, Garcıa-Landa B, Algarabel P A and Ibarra M R 1998 *Appl. Phys. Lett.* **73** 3462
[61] Sechovsky V, Havela L, Prokes K, Nakotte H, Boer F R and Bruck E 1994 *J. Appl. Phys.* **76** 6913
[62] Chien C L, Xiao J Q and Jiang J S 1993 *J. Appl. Phys.* **73** 5309
[63] Xiao J, Jiang J and Chien C 1992 *Phys. Rev. Lett.* **68** 3749
[64] Allia P, Knobel M, Tiberto P and Vinai F 1995 *Phys. Rev. B* **52** 15398
[65] Sengupta K, Rayaprol S and Sampathkumaran E V 2005 *Europhys. Lett.* **69** 454
[66] Walline R E and Wallace W E 1964 *J. Chem. Phys.* **41** 1587
[67] Isikawa Y, Mori K, Sato K, Ohashi M and Yamaguchi Y 1984 *J. Appl. Phys.* **55** 2031
[68] Pecharsky A, Mozharivskyj Y, Dennis K, Gschneidner K, McCallum R, Miller G and Pecharsky V 2003 *Phys. Rev. B* **68** 134452
[69] Gignoux D and Shah J S 1972 *Solid State Commun.* **11** 1709
[70] Pospisil J, Vejpravova J P and Sechovsky V 2007 *J. Magn. Magn. Mater.* **316** e552
[71] Wang D, Li Y, Long Y, Ye R, Chang Y and Wan F 2007 *J. Magn. Magn. Mater.* **311** 697
[72] Sato K, Yosida Y, Isikawa Y and Mori K 1986 *J. Magn. Magn. Mater.* **54–57**, Part 1 467
[73] Tajiri Y, Nishimura K, Li L and Hutchison W D 2008 *Solid State Commun.* **148** 365
[74] Nishimura K, Mori K, Narita Y and Hutchison W D 2007 *J. Magn. Magn. Mater.* **310** 1730
[75] Tajiri Y, Nishimura K, Li L, Kawabata T, Sato K, Kindo K and Hutchison W D 2009 *J. Alloys Compd.* **487** 5
[76] Zheng X Q, Zhang B, Wu H, Hu F X, Huang Q Z and Shen B G 2016 *J. Appl. Phys.* **120** 164101
[77] Tripathy S K, Suresh K G, Nirmala R, Nigam A K and Malik S K 2005 *Solid State Commun.* **134** 323
[78] Kumar P, Suresh K G, Nigam A K and Gutfleisch O 2008 *J. Phys. D: Appl. Phys.* **41** 245006
[79] Shen J, Xu Z Y, Zhang H, Zheng X Q, Wu J F, Hu F X, Sun J R and Shen B G 2011 *J. Magn. Magn. Mater.* **323** 2949
[80] Sato K 1982 *J. Appl. Phys.* **53** 8222
[81] Sato K, Iwasaki S, Ishikawa Y and Mori K 1982 *J. Appl. Phys.* **53** 1938
[82] Sato K, Iwasani S, Mori K and Isikawa Y 1983 *J. Magn. Magn. Mater.* **31–34**, Part 1 207
[83] Maezawa K, Wakabayashi S and Sato K 1985 *J. Appl. Phys.* **57** 3219
[84] Pecharsky V K and Gschneidner K A 1997 *Phys. Rev. Lett.* **78** 4494
[85] Wada H, Tanabe Y, Shiga M, Sugawara H and Sato H 2001 *J. Alloys Compd.* **316** 245
[86] Zhang Q, Cho J H, Li B, Hu W J and Zhang Z D 2009 *Appl. Phys. Lett.* **94** 182501
[87] Buschow K H J 1971 *Philips Res. Rep.* **26** 49
[88] Adams W, Moreau J M, Parthe E and Schweizer J 1976 *Acta Cryst.* **B32** 2697
[89] Deng J Q, Zhuang Y H, Li J Q and Huang J L 2007 *Physica B* **391** 331
[90] Chen X and Zhuang Y H 2008 *Solid State Commun.* **148** 322
[91] Dong Q Y, Chen J, Zhang X Q, Zheng X Q, Sun J R and Shen B G 2013 *J. Appl. Phys.* **114** 173911
[92] Zheng Z G, Zhong X C, Yu H Y, Liu Z W and Zeng D C 2011 *J. Appl. Phys.* **109** 07A919
[93] Zheng X, Zhang B, Li Y, Wu H, Zhang H, Zhang J, Wang S, Huang Q and Shen B 2016 *J. Alloys Compd.* **680** 617
[94] Buschow K H J 1977 *Rep. Prog. Phys.* **40** 1179
[95] Ehlers G, Ahlert D, Ritter C, Miekeley W and Maletta H 1997 *Europhys. Lett.* **37** 269
[96] Mallik R, Sampathkumaran E and Paulose P L 1998 *Solid State Commun.* **106** 169
[97] Arora P, Tiwari P, Sathe V G and Chattopadhyay M K 2009 *J. Magn. Magn. Mater.* **321** 3278
[98] Gignoux D and Schmitt D 1991 *J. Magn. Magn. Mater.* **100** 99
[99] Zhang X X, Wang F W and Wen G H 2001 *J. Phys.: Condens. Matter* **13** L747
[100] Duc N H, Anh D T and Brommer P E 2002 *Physica B* **319** 1
[101] Singh N K, Kumar P, Suresh K G, Nigam A K, Coelho A A and Gama S 2007 *J. Phys.: Condens. Matter* **19** 036213
[102] Singh N K, Suresh K G, Nirmala R, Nigam A K and Malik S K 2006 *J. Appl. Phys.* **99** 08K904
[103] Li B, Hu W J, Liu X G, Yang F, Ren W J, Zhao X G and Zhang Z D 2008 *Appl. Phys. Lett.* **92** 242508
[104] von Ranke P, Mota M, Grangeia D, Carvalho A, Gandra F, Coelho A, Caldas A, de Oliveira N and Gama S 2004 *Phys. Rev. B* **70** 134428
[105] Dong Q Y, Chen J, Shen J, Sun J R and Shen B G 2011 *Appl. Phys. Lett.* **99** 132504

[106] Zhang H, Sun Y J, Niu E, Yang L H, Shen J, Hu F X, Sun J R and Shen B G 2013 *Appl. Phys. Lett.* **103** 202412

[107] Zhang H, Shen B G, Xu Z Y, Shen J, Hu F X, Sun J R and Long Y 2013 *Appl. Phys. Lett.* **102** 092401

[108] Wang L C, Dong Q Y, Lu J, Shao X P, Mo Z J, Xu Z Y, Sun J R, Hu F X and Shen B G 2014 *J. Alloys Compd.* **587** 10

[109] Zhang H, Li Y, Liu E, Ke Y, Jin J, Long Y and Shen B 2015 *Sci. Rep.* **5** 11929

[110] Nagai H, Ogiwara F, Amako Y, Yoshie H, Koga K and Adachi K 1995 *J. Magn. Magn. Mater.* **140–144** Part 2 793

[111] Tristan N V, Nenkov K, Palewski T, Skokov K P and Nikitin S A 2003 *Phys. Status Solidi A* **196** 325

[112] Baranov N V, Pirogov A N and Teplykh A E 1995 *J. Alloys Compd.* **226** 70

[113] Baranov N V, Bauer E, Hauser R, Galatanu A, Aoki Y and Sato H 2000 *Eur. Phys. J. B* **16** 67

[114] Teplykh A E, Pirogov A N and Baranov N V 2000 *Mater. Sci. Forum* **321–324** 653

[115] Baranov N V, Hilscher G, Korolev A V, Markin P E, Michor H and Yermakov A A 2002 *Physica B* **324** 179

[116] Tripathy S K, Suresh K G and Nigam A K 2006 *J. Magn. Magn. Mater.* **306** 24

[117] Baranov N V, Markin P E, Nakotte H and Lacerda A 1998 *J. Magn. Magn. Mater.* **177–181**, Part 2 1133

[118] Baranov N V, Gubkin A F, Vokhmyanin A P, Pirogov A N, Podlesnyak A, Keller L, Mushnikov N V and Bartashevich M I 2007 *J. Phys.: Condens. Matter* **19** 326213

[119] Li B, Du J, Ren W J, Hu W J, Zhang Q, Li D and Zhang Z D 2008 *Appl. Phys. Lett.* **92** 242504

[120] Shen J and Wu J F 2011 *J. Appl. Phys.* **109** 07A931

[121] Shen J, Zhao J L, Hu F X, Wu J F, Sun J R and Shen B G 2010 *Chin. Phys. B* **19** 047502

[122] Mo Z J, Shen J, Yan L Q, Wu J F, Tang C C and Shen B G 2013 *J. Appl. Phys.* **113** 033908

[123] Mo Z J, Shen J, Yan L Q, Wu J F, Tang C C and Shen B G 2013 *J. Alloys Compd.* **572** 1

[124] Kumar P, Singh N K, Nayak A K, Haldar A, Suresh K G and Nigam A K 2010 *J. Appl. Phys.* **107** 09A932

[125] Podlesnyak A, Daoud-Aladine A, Zaharko O, Markin P and Baranov N 2004 *J. Magn. Magn. Mater.* **272–276**, Part 1 565

[126] Baranov N V, Goto T, Hilscher G, Markin P E, Michor H, Mushnikov N V, Park J G and Yermakov A A 2005 *J. Phys.: Condens. Matter* **17** 3445

[127] Akiko Takahashi S, Akihiko T, Masashi S and Takasu H 1995 *Jpn. J. Appl. Phys.* **34** L171

[128] Sherwood R C, Williams H J and Wernick J H 1964 *J. Appl. Phys.* **35** 1049

[129] Hashimoto Y, Fujii H and Okamoto T 1976 *J. Phys. Soc. Jpn.* **40** 1519

[130] Sugiyama K, Nakashima M, Yoshida Y, Settai R, Takeuchi T, Kindo K and Onuki Y 1996 *Physica B* **259** 896

[131] Loewenhaupt M, Doerr M, Jahn L, Reif T, Sierks C, Rotter M and Muller H 1998 *Physica B* **246** 472

[132] Doerr M 2003 *Physica B: Condensed Matter* **329–333** 633

[133] Birss R R, Houldsworth R V and Lord D G 1980 *J. Magn. Magn. Mater.* **15** 917

[134] Lord D G and McEwen K A 1980 *J. Magn. Magn. Mater.* **15** 523

[135] Luong N H, Franse J J M and Hien T D 1985 *J. Magn. Magn. Mater.* **50** 153

[136] Bischof J, Diviš M, Svoboda P and Smetana Z 1989 *Phys. Status Solidi A* **114** K229

[137] Doerr M, Rotter M, Loewenhaupt M, Reif T and Svoboda P 2000 *Physica B* **284** 1331

[138] Gratz E, Sechovsky V, Sima V, Smetana Z and Ström-Olson J O 1982 *Phys. Status Solidi B* **111** 195

[139] Smetana Z, Šıma V and Lebech B 1986 *J. Magn. Magn. Mater.* **59** 145

[140] Lebech B, Smetana Z and Šıma V 1987 *J. Magn. Magn. Mater.* **70** 97

[141] Karmakar S K, Giri S and Majumdar S 2015 *J. Appl. Phys.* **117** 193904

[142] Zheng X Q, Xu Z Y, Zhang B, Hu F X and Shen B G 2017 *J. Magn. Magn. Mater.* **421** 448